High-Fidelity Simulation and Analysis of Ignition Regimes and Mixing Characteristics for Low Temperature Combustion Engine Applications

by

Saurabh Gupta

A dissertation submitted in partial fulfillment
of the requirements for the degree of
Doctor of Philosophy
(Mechanical Engineering)
in The University of Michigan
2012

Doctoral Committee:

Professor Hong G. Im, Chair
Professor Mauro Valorani
Professor Arvind Atreya
Associate Professor Angela Violi
Assistant Professor Matthias Ihme

To you, Dear Baba, for your unconditional love and support

ACKNOWLEDGEMENTS

There are many people without whose support this work would not have been possible. First and foremost, I would like to thank my advisor Prof. Hong Im, for showing trust in my abilities and guiding me at every step of this journey. He has always given me independence to pursue my thoughts and research ideas. I have learnt so much from him, both technically and as a human being.

I would like to thank Prof. Valorani for sharing his valuable tool of CSP analysis, without which this work would have been impossible. He showed a lot of patience in explaining the minute details about the workings of the code, and I really appreciate his time and effort. I also acknowledge Prof. Lu and Prof. Yoo for helping out with DNS of n-heptane/air systems. They both have been very kind to answer my each and every question about the mechanism and code debugging. I thank Dr. Keum to have given me insights into modeling of mixing. Our discussions at Panera helped me a great deal.

I would also like to thank my labmates Gaurav, Paul, Johny, Songtao, Jingjin, Pinaki and LC, for making the environment of the lab so friendly. Especially Gaurav has given me a lot of guidance over many technical and non-technical matters. Discussions with him have helped me a great deal in my research. Paul has been ever so kind in introducing me to the S3D code, and helping me out with code debugging issues. Johny's ever smiling face helped me relax whenever I went through a rough patch. I've learnt dedication and hard work from Songtao and Jingjin. Over the last few months, it's been nice to have known Pinaki and LC. I've learned a lot in my

interactions with them.

I have made some very good friends for lifetime during my stay here. Over the years, we have become more like family members, sharing everything with one another. I would especially like to thank Prasanna, Biju, Kaustub and Krithika for their friendship.

I have been very fortunate to have met some of the best people, who have been ever so kind and generous. How can I thank sister Lakshmi and Indu mataji who have taken care of me like a mother over all these years. The love and support of sister Tina, sister Kristina and sister Aarti have been incredible and I cherish all the moments we've spent together. I look upto all these people for inspiration.

Lastly, I would like to thank my parents, my sister Swati and my brother-in-law Nishant for their emotional support throughout my doctoral work. They are the backbone of whatever I've achieved in life.

Finally, I dedicate this entire work to my eternal companion, God, the Supreme, whose unconditional love and support have been the guiding force in my life. I owe everything to Him !

TABLE OF CONTENTS

LIST OF FIGURES

Figure

ABSTRACT

High-Fidelity Simulation and Analysis of Ignition Regimes and Mixing Characteristics for Low Temperature Combustion Engine Applications

by

Saurabh Gupta

Chair: Hong G. Im

Low temperature combustion (LTC) technology is considered a viable option in the near future for its promises of low emissions and high efficiencies. However, the technical challenges of lack of control of ignition timing and combustion phasing are the roadblocks in its implementation. Introduction of thermal and compositional stratifications has been found to be useful to overcome these challenges. Under the presence of such stratifications, multiple ignition regimes are found to co-exist, and the influence of turbulent mixing on combustion becomes much more significant. In this dissertation, high-fidelity direct numerical simulation (DNS) is performed, and various analysis tools are used to obtain fundamental insights into classification of ignition regimes and modeling of turbulent mixing under such conditions.

Computational singular perturbation (CSP) technique is applied as an automated diagnostic tool to classify ignition regimes, especially spontaneous ignition front and deflagration. Various model problems representing LTC are simulated using high-fidelity computation with detailed chemistry for hydrogen-air system. The simulation data are then analyzed by CSP. In a homogeneous system, the occurrence of two

branches of explosive eigenvalues characterizes chain-branching and thermal ignition. Their merging point serves as a good indicator of the completion of the explosive stage of ignition. However, the merging point diagnostics is insufficient to differentiate spontaneous ignition from deflagration. As an alternate method, the active reaction zones are first identified by the locus of minimum number of fast exhausted time scales (based on user-specified error thresholds). Subsequently, the relative importance of transport and chemistry is determined in the region ahead of the reaction zone. A new index I^T, defined as the sum of the absolute values of the importance indices of diffusion and convection of temperature to the slow dynamics of temperature, serves as a criterion to differentiate spontaneous ignition from deflagration regimes. These diagnostic tools are applied to 1D and 2D ignition problems under laminar and turbulent mixture conditions, respectively, allowing automated detection of different ignition regimes at different times and location during the ignition events.

The same strategy is then used to gain fundamental insights into classification of ignition regimes in n-heptane/air mixtures in the presence of temperature and composition inhomogeneities. Parametric studies are conducted using high-fidelity simulations with detailed chemistry and transport. In particular, a key interest is to understand different ignition behavior of the n-heptane mixture at the negative-temperature coefficient (NTC) versus the non-NTC conditions. The CSP analysis for the reference homogeneous system yields the number of exhausted modes (M) at various stages during the ignition event. In addition, the merging of two explosive modes is observed at the onset of auto-ignition. For the one-dimensional system, the M profiles along with the importance index (I^T) measured in the upstream of the ignition front are used to determine whether the front propagation is the spontaneous ($I^T \sim 0$) or deflagrative ($I^T \sim 1$) regime. At a relatively large temperature fluctuation considered herein, the mixture at non-NTC conditions shows initially a deflagration front which is subsequently transitioned into a spontaneous ignition front. For the

mixtures at the NTC conditions which exhibit two-stage ignition behavior, the 1st stage ignition front is found to be more likely in the deflagration regime. On the other hand, the 2nd stage ignition front occurs almost always in the spontaneous regime because the upstream mixture contains active radical species produced by the preceding 1st stage ignition front. The effects of differently correlated equivalence ratio stratification are also considered and the results are shown to be consistent with previous findings. Next, 2D turbulent auto-ignition problems with same thermal fluctuation level, but different mean temperatures, corresponding to NTC and non-NTC chemistry are considered. The results are found to be consistent with the 1D studies, suggesting that for the levels of thermal fluctuations considered herein, turbulence did not have any significant influence on ignition regimes.

Finally, we look into the modeling of turbulent mixing in the context of flamelet approach. Flamelet modeling is considered to be a viable approach under stratified LTC. However, there are several issues that need further improvement. In particular, accurate representation of the scalar dissipation rate, which is the key parameter to connect the physical mixing space to the reactive space, requires further investigation. This involves a number of aspects: (i) probability density functions, (ii) mean scalar dissipation rates, and (iii) conditional scalar dissipation rates, for mixture fraction (Z) and total enthalpy (H). The validity of existing models both in the RANS and LES contexts is assessed, and alternative models are proposed to improve on the above three aspects.

CHAPTER I

Introduction

Over the last few decades, global concerns of climate change and dwindling petroleum reserves have become more serious than ever. Owing to rapidly increasing consumption, world oil prices are expected at $125 per barrel in 2035 (as compared to $84.5 per barrel in 2012) [3]. Furthermore, new environmental regulations such as Tier 3 Emission Standards [4] demand ultra-low NO_x and particulate emissions. These pose great challenges in the development of next generation transportation systems.

The existing spark ignition (SI) and compression ignition (CI) technologies are unable to meet the above requirements simultaneously. Due to higher thermal efficiency and better reliability, CI engines dominate the engineering applications requiring high power density, such as heavy duty vehicles, locomotive and marine engines. Due to high in-cylinder temperature and fuel-rich burning, however, the conventional CI engines suffer from large NO_x and soot emissions. In contrast, SI engines are commonly used in smaller passenger cars, in favor of lower soot emissions due to premixed burning, followed by after-treatment systems that can further reduce NO_x emissions to a large extent. However, SI engines face the challenge of low thermal efficiency as the compression ratio is limited due to the knocking problem. Furthermore, NO_x after-treatment systems increase the cost of vehicle enormously.

The above situation calls for a technology breakthrough to find new ways of highly

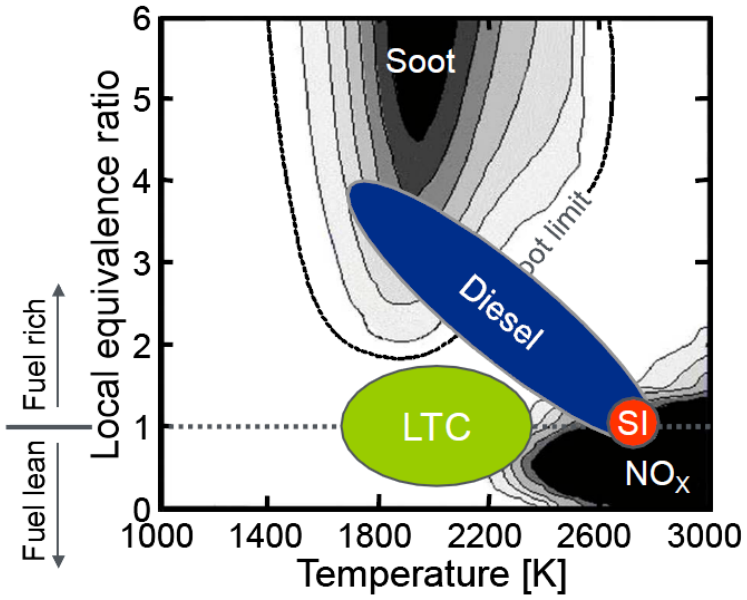

Figure 1.1: LTC operating regime. LTC engines operate at fuel lean and low temperature conditions, thereby preventing the formation of soot and NO_x, respectively. Figure from [1].

efficient and clean combustion. Low temperature combustion (LTC) technology refers to a general category of various types of new internal combustion (IC) engine concepts that can achieve these goals. The present doctoral dissertation is aimed at gaining fundamental insights into ignition and turbulent mixing characteristics in LTC engine environments, thereby enabling the design and development of modern engines at higher efficiency and lower emissions.

1.1 LTC concept and technology

The central concept of the LTC engine is to dilute the fuel-air mixture which allows for a low peak temperature, hence the term low temperature combustion [5, 6, 7]. Fuel-lean burning ensures low soot production, and low temperature accounts for low NO_x emissions. High level of dilution allows the engine to operate essentially unthrottled, thereby reducing pumping work and increasing fuel economy. Low peak combustion temperature reduces the closed-cycle heat losses and increases the in-

dicated thermal efficiency to levels approaching those of a CI engine. In addition, compared to SI engine, higher compression ratios are achieved due to self-ignition of the mixture, thereby increasing the thermal efficiency. Furthermore, LTC engines can potentially reduce cycle-to-cycle variations in comparison to SI engines. Large cycle-to-cycle variations occur with SI combustion [8] since the early flame development varies significantly with the variation of air/fuel mixture strength in the vicinity of a spark plug. However, the combustion initiation in LTC takes place at many points simultaneously, and the unstable flame propagation is avoided.

While LTC refers to a general class of IC engine approach, there are a number of variants depending on the specific implementations. For example, homogeneous charge compression ignition (HCCI) [9], compression ignited homogeneous charge (CIHC) combustion [10], premixed charge compression ignition (PCCI), controlled auto-ignition (CAI) combustion [11], Diesel combustion under uniform higher-dispersed mixture formation (UNIBUS) [12].

1.2 LTC challenges

Despite the promises of LTC engines, there are a few challenges which need to be tackled before this technology can be implemented practically: (i) difficulty in controlling ignition timing and combustion phasing, (ii) a narrow operating regime, and (iii) high hydrocarbon and CO emissions.

Unlike SI or CI engines, which utilize spark plug and fuel injector, respectively, there are no direct means to trigger ignition in LTC engines. This makes the control of ignition timing and subsequent combustion phasing very difficult. For high load conditions, heat release rate and pressure rise rate are so large that they can cause engine damage [13]. On the other hand, for very light loads, peak combustion temperature is too small to completely oxidize CO into CO_2 [14], resulting in a steep decline in combustion efficiency. Therefore, the stable operating regime is very nar-

row for LTC engines. Moreover, a large portion of unburned fuel stored in crevices is not completely burned because of relatively low peak temperature as compared to SI engines. This results in unwanted hydrocarbon and CO emissions.

A lot of research attention over the past few years has been focused to develop methods to resolve the above challenges, more specifically to control ignition timing and combustion phasing [7]. They can be generally divided into two categories:

- Modification of air/fuel mixture properties: by increasing intake temperature [15], adjusting air/fuel ratio, using exhaust gas recirculation (EGR) [16], using additives (promoters and inhibitors of ignition), and modifying fuels by blending or preconditioning.

- Modification of engine operation and design parameters: such as the variable compression ratio [17], variable valve timing [18], supercharging, and using different concepts of fuel injection.

Ultimately, all of these techniques provide means to adjust the compressed gas temperature and composition so that the charge mixture auto-ignites at the desired crank angle. In the following, we will look into further details on the effect of thermal and compositional stratifications.

1.3 Stratified LTC

Mixture stratifications (both thermal and compositional) play an important role in LTC combustion. On a conceptual level, one would expect that stratifications will favor directional burning of the fuel-air mixture (from hot-to-cold, and from rich-to-lean), which will allow the heat release to spread over several crank angle degrees, thereby extending the LTC high load limit. Moreover, stratifications also render control over the ignition timing and combustion phasing by optimal control of the mean and fluctuation magnitudes, as elucidated in a computational study [19].

Several experimental studies have also dealt with the role of stratifications in controlling LTC. In particular, the work by Sjoberg et al.[20], through a combination of multi-zone chemical-kinetics modeling and experiments, found that thermal stratifications have a large potential for extending the upper load limit. Dec et al. [21] conducted a chemiluminescence imaging study to conclude that thermal stratifications extending into the bulk gases will be effective in controlling the maximum pressure rise rate. Morimoto et al.[22] performed experiments with natural gas in a single-cylinder diesel engine, and concluded that mixture inhomogeneity could be used as an effective control for LTC.

On the other hand, other experimental studies, such as the direct observation of LTC in a four-stroke engine by Richter et al.[23], planar laser-induced fluorescence (PLIF) imaging study by Zhao et al.[24], a single-cylinder engine experiment by Girard et al.[25], and a recent PLIF study by Herold et al.[26], concluded that inhomogeneities have only a moderate to minimal effect on controlling LTC operation.

Nevertheless, low levels of mixture inhomogeneities are in fact found to be naturally present in LTC engines, mainly attributed to incomplete turbulent mixing, and heat loss to the cylinder wall. Experimentally observed LTC heat release is slower than that expected from kinetic rates for a thermally uniform charge. This natural slow-down in combustion duration is primarily attributed to thermal nonuniformities in the in-cylinder charge [27]. In another PLIF study [23], acquired sample images of the OH radical revealed a non-uniformly igniting charge in spite of efforts to make the most homogeneous fuel, temperature, and residual gas distribution possible for that engine configuration.

1.4 Ignition Regimes in LTC

Under such stratified mixture conditions, the auto-ignition and subsequent combustion processes become highly complex as observed by some recent experimental stud-

ies. By combining PLIF with chemiluminescence imaging, Hultqvist et al.[28] observed that ignition is not purely homogeneous, but there is formation of ignition kernels at favorable locations (the location being dependent on location mixture composition and temperature), which eventually merge together. Kaiser et al.[29] observed an occurrence of ordinary flame propagation between isolated ignition sites over distances short relative to the cylinder diameter in their research engine operated under HCCI mode using gasoline fuel. In their chemiluminescence study, Dec et al.[21] found evidence of combustion occurring as sequential autoignition of progressively cooler regions. Walton et al.[30], in an RCF study using iso-octane/air mixtures observed two distinct ignition regimes demarcated by a critical fuel mole fraction, below which volumetric ignition occurs, and above which there is formation and propagation of reaction fronts. In a recent optical imaging study by Zigler et al.[31], it was revealed that local hot zones result in preferential ignition sites for different fuels like iso-octane, indolene and gasoline.

All these experimental studies provide evidence that in the presence of stratifications, ignition and subsequent combustion processes in LTC engines occur in fundamentally different modes depending on the level of inhomogeneities. Therefore, it is important to gain fundamental understanding of different auto-ignition characteristics as a result of various physical parameters in order to develop a predictive combustion model applicable to LTC engines for a wide range of operating conditions.

The pioneering work by Zeldovich [32] established a theoretical framework to classify various ignition regimes depending on the level of temperature gradient. In the context of IC engines, various ignition regimes that can exist are: (i) *Homogeneous auto-ignition*, where the entire reactant mixture auto ignites simultaneously, (ii) *Deflagration*, where the reactant mixture is burned in succession by virtue of transport of radicals from the burning to the unburned region, and (iii) *Spontaneous ignition front*, where the reactant mixture sequentially auto-ignites owing to increasing ig-

nition delays, giving the appearance of front propagation. The distinction between these three ignition regimes, and in particular between spontaneous ignition front versus deflagration, is of primary interest. Subsequently, a number of computational studies have followed to develop a rational way to identify distinct ignition regimes.

Gu et al.[33] proposed ignition regime distinction based on initial hot spot temperature gradient. The issue has since been investigated by using direct numerical simulation (DNS). Sankaran et al.[34] proposed a temperature gradient cut off criterion, below which the front propagation was considered as spontaneous ignition, and above which front propagation was deflagration. The above studies based on temperature gradients provide good initial exploration on the topic, but are very case specific and based on ad hoc assumptions. To improve on the above criteria, Hawkes et al.[35] proposed an alternative criterion based on the comparison of the instantaneous displacement front speed with steady laminar flame speed at the same local mixture conditions. But use of steady propagation speeds in highly transient turbulent auto-ignition event inside an IC engine is highly questionable. Furthermore, this criterion might not hold true in case of multidimensional front propagation where displacement speed is not the ignition front speed. More recently, Bansal et al.[36] proposed a Damköhler number criterion based on the non-collocated peaks of reaction and diffusion of the radical HO_2 in a front, the peaks being tracked by a gradient descent algorithm. Although this approach is more comprehensive than the earlier ones, the choice of radical species may vary for different fuels or different stages of ignition. Moreover, in case of highly complex turbulent auto-ignition with multiple ignition fronts interacting with one another, the possibility of keeping track of the peaks of a specific ignition front is difficult. From a more practical standpoint towards reduced order full-cycle engine simulations, Martz et al.[37, 38] considered a one-dimensional configuration with an iso-octane mixture, and provided simpler criteria for ignition regime identification based on global physical parameters.

Although all the above computational studies provide useful insights into ignition regime distinction, there is still a need for an automated diagnostic tool which does not depend on ad hoc assumptions, has a broader applicability, and is based on sound physical and mathematical grounds. Computational singular perturbation (CSP) is an approach which caters to the above needs.

1.5 CSP analysis

The basic concept of CSP was established in late 1980s to early 1990s by Lam and coworkers [39, 40, 41, 42] and finds wide applications in essentially three areas: (i) chemical mechanism reduction, (ii) numerical stiffness reduction, and (iii) gaining insights into complex chemical kinetic behavior. In this study, we mainly utilize the third aspect.

The central idea of CSP is to find an alternative representation of the chemical source term vector ($\mathbf{g}$) of a given chemical kinetic system, such that the system can be decoupled into slow (active) and fast (exhausted) modes, thereby revealing useful physical insights into system timescales and stiffness.

In CSP, all processes (chemical reactions, diffusive and convective transport) are locally projected onto a curvilinear frame of reference identified by the right eigenvectors of the Jacobian matrix ($d\mathbf{g}/d\mathbf{Z}$), of the chemical source term vector ($\mathbf{g}$), where $\mathbf{Z}$ is the scalar solution variable vector (N_s species and temperature), thereby identifying the local eigenmodes of the characteristic processes of chemical nature. This also allows an identification of the contribution of each process to a specific chemical time scale, defined as the reciprocal of the modulus of the eigenvalue corresponding to the associated eigenmode. The number of modes, $N = N_s + 1$, is equal to the number of scalar variables.

The chemical time scales can be classified as explosive/dissipative and the corresponding modes are distinguished as exhausted/active/dormant. Explosive scales are

associated with eigenvalues with a positive real part and control the explosive behavior of the system through chain-branching and/or thermal ignition. Dissipative scales are associated with eigenvalues with a negative real part and can be associated with both fast exhausted and slow active/dormant modes. An automatic characterization of the reacting flow can be carried out by partitioning the physical space as the union of zones having an equal number of fast exhausted modes, M, where the criterion to declare a mode exhausted is based on a user-specified threshold.

Further analysis within a particular zone of interest is carried out through the importance and participation indices of various physical and chemical processes. The participation index of a process to a mode measures its relative contribution to the magnitude of that mode amplitude. The slow/fast importance indices of a process for a species are the non-dimensional measure of its relative contribution to the slow/fast dynamics of that species. Theoretical formulation of CSP will be discussed in the next chapter.

There have been a large number of studies employing CSP analysis to gain insights into the complex chemical kinetic behavior. Valorani et al.[43] used CSP analysis to identify various flow regimes in transient methane-air flame-vortex interactions. Kazakov et al.[44] employed CSP analysis to understand the cause of two-stage ignition behavior of large hydrocarbons at large pressures. Goussis et al.[45] even analyzed biochemical systems with the help of CSP analysis. Further, Lu et al.[46] used CSP analysis to identify quasi steady state species for methane oxidation with NO chemistry. More recently, a CSP based chemical explosive mode analysis (CEMA) has been introduced by Lu et al.[47] to identify flame and ignition structure.

In this dissertation, we use CSP analysis to formulate a quantitative criterion or metric to identify various ignition regimes, which is an original contribution.

1.6 Objectives I

Based on the above discussion on ignition regimes and CSP analysis, the objectives of the first part of this thesis are as follows:

- To formulate a novel strategy based on CSP to identify various ignition regimes in LTC engines. The strategy is developed and validated using various test cases of 0D and 1D laminar systems of hydrogen-air chemistry. Subsequently, the method is used to detect ignition regimes in multi-dimension, turbulent, mixed-mode combustion events. This will be discussed in Chapter 3.

- To use the above strategy to gain fundamental insights into the auto-ignition characteristics and ignition regimes for the two-stage ignition of n-heptane/air systems. One of the key fundamental questions of the study is regarding how the negative temperature coefficient (NTC) behavior affects the relative importance among different ignition regimes at given parametric conditions, such as temperature, pressure, and the level of temperature/composition fluctuations. Various 0D, 1D laminar and 2D turbulent systems are considered and useful insights are revealed into the two-stage ignition behavior and its effect on ignition regimes. This will be discussed in Chapter 4.

1.7 Turbulent mixing in LTC engines

Another important issue in turbulent combustion modeling is an accurate representation of turbulent mixing effects on auto-ignition and combustion within the LTC engines. Since all full-cycle IC engine simulations cannot afford DNS-like grid resolution, turbulent mixing and combustion events occurring at a subgrid level must be modeled.

If the LTC ignition occurs in perfectly homogeneous conditions, there is no significant influence of turbulence. In the presence of thermal and compositional strat-

ifications, however, there is a large impact of turbulence mixing on ignition timing and pollutant formation processes. The role of turbulence in LTC engines is two-fold: turbulence affects combustion indirectly through its influence on wall heat transfer, and also directly affects the mean reaction rate under certain mixture conditions when the fuel and air are not perfectly mixed. The direct effect will be more prominent in the presence of stratifications.

Christensen et al.[48, 49] considered two different piston geometries - flat and square-bowl respectively - to study the effects of engine turbulence on LTC. Square-bowl geometry induces larger in-cylinder turbulence, and consequently larger wall heat loss. The experiments indeed showed longer combustion duration in the square bowl piston as compared to that in the flat piston. In a computational study replicating the above experiments, Kong et al.[50] also reached to the conclusion that turbulence has a large impact on ignition timing and combustion duration. In another computational study, Zhang et al.[51] implemented transported PDF method in order to elucidate the role of turbulence-chemistry interactions on LTC. They found that for nearly homogeneous mixtures, even though the effect of turbulence on ignition timing can be neglected, its effect on emissions is non-negligible. Furthermore, with increasing levels of inhomogeneity, the effects of turbulence on both ignition timing and emissions become increasingly important. More recently, there have been 2D turbulent DNS studies with thermal stratifications [35, 52] and both thermal and compositional stratifications [36], which also reveal that turbulence results in a wider spread of heat release rate. Hence, it is clear from both experimental and computational standpoints, that turbulence influences LTC in a strong manner. Therefore, for a correct description of LTC, proper turbulence mixing models need to be incorporated.

The interactions of turbulent fluid motion with chemical reactions constitute a great modeling challenge, which has been the subject of research in the turbulent

combustion community for several decades [53]. Turbulence closure problem is in itself a difficult task for inert flows, and the difficulty is compounded by nonlinear reaction rates and large density variations for reacting flows.

A large number of modeling approaches have been developed over the past several years to account for the influences of thermal and compositional in-homogeneities and the role of turbulence in LTC. These include multiple-zone models [27, 54], stochastic models [55], and CFD based models [56, 50]. Within CFD models, the two main approaches that have been developed are PDF modeling [57] and flamelet modeling based on 1D enthalpy-based [58] and 2D enthalpy-mixture fraction-based [2] formulations. In this thesis, we look at the problem of transport closure in the flamelet modeling approach by the help of DNS data.

1.8 Flamelet modeling and transport closure

As a viable submodel for combustion processes in stratified LTC conditions, flamelet models have been proposed as an improved alternative to the multizone models (Cook et al.[58, 2]). Unlike the name may suggest, the flamelet approach [59] should be viewed as a general framework of describing chemical reactions in a reduced-dimensional space in which conserved scalar variables are used as the independent coordinate variables. The multi-dimensional computational fluid dynamics (CFD) simulation only considers transport equations for velocity and nonreactive scalar variables.

To accurately describe highly transient events such as auto-ignition encountered in LTC engines, the representative interactive flamelet (RIF) approach [60] solves the unsteady flamelet equation in the reactive space in conjunction with the time integration of the CFD solver. As for the conserved scalar variables, the mixture fraction, Z, is commonly used as the one-dimensional conserved scalar. To account for the nonuniform enthalpy levels due to exhaust gas mixing and heat losses, the

total enthalpy variable, H, can be added to construct a two-dimensional flamelet equation in the Z-H space [2]. One of the key parameters in the flamelet equation is the scalar dissipation rate, defined as

$$\chi_Z = 2\alpha|\nabla Z|^2 \tag{1.1}$$

where α is the diffusivity. For the two-dimensional flamelet approach, additional scalar dissipation rate for H needs to be defined as

$$\chi_H = 2\alpha|\nabla H|^2 \tag{1.2}$$

The scalar dissipation rate is the key parameter that connects the physical transport space and the reactive space. At each time step of the numerical solution, at first the equations in the physical space are solved to obtain the mean scalar dissipation rate at stoichiometric conditions. This is then used to calculate the conditional scalar dissipation rate through an analytical model [61, 62]. Conditional scalar dissipation rate is further used as an input to the flamelet equations (in the transformed space). The output parameters from the transformed space (species mass fractions as a function of Z and H) are then fed into the physical space to complete one time step cycle. The theoretical framework of flamelet modeling and the corresponding transport closure will be discussed in Chapter 2.

1.9 Objectives II

Although flamelet models have been successfully used in modeling LTC under stratified conditions, there still remain open issues. In particular, there still has not been a thorough study to investigate modeling of the scalar dissipation rate. Modeling scalar dissipation rate involves a number of aspects, the most important being the

probability density functions, mean scalar dissipation rates, and conditional scalar dissipation rates for Z and H. Therefore, the objectives of the present study are to validate various existing models, and to propose improved alternatives for:

- Probability density functions of Z and H
- Mean Z and H scalar dissipation rates
- Conditional Z and H scalar dissipation rates

This will be discussed in Chapter 5 of the thesis.

1.10 Outline of Dissertation

The main technical contents of the present dissertation is organized as follows.

- In Chapter 2, the theoretical formulation of CSP analysis is given. Mathematical derivations of the diagnostic tools (exhausted modes, explosive modes, importance index, participation index etc.) used in the thesis are provided. Next, formulation of the numerical interface between the CSP analysis code and S3D, the direct numerical simulation (DNS) code, which computes the numerical jacobian ($\mathrm{d}\mathbf{g}/\mathrm{d}\mathbf{Z}$) at each point of the spatio-temporal domain, is provided. This numerical interface was developed during this doctoral work. Finally, a brief description of the S3D code, which is used for 1D laminar and 2D turbulent DNS model problems is given.
- In Chapter 3, we look to develop a new strategy of ignition regime identification based on CSP analysis. Owing to its simplicity, hydrogen-air chemistry is used. Firstly, in order to find a proper metric to identify the auto-ignition event, a purely homogeneous 0D model problem is considered. Subsequently, for differentiation of spontaneous ignition and deflagration regimes, 1D model

problems are studied. The diagnostic tools thus developed are applied to the 2D turbulent ignition problem.

- The main purpose of Chapter 4 is to use the above CSP based diagnostic tools to gain insights into ignition regimes in highly complex n-heptane/air mixtures exhibiting 2-stage ignition. Again, we start with 0D homogeneous systems. The diagnostic tools are able to give insights into the chemical pathways for NTC vs. non-NTC chemistry. Next, DNS of 1D laminar and 2D turbulent ignition problems with varying levels of thermal and compositional fluctuations are conducted, and the results are analyzed by CSP. Various ignition regimes corresponding to different stages of ignition are identified.

- In Chapter 5, the aim is to gain fundamental insights into turbulent mixing in LTC engines, in particular we look at modeling of scalar dissipation rates in the context of RANS and LES. Three DNS test cases of 2D turbulent auto-ignition with different correlations of temperature and mixture fraction, representing different ignition regimes are considered. Firstly, the existing models of mean and conditional scalar dissipation rates, and probability density functions (PDFs) of mixture fraction and total enthalpy are tested against the DNS data. Next, the underlying reasons for the performance of the existing models are explored by looking into the local and global dynamics of mixing. Based on that understanding, new mixing models are proposed both in the context of RANS and LES and are shown to give better results.

- Finally, conclusions and directions for future work are presented in Chapter 6.

CHAPTER II

Formulation and Numerical Method

In this chapter, relevant mathematical formulations and the numerical method used in this dissertation are discussed. Firstly, theoretical and mathematical background of CSP analysis is given. Next, the DNS/CSP interface, developed during the course of this doctoral work is explained. Subsequently, a brief description of the DNS code, which is used for all the simulations in this dissertation, is provided. Finally, the computational framework of scalar dissipation rate modeling in the context of flamelet approach is presented.

2.1 CSP Analysis: Mathematical Formulation

A brief introduction to CSP analysis has already been given in Section 2.1. In the following, we provide the underlying mathematical formulation of CSP analysis. We will first consider the simplistic homogeneous case, and establish the criterion to compute the number of exhausted modes (M). Next, the formulation will be extended to non-homogeneous systems where transport processes (diffusion and convection) come into picture. Finally, conceptual and mathematical insights into the importance and participation indices, CSP steady state species and driving timescales will be given. All these parameters are computed in the CSP code, developed by Valorani et al.[43].

2.1.1 Homogeneous auto-ignition

Governing equations for species and energy conservation are given as:

$$\frac{d\mathbf{y}}{dt} = \mathbf{g}(\mathbf{y}) \tag{2.1}$$

Differentiating Equation 2.1 once w.r.t. time, we get

$$\frac{d\mathbf{g}(\mathbf{y})}{dt} = \frac{d\mathbf{g}(\mathbf{y})}{d\mathbf{y}}\frac{d\mathbf{y}}{dt} \tag{2.2}$$

where $\mathbf{J} = \frac{d\mathbf{g}(\mathbf{y})}{d\mathbf{y}}$ is the Jacobian of the source term

Eigenvalue analysis of $\mathbf{J}$ leads to

$$\mathbf{J} = \mathbf{A}\Lambda\mathbf{B} \tag{2.3}$$

where $\mathbf{A}$ and $\mathbf{B}$ are the right and left eigenvectors matrices respectively, and Λ is the diagonal matrix containing eigen-values of $\mathbf{J}$

Pre-multiplying Equation 2.2 by $\mathbf{B}$, and noting that $\mathbf{BA} = \mathbf{I}$, we get

$$\frac{d(\mathbf{Bg})}{dt} = \mathbf{BA}\Lambda(\mathbf{Bg}) = \Lambda(\mathbf{Bg}) \tag{2.4}$$

In Equation 2.4, $\frac{d\mathbf{B}}{dt}$ has been neglected. Ideally, $\mathbf{A}$ and $\mathbf{B}$ are computed through CSP refinement procedure [41] such that the resulting Λ is close to being diagonal.

Let $\mathbf{f} = \mathbf{Bg}$, then from Equation 2.4, we get

$$\frac{d\mathbf{f}}{dt} = \Lambda\mathbf{f} \tag{2.5}$$

Solution for Equation 2.5 is given by

$$f^i = f_0 \exp(\lambda_i t) \quad i = 1, 2, 3, ...N(number\ of\ modes) \tag{2.6}$$

From Equation 2.6,

f^i can be identified as the amplitude of the i^{th} mode

Chemical timescale of the i^{th} mode τ_i can be identified as

$$\tau_i = \frac{1}{|\lambda_i|} \tag{2.7}$$

2.1.2 Criterion to determine M

In physical space,

$$\mathbf{g}(\mathbf{y}) = \mathbf{S}_1 R_1 + \mathbf{S}_2 R_2 + ... + \mathbf{S}_{N_r} R_{N_r} \tag{2.8}$$

where, $\mathbf{S}_k$ is the k^{th} stoichiometric vector, R_k is the the reaction rate of k^{th} reaction, and N_r is the total number of reactions.

In the eigen-space spanned by the eigen-vectors $\mathbf{a}_i$ and $\mathbf{b}_i$, $\mathbf{g}(\mathbf{y})$ can be written as

$$\mathbf{g}(\mathbf{y}) = \mathbf{a}_1(\mathbf{b}_1.\mathbf{g}) + \mathbf{a}_1(\mathbf{b}_1.\mathbf{g}) + ... + \mathbf{a}_N(\mathbf{b}_N.\mathbf{g}) \tag{2.9}$$

M modes are declared to be exhausted if they satisfy

$$|\tau_{M+1}(\sum_{i=1}^{M} a_i^j f^i)| \leq \varepsilon_r y^j + \varepsilon_a \tag{2.10}$$

for all $j = 1, 2, 3, ..., N$

where ε_r and ε_a are the user-specified relative and absolute error thresholds, respectively.

2.1.3 Extension to non-homogeneous systems

For the general problem including transport, the governing equations become:

$$\frac{\partial \mathbf{y}}{\partial t} = \mathbf{g}(\mathbf{y}) + \mathbf{L}_c(\mathbf{y}) + \mathbf{L}_d(\mathbf{y}) \tag{2.11}$$

For this case, local approach [63] is adopted and the Jacobian is computed w.r.t. the source term only. The mode amplitudes are now computed as:

$$f^i = \mathbf{b}^i.(\mathbf{g} + \mathbf{L}_c + \mathbf{L}_d) \tag{2.12}$$

The criterion for selection of M remains the same. However, for each mode, in addition to the chemical time scale, we have convective and diffusive time scales, which are defined as:

$$\tau^i_{diff} = \frac{|\mathbf{b}_i.\mathbf{y}_0|}{|\mathbf{b}_i.\mathbf{L}_{d,0}|} \tag{2.13}$$

$$\tau^i_{conv} = \frac{|\mathbf{b}_i.\mathbf{y}_0|}{|\mathbf{b}_i.\mathbf{L}_{c,0}|} \tag{2.14}$$

where $\mathbf{y}_0$ is the state vector at the point of interest; $\mathbf{L}_{d,0} = \mathbf{L}_d(\mathbf{y}_0)$ and $\mathbf{L}_{c,0} = \mathbf{L}_c(\mathbf{y}_0)$ Now that M can be calculated based on the user-specified thresholds ε_r and ε_a, further insights into the problem can be obtained by looking at the dimension M of the fast subspace at various stages of auto-ignition.

2.1.4 Importance and participation indices

The topology of M represents the rapid changes of the variables in the phase space - species and temperature, which can then be understood by further analysis in each region of the M profile. This detailed analysis is carried out through the importance and participation indices of various physical and chemical processes. The slow (or fast) importance index of a process is the non-dimensional measure of its relative contribution to the slow (or fast) dynamics of a particular species. Mathematically, the slow (or fast) importance index for k^{th} process in the slow (or fast) dynamics of

i^{th} species is defined as [64]:

$$(\mathbf{I}_k^i)_{slow} = \frac{\sum_{s=M+1}^{N-N_c} a_s^i(\mathbf{b}^s.\mathbf{S}_k)R^k}{\sum_{j=1}^{N_p}\left|\sum_{s=M+1}^{N-N_c} a_s^i(\mathbf{b}^s.\mathbf{S}_j)R^j\right|} \tag{2.15}$$

$$(\mathbf{I}_k^i)_{fast} = \frac{\sum_{r=1}^{M} a_r^i(\mathbf{b}^r.\mathbf{S}_k)R^k}{\sum_{j=1}^{N_p}\left|\sum_{r=1}^{M} a_r^i(\mathbf{b}^r.\mathbf{S}_j)R^j\right|} \tag{2.16}$$

where N_p is the total number of processes (chemical reactions + transport processes), N is the total number of modes and N_c is the number of modes corresponding to atomic and energy conservation laws. $\mathbf{a}_i$ and $\mathbf{b}_i$ are the right and left eigenvectors, respectively of the Jacobian of the chemical source term. $\mathbf{S}_i$ is defined such that it is the stoichiometric vector for chemical reactions and unit vector with j^{th} entry as unity corresponding to diffusion or convection of j^{th} species. R^k is defined the reaction rate for chemical reactions and the corresponding diffusion or convection term for transport processes.

The participation index of the k^{th} process measures its relative contribution in the modal amplitude of i^{th} mode. It is defined as

$$(P_k^s) = \frac{\mathbf{b}_r.\mathbf{S}_k R^k}{\sum_{j=1}^{N_p}\left|\mathbf{b}_r.\mathbf{S}_k R^k\right|} \tag{2.17}$$

These indices provide more valuable information than the mere ratio of individual reaction or transport terms to the net time rate of change of a particular variable appearing in the governing equations in the physical space. This is in part because the contribution of a particular process is measured relative to all the processes pertaining

to the solution variables having different physical dimensions, such as those appearing in species equation and those in energy equation. Furthermore, the separation of the fast and slow components of the solution trajectory allows for a systematic way to measure the contributions only in either the fast or the slow subspace, which is better than considering the entire space all at once. An illustrative example explaining this point can be found in [64].

2.1.5 Identification of steady state species

A significant outcome of the CSP analysis is the identification of steady state species, which gives insights into the possibility of mechanism reduction. In the past, such species were identified based on the detailed inspection of the production and destruction rates of individual reaction steps; relying on sensitivity analysis tools [65], [42]; by measuring the species lifetime [66]; or by observing the magnitude of properly scaled candidate species concentration [67]. However, these methodologies are only based on a portion of the underlying physics. CSP identifies steady state species (CSP radicals) as those: (i) which are most affected by the exhausted chemical time scales, (ii) which contribute most to the algebraic relations responsible for mode exhaustion.

2.1.6 Driving timescales

CSP analysis can also give insights about the driving timescale at each spatio-temporal location. The driving chemical timescale, τ_{M+1}, is identified as the fastest active time scale. The driving diffusion timescale of the system, $\tau_{d,min}$ is the minimum of the diffusive timescales of all active modes, and similarly the driving convection timescale of the system, $\tau_{c,min}$ is the minimum of the convective timescales of all the active modes. By comparing these timescales, an overall estimate can be made as to which physical process plays a role as the driving process at a given position and time during the evolution of combustion event.

2.2 Formulation of DNS/CSP interface

The DNS/CSP interface takes the local state vector as an input from DNS, and outputs the refined data set to the CSP code. This refined data set includes:

(i) Matrix **Q** obtained from splitting of the source term

$$\mathbf{g}_{(N_s+1,1)} = \mathbf{Q}_{(N_s+1,N_s)}\mathbf{S}_{(N_s,N_r)}\mathbf{R}_{(N_r,1)} \tag{2.18}$$

S is the stoichiometric matrix and **R** is the reaction rate vector

For the constant volume problems considered, we get

$$\mathbf{Q} = \begin{bmatrix} \frac{W_1}{\rho} & 0 & \cdots & 0 & 0 \\ 0 & \frac{W_2}{\rho} & \cdots & 0 & 0 \\ 0 & 0 & \cdots & 0 & \frac{W_{N_s}}{\rho} \\ \frac{-u_1 W_1}{\rho C_v} & \frac{-u_2 W_2}{\rho C_v} & \cdots & \frac{-u_{N_s-1} W_{N_s-1}}{\rho C_v} & \frac{-u_{N_s} W_{N_s}}{\rho C_v} \end{bmatrix} \tag{2.19}$$

For constant pressure problems, u (internal energy) is replaced by h (enthalpy) and C_v is replaced by C_p

(ii) Jacobian $\mathbf{J} = \frac{d\mathbf{g}}{d\mathbf{y}}$ of the source term. It is computed numerically by finite central differencing scheme. A very small perturbation is given to $\mathbf{y}$, and $\mathbf{g}$ is calculated using CHEMKIN sub-routines.

(iii) Diffusion and Convection terms of the species and energy conservation equations.

2.3 Numerical method: DNS

In this doctoral work, the high-fidelity DNS code named S3D, originally developed at Sandia National Labs has been used to solve compressible, multi-component, reacting Navier-Stokes equations [68, 69, 70]. S3D employs eighth-order explicit finite difference scheme for spatial derivatives, and fourth-order explicit Runge-Kutta method

for time integration with PID error controller [71]. Tenth order spatial filter is implemented to remove any spurious oscillations in the solution. S3D has been designed for massive parallelization using MPI.

The mixture specific heat is computed locally based on mixture composition using the CHEMKIN thermodynamic database [72]. Hydrogen/air simulations (chapters 3 and 5) use a detailed chemical mechanism with 9 species and 21 reactions (Mueller et al.[73]). A reduced chemical mechanism with 58 species and 387 reactions (Yoo et al.[74]), derived from the 88 species skeletal mechanism is implemented for n-heptane/air system (chapter 4). Transport properties are handled differently for hydrogen/air and n-heptane/air simulations. For the former, temperature dependent viscosity, and constant Prandtl and Lewis numbers are assumed, whereas for the latter, mixture-averaged transport properties are computed by linking CHEMKIN and TRANSPORT libraries with S3D [75, 76]. Periodic boundary conditions have been imposed in all directions such that ignition occurs at constant volume.

2.4 Mixing Models: Computational framework

A brief discussion of the flamelet modeling approach and transport closure was already given in Section 1.8. Here, we will describe the underlying computational framework and the corresponding mathematical formulation of the mixing models.

The coupling between the CFD code and the combustion code has been shown in Figure 2.1. The CFD code solves the RANS/LES transport equations of the mean and variance of the mixture fraction (Z) and total enthalpy (H)

$$\overline{\rho}\frac{\partial \widetilde{Z}}{\partial t} + \overline{\rho}\widetilde{\mathbf{v}}.\nabla\widetilde{Z} = \nabla.(\overline{\rho}D_t\nabla\widetilde{Z}) \tag{2.20}$$

$$\overline{\rho}\frac{\partial \widetilde{Z''^2}}{\partial t} + \overline{\rho}\widetilde{\mathbf{v}}.\nabla\widetilde{Z''^2} = \nabla.(\overline{\rho}\widetilde{\mathbf{v}''Z''^2}) + 2\overline{\rho}D_t(\nabla\widetilde{Z})^2 - \overline{\rho}\widetilde{\chi_Z} \tag{2.21}$$

In Equation 2.21, $\widetilde{\chi_Z}$, the mean scalar dissipation rate term for Z is unclosed, and

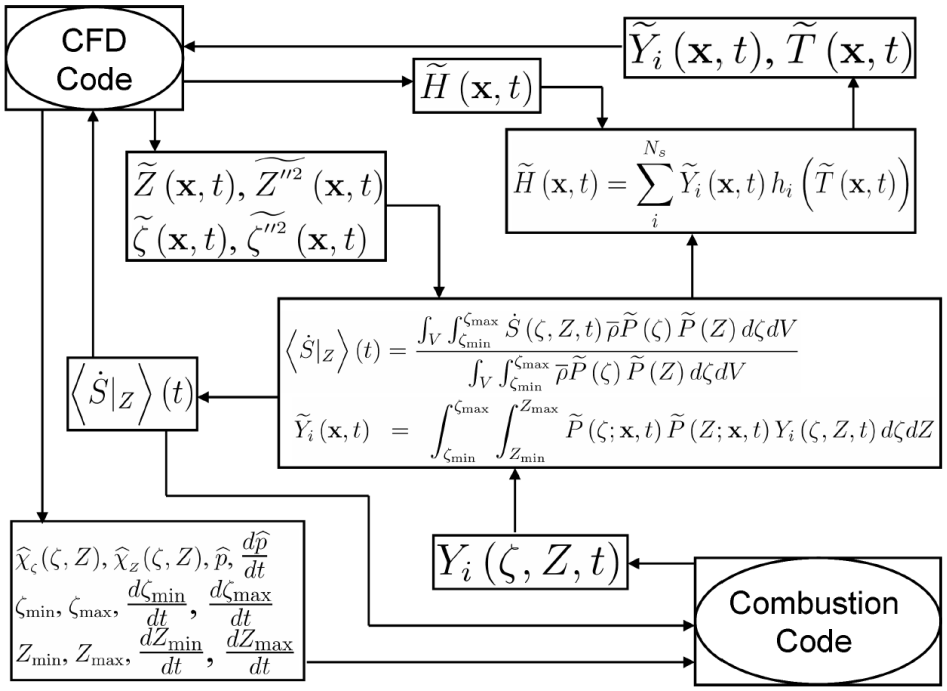

Figure 2.1: Coupling between the CFD and combustion code. Figure from [2]

needs to be modeled. A similar term, $\widetilde{\chi_H}$ will appear in the corresponding transport equation for $\widetilde{H''^2}$. The most commonly used model for mean scalar dissipation rates is based on the assumption of proportionality of the mixing timescale with the turbulence time scale. The constant of proportionality is generally taken as 2.0 [77, 61]. In earlier DNS studies of a single passive scalar mixing, [78], and two passive scalars mixing [79], the constant has also been reported as 2.0 and 3.0, respectively.

$$\widetilde{\chi_Z} = C_Z \frac{\widetilde{\varepsilon}}{\widetilde{\kappa}} \widetilde{Z''^2} \tag{2.22}$$

$$\widetilde{\chi_H} = C_H \frac{\widetilde{\varepsilon}}{\widetilde{\kappa}} \widetilde{H''^2} \tag{2.23}$$

In chapter 5, we will explore the magnitudes of the constant relevant for mixing under LTC conditions.

The modeled values of $\widetilde{\chi_Z}$ and $\widetilde{\chi_H}$ are used as an input to the combustion code which solves the flamelet equations. For 1D Z based flamelet approach, the classical flamelet

equations under the assumption of unity Lewis numbers for all species are given as [61]:

$$\frac{\partial y_i}{\partial t} = \frac{\langle \chi | Z \rangle}{2} \frac{\partial^2 y_i}{\partial Z^2} + \frac{\omega_i}{\rho} \tag{2.24}$$

$\langle \chi | Z \rangle$ is termed as the conditional scalar dissipation rate based on Z. It is generally modeled as [80]:

$$\langle \chi | Z \rangle = \frac{\widetilde{\chi_Z} f(Z)}{\int_0^1 f(Z) P(Z)\, dZ} \tag{2.25}$$

where $f(Z)$ gives the functional dependence of scalar dissipation rate on Z. $f(Z)$ can have many different forms, for example: 1D mixing layer profile [81], infinite 1D mixing layer profile [82], counterflow profile [59] etc. In Chapter 5, we test the infinite 1D mixing layer profile [82], for which $f(Z)$ is modeled as:

$$f(Z) = \frac{(Z/Z_{max})^2 \log\left(Z/Z_{max}\right)}{(Z_{ref}/Z_{max})^2 \log\left(Z_{ref}/Z_{max}\right)} \tag{2.26}$$

$P(Z)$ is the probability density function(PDF) of Z. The commonly used PDF is the Beta PDF, given as:

$$P(Z) = \frac{\Gamma(\alpha+\beta)}{\Gamma(\alpha)(\beta)} Z^{\alpha-1}(1-Z)^{\beta-1} \tag{2.27}$$

where,

$$\begin{aligned} \alpha &= \widetilde{Z}\gamma \\ \beta &= (1-\widetilde{Z})\gamma \\ \gamma &= \frac{\widetilde{Z}(1-\widetilde{Z})}{\widetilde{Z''^2}} - 1 \end{aligned} \tag{2.28}$$

In Chapter 5, the validity of Beta PDF will also be assessed.

In the above discussion, we considered Z based flamelet models. Corresponding

conditional scalar dissipation rate for H will have a similar formulation. For 2D $Z-H$ flamelet models however, an extra cross scalar dissipation rate term $\langle\chi|ZH\rangle$ will appear in the flamelet equations which also needs to be modeled.

CHAPTER III

Identification of Ignition Regimes in LTC Hydrogen/Air Mixtures Using CSP Analysis

LTC engines are considered a viable concept as an alternative to diesel engines in favor of their low NO_x and particulate emissions as well as high efficiencies (Section 1.1). However, a major challenge in their development is to enable accurate control of ignition timing and combustion phasing in order to achieve stable operation over a wide range of load conditions (Section 1.2). One way of providing ignition control is by utilizing temperature and composition stratifications through injection strategies and/or exhaust gas recirculation. The introduced inhomogeneities have an additional benefit of spreading the heat release over a longer duration, thereby alleviating the knock problems (Section 1.3). Inhomogeneities intrinsic to the combustion system may also arise due to incomplete turbulent mixing and heat loss to the cylinder wall. Therefore, description of combustion characteristics in LTC engines needs to account for various auto-ignition modes distinct from simple homogeneous processes.

Auto-ignition of a reactant mixture in the presence of temperature non-uniformity has been systematically studied in the past. Zeldovich [32] identified various ignition regimes depending on the level of temperature gradient, such as the deflagration and the spontaneous ignition regimes. Characterization of ignition regimes in LTC combustion is important in developing appropriate turbulent ignition and combustion

sub-models for full-cycle engine simulations. Some recent studies have provided insights into these issues [83, 52, 84], but the determination of the front propagation speed was based on the assumption of quasi-steady behavior of front propagation. Therefore, the identification of ignition regimes based on the front speed may be become invalid for highly transient auto-ignition events.

Computational singular perturbation (CSP) analysis [39, 40] is an automated diagnostic tool and therefore it alleviates the need for ad hoc assumptions. Introduction to CSP analysis has been given in Section 1.4 and its mathematical formulation is described in Section 2.1

The main objective of this chapter is to use CSP analysis to identify the ignition regimes occurring in LTC engine environments. The proposed diagnostic tools are tested first with reference to model problems of 0D ignition and 1D ignition (laminar flow) under LTC-like combustion environments of lean mixture, and are then applied to 2D ignition (turbulent flow) with thermal inhomogeneities. The 1D and 2D simulation data were taken from the previous study by Bansal and Im [36] using the DNS code named S3D (Section 2.3). The CSP analysis was carried out using a suite of tools developed by Valorani, Najm and Goussis [43]. An S3D/CSP interface (Section 2.2) was developed to compute the Jacobian of the chemical source terms in S3D and other relevant variables, which were used as input for the CSP analysis.

3.1 Homogeneous Ignition: 0D Analysis

As a baseline study to identify spontaneous ignition, we first start with the simplest case of homogeneous auto-ignition in an engine-like compression ignition environment (lean H_2-air mixture with $\phi = 0.1$, initial pressure of 41 atm, and initial temperature of 1100K). Hydrogen is chosen as the fuel for computational cost consideration and because the detailed chemical characteristics are well understood.

An eigenvalue with a positive real part (explosive) is an indicator of explosive

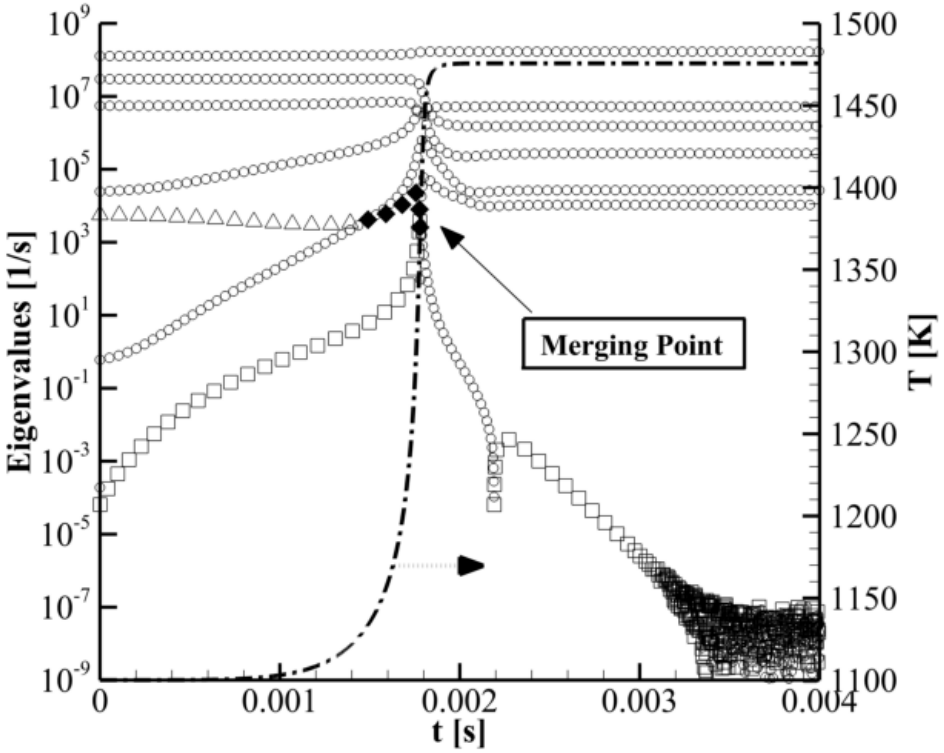

Figure 3.1: Real parts of the eigenvalues for homogeneous ignition. Circles denote magnitude of negative eigenvalues. Positive eigenvalues are denoted by triangles (mode 5), diamonds (mode 6) and squares (mode 7). The negative eigenvalues are plotted in magnitude in order to plot in a log scale.

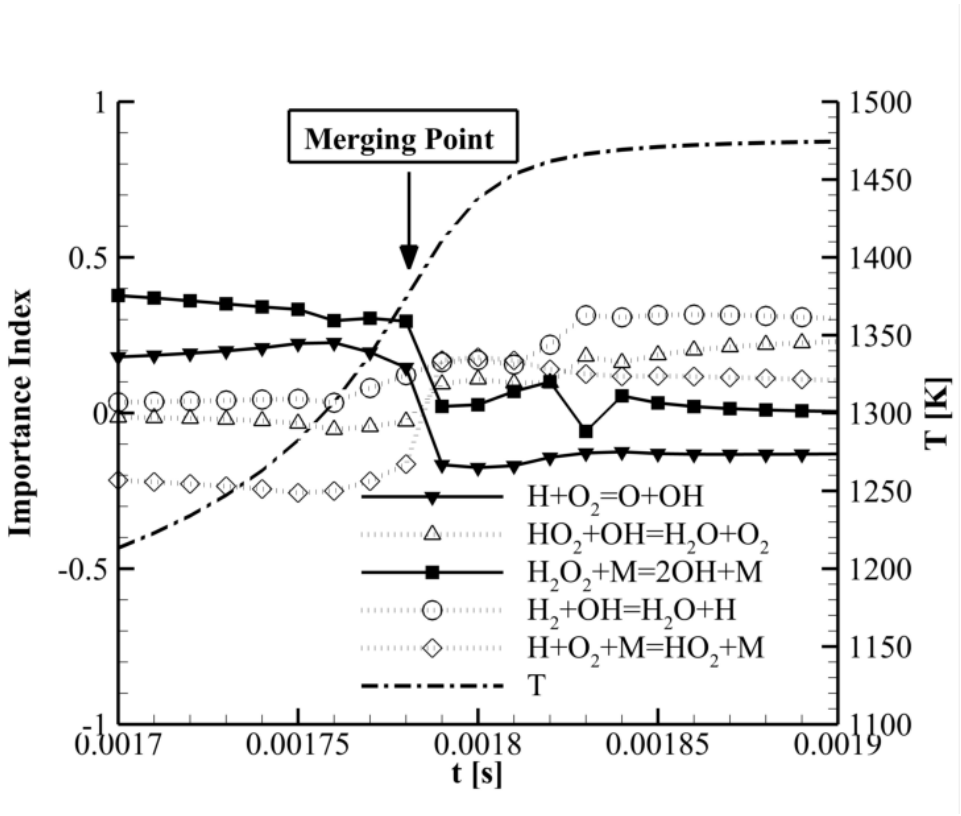

Figure 3.2: Evolution of the importance indices of reactions in the slow dynamics of temperature for homogeneous ignition, near the merging point shown in Figure 3.1

tendencies (chain branching or thermal runaway) in the system. A recent study [46] using CSP analysis identifies an abrupt discontinuity in the maximum explosive eigenvalue of the Jacobian of the chemical source term, as a boundary separating the unburned and burned regions at atmospheric pressure conditions. Diamantis et al. [85] investigated the two-stage ignition of n-heptane at moderately high pressures by analyzing the two branches of explosive eigenvalues. Following the same approach, in the present study both explosive and dissipative (negative real part) eigenvalues are examined in order to characterize the underlying mechanisms responsible for spontaneous ignition for high pressure LTC environments.

Figure 3.1 shows the temporal evolution of the real part of the eigenvalues during the homogeneous ignition event. Note that two branches of explosive eigenvalues merge at t=1.78ms. The upper branch (faster explosive time scale) corresponds to mode 5 (from 0ms to 1.5ms) and mode 6 (from 1.5ms to 1.78ms), whereas the lower branch (slower explosive time scale) corresponds to mode 7 all the way up to 1.78ms. The switch from mode 5 to 6 in the upper branch at t = 1.5ms (transition from open triangle to solid diamond in Fig. 1) is attributed to the shift in the contribution of the key chain-branching reaction $H_2O_2 + M = 2OH + M$. This suggests that the entire upper branch is a manifestation of the above chain branching reaction.

The behavior near the merging point is analyzed in further detail. For $t < 1.78ms$, mode 6 was found to be closely aligned with the direction of the temperature axis in the phase space. At t = 1.78ms, however, mode 7 rotates to become more aligned with the temperature axis. A measure of this alignment is the CSP pointer [43]. To understand the underlying processes behind the modal rotation, the key reactions most important to the slow dynamics of temperature are examined in Figure 4.4. For $t < 1.78ms$, the chain branching reaction $H_2O_2 + M = 2OH + M$ is the major contributor. Inspection of the participation indices indeed confirmed that $H_2O_2+M = 2OH + M$ is the dominant reaction for mode 6. The corresponding eigenvalues have

a larger magnitude, indicating that the process is controlled by the fast explosive branching reactions. At t=1.78ms, the exothermic reactions (dotted line with open circles) led by $H_2 + OH = H_2O + H$ (characterizing mode 7) start to take over and finally become the major contributors. The associated eigenvalues are negative, indicating that the reaction is decaying. The shift in the governing chemistry at 1.78ms is reflected in the phase space as the rotation of modes. Therefore, the merging point of modes 6 and 7 represents the completion of the explosive phase of ignition.

3.2 Spontaneous Ignition versus Deflagration: 1D Analysis

In spatially inhomogeneous systems, ignition occurs as a front propagation. The fundamental mechanism for the propagation, however, is distinguished into two different regimes: in the spontaneous front propagation regime, the ignition front primarily propagates due to sequential reactions in the neighboring mixtures with varying degrees of reactivity, whereas in the deflagration regime the reaction front propagates through the dynamic balance between reaction and diffusive transport. The CSP tool is now applied to model problems as a means to identify distinct ignition regimes. For this purpose, one dimensional constant-volume test cases provided by Bansal and Im [84] are utilized. The baseline mean condition is prescribed with a lean hydrogen-air mixture ($\phi = 0.1$) at a pressure of 41 atm and a mean temperature of 1095K. A sinusoidal variation in the temperature with an amplitude of 10K (Case 1A) and 100K (Case 1B) with wave length of 1mm is superimposed to the baseline condition. Both boundaries are set to be periodic such that compression heating effects are incorporated. In both cases, a homogeneous igniting kernel at the center of the domain develops two fronts propagating in opposite (left and right) directions. The average front speeds for Cases 1A and 1B are approximately 200 and 50cm/s, respectively. The latter value matches well with the expected value of a deflagration front under high pressure conditions, as found and reported in [14]. Hence, the ignition behavior

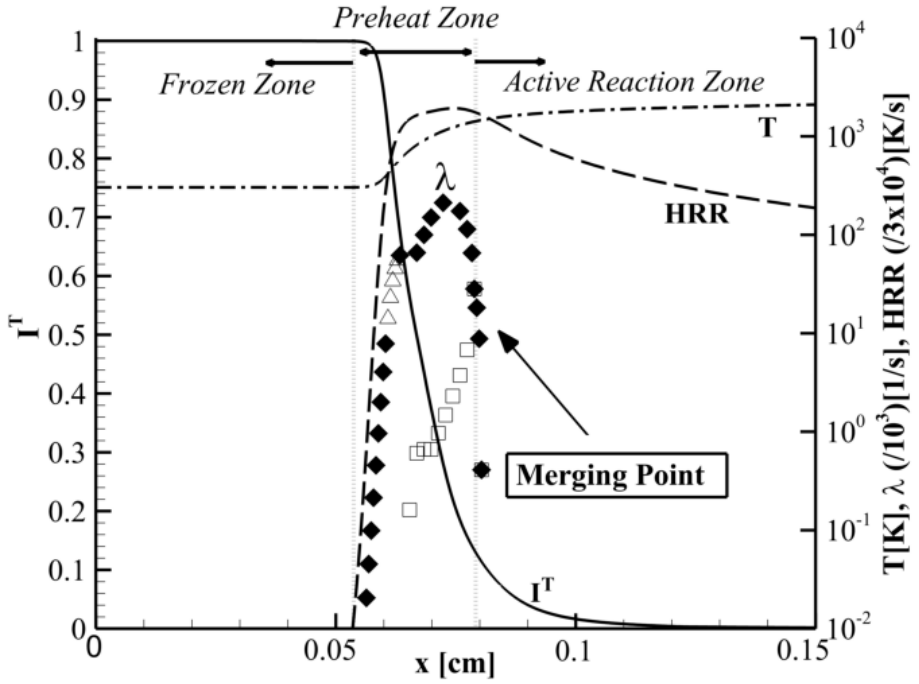

Figure 3.3: Eigenvalues and I^T in a freely propagating laminar premixed flame with a stoichiometric H_2-air mixture under STP. Explosive eigenvalues are denoted by triangles (mode 5), diamonds (mode 6) and squares (mode 7).

of Cases 1A and 1B is expected to be in the spontaneous ignition and deflagration regime, respectively.

The ignition proceeds at constant volume and high pressure, such that the upstream end-gas may autoignite due to compression heating. Therefore, although not shown here, the eigenvalue plots for both cases appear similar to Fig. 1, with the time axis replaced by the spatial axis. That is, the eigenvalues change from the explosive mode in the unburned region to the dissipative mode in the burned region. However, the qualitative pattern is similar between the two cases, such that both cases may be ambiguously identified as spontaneous ignition fronts. Therefore, the merging point diagnostics is not able to provide a rigorous identification of ignition regimes.

As a reference, the CSP analysis was also performed with a steady freely-propagating flame and the results are shown in Figure 3.3. Temperature and heat release rate pro-

files are also overlaid (in log scale). The region to the right of the merging point is the active reaction zone, whereas to its left is the preheat zone. Furthermore, since explosive eigenvalues disappear after a certain distance to further left of the merging point, this far upstream region (with no explosive eigenvalues, hence no explosive tendencies) can be described as chemically frozen. On the contrary, for a spontaneous ignition front, since the mixture ahead of the front is not frozen (a spontaneous ignition front propagates by virtue of reactions), explosive eigenvalues are found throughout the region ahead of the front. Hence, the presence of a steep jump in positive eigenvalues (in addition to the one at the merging point) upstream of the active reaction zone could be used to differentiate between a freely propagating laminar premixed flame and a spontaneous ignition front. Such a detection technique has recently been reported in [46]. However, such a criterion is not easily applicable under multi-dimensional turbulent HCCI-like conditions where an unambiguous identification of upstream frozen zone becomes difficult. Furthermore, Case 1B was found to have the characteristics of a deflagration front [84], such that a proper diagnostic analysis is required in order to identify it accordingly. Therefore, an alternative diagnostic tool is proposed in the following.

3.2.1 Exhausted Mode Analysis

To provide better insights into the nature of front propagation, a more detailed analysis is given for the frozen, preheat, and active reaction zones by establishing a relative comparison of the transport (diffusion and convection) and chemistry.

To identify the zones of interest, the number of fast exhausted modes, M, is determined in order to partition the time scales into fast exhausted and slow active scales (based on user-specified relative and absolute error thresholds) at each spatio-temporal location [43]. If the problem exhibits a wide slow/fast time-scale gap, the value of M is insensitive to the user-specified error threshold. This was found to be

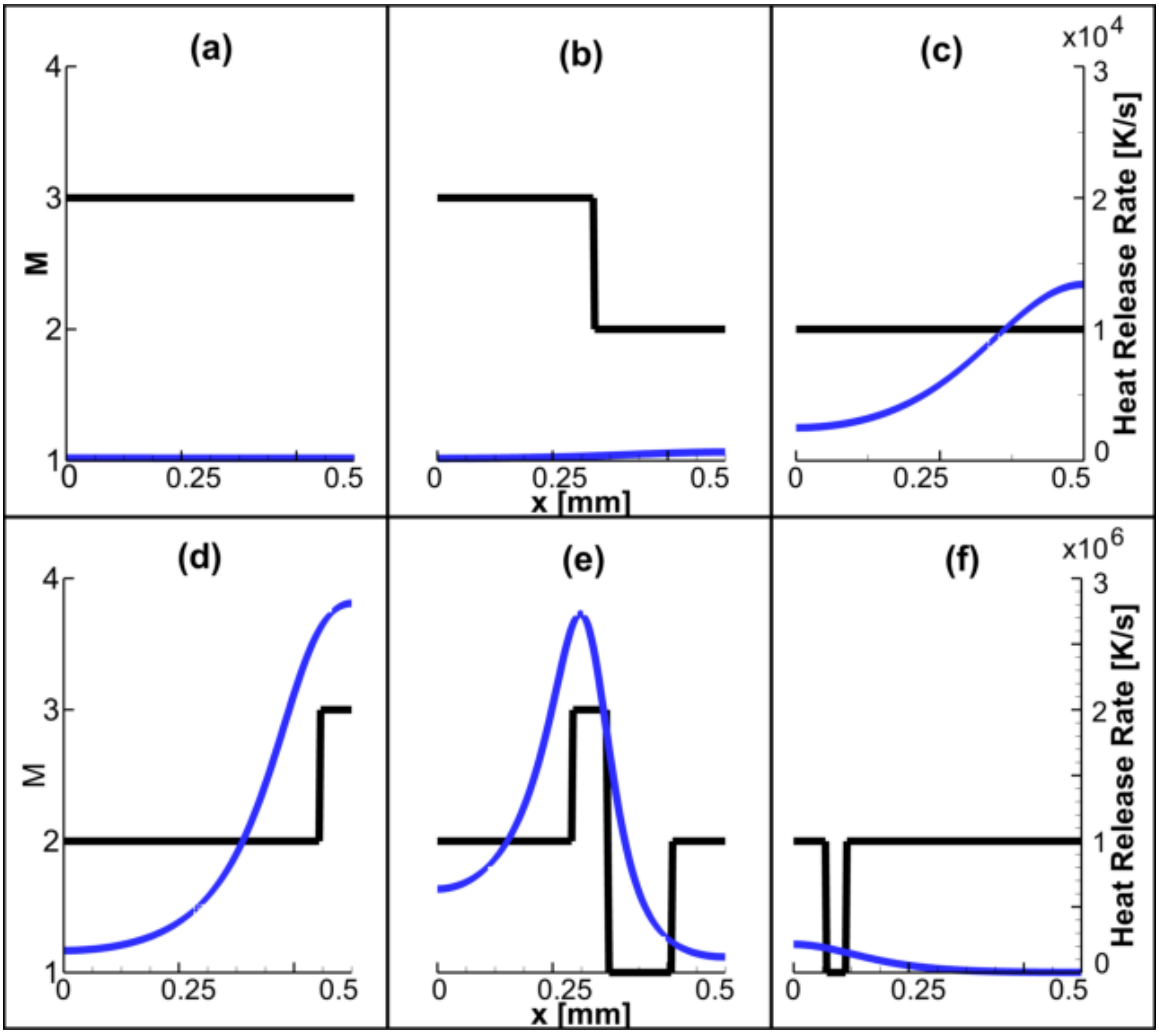

Figure 3.4: M-profile (black) overlaid on heat release rate (blue) for Case 1A: 0ms (b) 0.3ms (c) 0.8ms (d) 1.6ms (e) 1.7ms (f) 1.9ms

the case for the 1-D test cases. The relative error threshold was taken to be 10^{-3}. The value of the absolute error threshold depends on the minimum species concentration in the mixture [43]. After a careful comparison of different test cases, an absolute error threshold of 10^{-7} was used for the present analysis.

The M profile provides useful information about the flow characterization based on the decoupling of exhausted and active modes. Figure 3.4 show the M profile overlaid with the heat release rate Cases 1A. Because of the symmetry in the front propagation, only the left half of the domain is shown. Initially (Figure 3.4a), there is negligible heat release and the mixture is frozen with $M = 3$ everywhere. As the ignition proceeds, chemical reactions start to take place, and M decreases to 2 in the active reaction zone (Figures 3.4a to 3.4c). As the ignition front further develops, however, an $M = 3$ zone reappears in the large heat release zone (Figure 3.4d). Note that this downstream M= 3 zone should be distinct from the upstream $M = 3$ frozen zone. The physical processes responsible for the emergence of this downstream $M =$ 3 zone are explained in detail later in this section. Further downstream, the M value dips down to 1 and then recovers 2 (Figures 3.4e and 3.4f). In summary, near the front region the sequence of $M =$ 2-3-1-2 (from upstream to downstream) appears to be typical for the hydrogen-air mixture under the conditions considered.

The M =1 region identified in the downstream region is the active reaction zone where most of the fast key reactive processes occur. M increases to 2 further downstream where the mixture reaches a near equilibrium condition. For hydrocarbon fuels, the downstream near-equilibrium region typically has a number of exhausted modes much larger than that in the upstream unburned zone [43]. Such was not the case in the present study due in part to the simplicity of the hydrogen chemistry, and also in part to the short domain length. By increasing the domain length by a factor of 5, a near-equilibrium region with 4 exhausted modes was observed.

The emergence of the $M = 3$ region ahead of the active reaction zone has not been

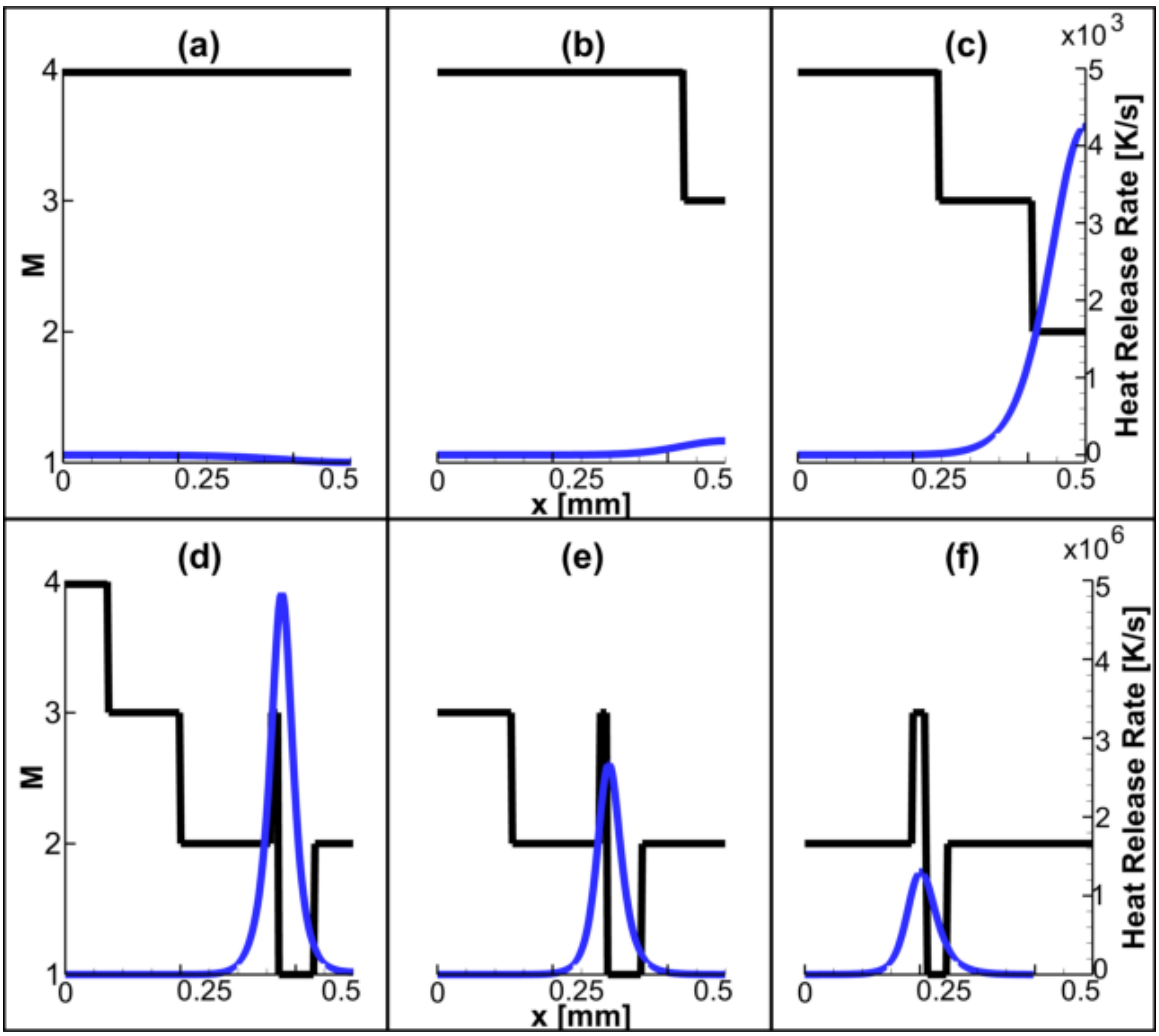

Figure 3.5: M-profile (black) overlaid on heat release rate (blue) for Case 1B: (a) 0ms (b) 0.02ms (c) 0.1ms (d) 0.4ms (e) 0.8ms (f) 1.0ms

observed in previous studies [43]. This region is marked by the merging of timescales τ_3 and τ_4, implying that the eigenvalues corresponding to modes 3 and 4 become complex conjugates at that point. This indicates that the dynamics over the plane defined by the complex pair is associated to a single dissipative/explosive time scale defined by the real part of the complex pair. After examining the participation indices of the driving mode, it was found that the conversion of HO_2 into H_2O_2 through $HO_2 + HO_2 = H_2O_2 + O_2$ was primarily responsible for this behavior, thereby increasing H_2O_2 concentration downstream which finally breaks down into OH radicals in the reaction zone to yield $M = 1$.

Figure 3.5 shows similar plots for Case 1B, in which the M = 2-3-1-2 pattern is again observed across the reaction front. The only difference is the $M = 4$ region far upstream, which is attributed to the chemical inactivity as a result of the lower temperature because of the way the initial temperature field is prescribed. Nevertheless, the general pattern of the M variation across the reactive front is clearly demonstrated. The goal is to investigate the near-upstream region of the reaction front. To this end, the $M = 3$ region in the vicinity of the reaction front is found to be a useful diagnostic signature to locate the upstream direction of the front, as otherwise the primary reaction zone ($M = 1$) would be surrounded by the $M = 2$ regions in both directions. As will be discussed next, the characteristics in the $M = 2$ zone in the upstream side are found to be important in determining the ignition regime.

3.2.2 The Importance Index Criterion

After identification of the zone of interest, the relative magnitudes of transport and reaction are compared in the region ahead of the fronts. To this end, we introduce the importance index, I^T, defined as:

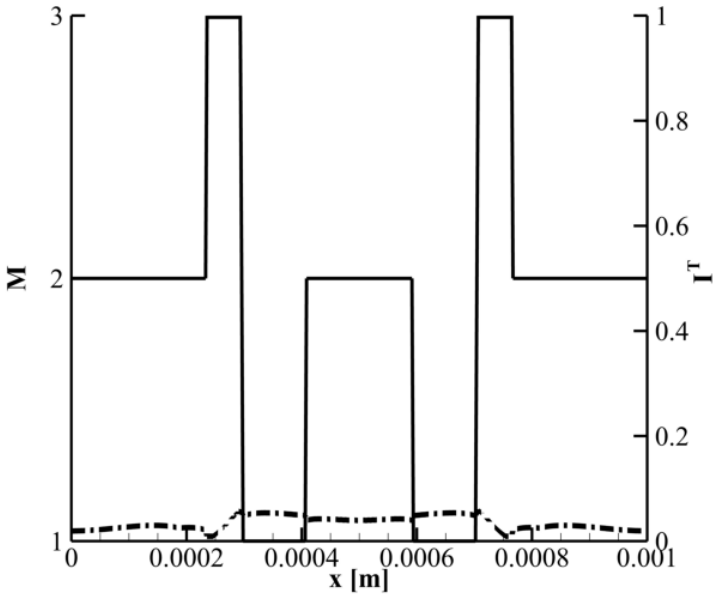

(a)

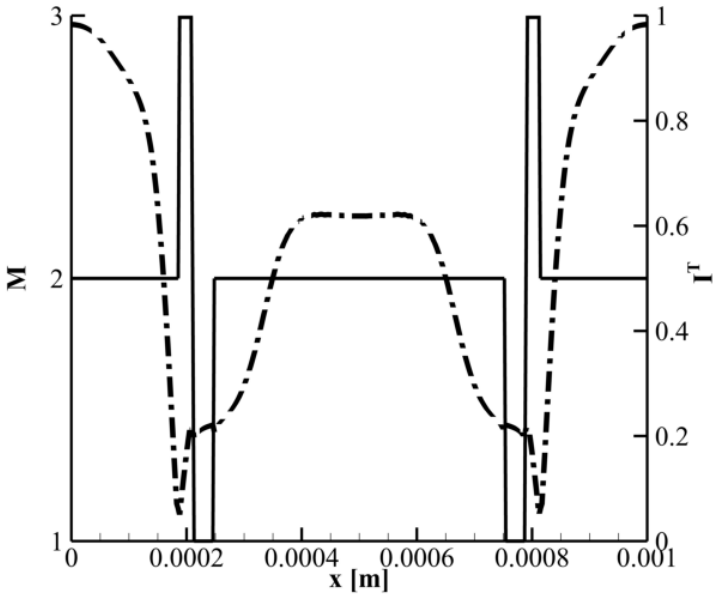

(b)

Figure 3.6: Spatial distribution of Index I^T (dash-dot) for (a) Case 1A at 1.7ms (b) Case 1B at 1.0ms

$$\boxed{I^T = |(I^T_{T-diffusion})_{slow}| + |(I^T_{T-convection})_{slow}|} \tag{3.1}$$

where $|(I^T_{T-diffusion})_{slow}|$ and $|(I^T_{T-convection})_{slow}|$ are the importance indices of temperature diffusion and convection, respectively, to the slow dynamics of the temperature variable. In other words, these two terms represent the importance of diffusive and convective transport of heat (sensible enthalpy) on the slow dynamics of the temperature field. By definition, I^T ranges from 0 to 1. I^T approaching zero implies that the ignition front propagation is primarily driven by chemical explosion in the upstream, while I^T being close to unity implies that the reaction zone propagates upstream by virtue of transport (diffusion and convection), that is, as a deflagration front.

Figure 3.3 shows the variation of I^T for a freely propagating laminar premixed flame. As expected, I^T is unity in the frozen zone and falls down in the preheat zone toward the active reaction zone. Therefore, the importance index adequately detects the deflagration characteristics that heat transport is the dominant process in the upstream preheat zone.

Following this observation, the distribution of the importance index for the two ignition fronts in Cases 1A and 1B, after the front structure is well established, is shown in Figure 3.6. Despite the similar behavior in the reactive eigenvalues, the two cases reveal distinct characteristics in the upstream $M = 2$ region; while Case 1A is clearly identified as a reaction-driven spontaneous ignition front, the importance index distribution for Case 1B appears much closer to a deflagration front in that I^T reaches a larger value within the bulk of the upstream $M = 2$ region. Therefore, the proposed importance index diagnostics properly captures the characteristics of the ignition front and is suggested as a rational tool to identify the ignition regime.

Figure 3.6 shows that a higher I^T value appears in the downstream $M = 2$ region for Case 1B as compared to Case 1A. This implies that the near-equilibrium region is

also transport-dominant on the slow time scales in a deflagration front, since the fast kinetics is in quasi-equilibrium. For a spontaneous ignition front, however, reactions are still active on the slow time scales. This information can be used to predict deflagration-to-spontaneous-ignition transition, as would occur in the end gas near the cylinder wall due to compression heating; during the transition, the region ahead of the front exhibits a low value of I^T, while the region behind the front remains at a high value of I^T. Although not shown here, such a transition event was identified for Case 1B as the fronts approach the boundaries.

Note that the importance index originates from an eigenvalue analysis of the system dynamics, and as such it is a valid metric of the relative importance between the reaction and transport processes, irrespective of the unsteadiness of the problem. Therefore, the present analysis is believed to be valid for a wider range of combustion problems associated with highly transient phenomena, in contrast to other diagnostic methods relying on the determination in the physical space of the front propagation speed under the quasi-steady approximation. Furthermore, the importance index ranges from 0 to 1, thus providing a quantitative measure of the relative contributions of the transport process.

3.3 Ignition Regimes in Turbulent Mixture: 2D Analysis

We now analyze the more complicated two-dimensional constant volume turbulent auto-ignition flow with temperature inhomogeneities. The DNS data by Bansal and Im [84] for Case 2A were used for analysis. In particular, the results from the solution field at 50 percent of the total heat release are presented here. As before, the relative and absolute tolerance values of 10^{-3} and 10^{-7} were used for the CSP analysis.

As discussed in the 1D analysis, the M distribution serves as a useful diagnostic tool to depict the reaction front locations and its direction of propagation. Figure 3.7 shows the isocontours of M which varies from 1 to 3. The active reaction region is

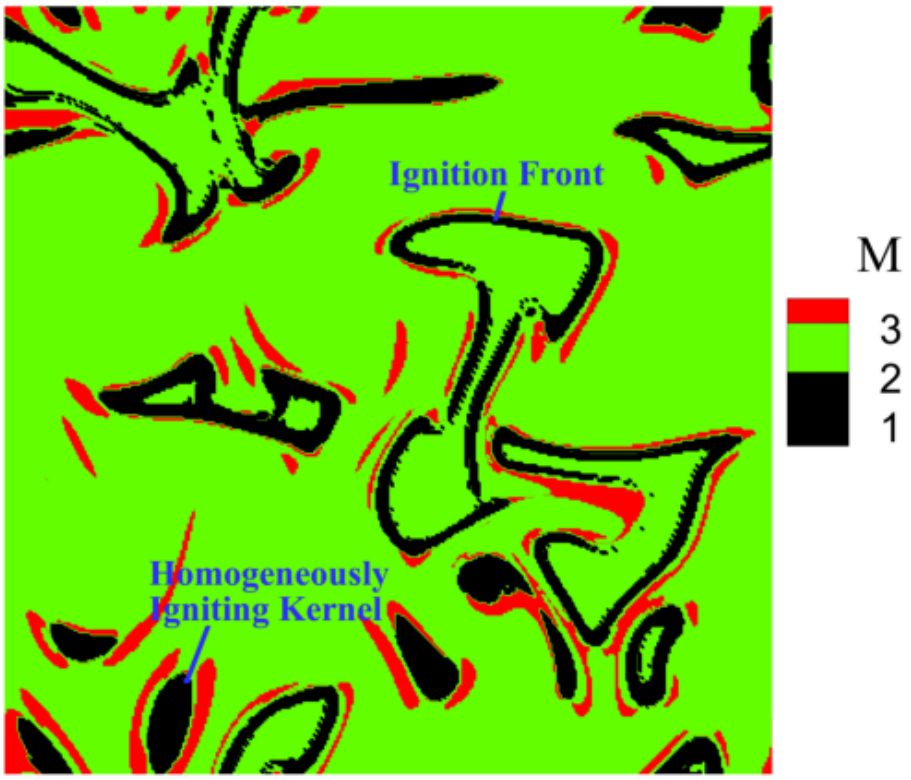

Figure 3.7: Isocontours of the number of exhausted modes during the ignition of hydrogen-air mixture in the presence of turbulent velocity and temperature distribution. Black regions are the highly active reaction zones. Red layers indicate the direction of propagation.

identified by $M = 1$ (black) and the $M = 2$ regions are found in both upstream fresh reactants and downstream products. The $M = 3$ layers (red) adjacent to the reaction zone clearly indicate the direction of the reaction front propagation. There exists some $M = 3$ layers which are not adjacent to $M = 1$ regions. These correspond to regions where a reaction front is about to form (see figure 3.4d). At the top left of the domain, some thin black layers are not surrounded by red layers. They correspond to the case shown in figure 3.4f for which the reaction front is significantly weakened to a near-extinction condition. Some black regions surrounded by the red layers but not followed by an $M = 2$ equilibrium region (shown in the lower part of the domain) are identified as homogeneously igniting kernels as indicated.

Based on the M-distribution diagnostics, the importance index provides the key information to characterize the ignition regime. As before, we focus on the $M = 2$ regions close to the upstream of the active reaction zone. Figure 3.8 shows the isocontours of I^T superimposed over the active reaction regions (black). Red layers upstream of $M = 1$ region imply that transport is dominant in that region and hence these are identified as deflagration fronts. On the other hand, the blue layers ahead of the $M = 1$ regions indicate that these are spontaneous ignition fronts. Note that, even within the continuously connected front (such as the closed isocontour denoted as C), mixed ignition regimes are observed; parts of the same continuous front propagate in either the deflagration or spontaneous ignition regime.

The $M = 1$ regions without the near-equilibrium downstream zone is classified as homogeneously igniting kernels. These kernels are likely to grow into fronts. Whether the kernels will become spontaneous ignition front or deflagration can also be predicted by the importance index ahead of them.

In summary, for the 2D turbulent ignition condition considered herein, the ignition regimes are categorized into four types, as denoted in Figure 3.8

- FD: ignition front propagation in the deflagration mode

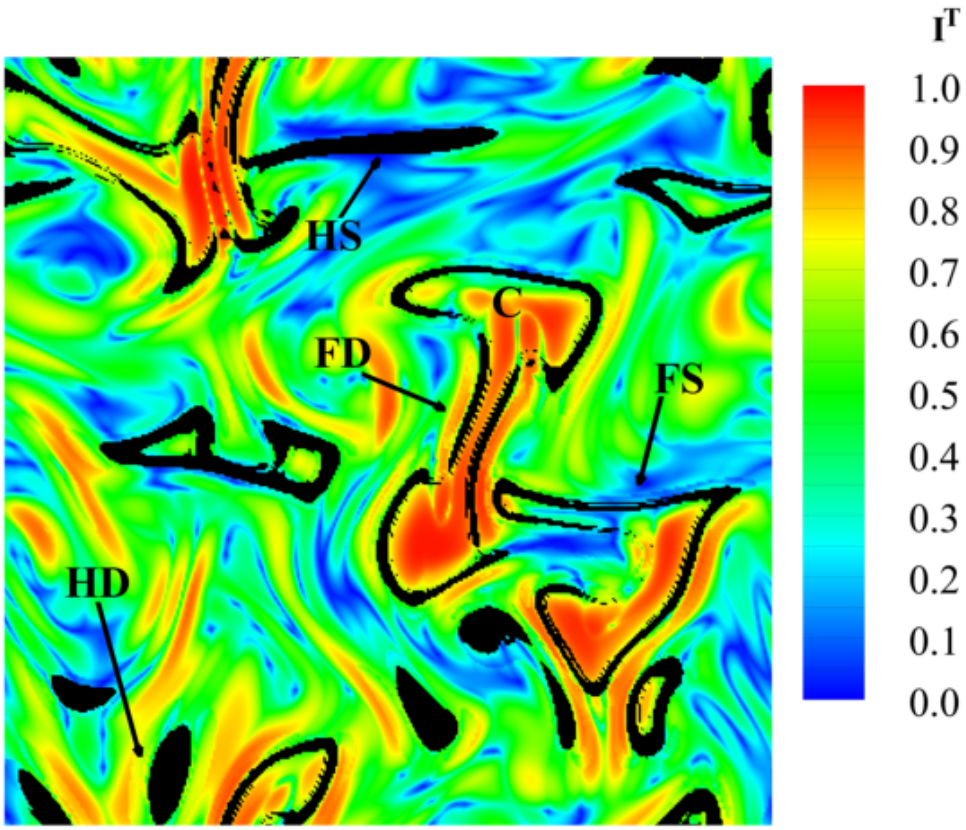

Figure 3.8: Isocontours of I^T for the data field shown in Figure 3.7. $M = 1$ region is overlaid in black.

- FS: ignition front propagating in the spontaneous ignition mode
- HD: homogeneous ignition kernel that will subsequently grow into deflagration
- HS: homogeneous ignition kernel that will subsequently grow into spontaneous ignition front

The results show that, under the test simulation condition, both deflagration and spontaneous ignition regimes occur in LTC-like combustion environment. The proposed criterion combining information from the M and the I^T fields provides a good measure to characterize both kinds of ignition modes.

3.4 Concluding Remarks

In this chapter, a novel strategy based on CSP analysis was developed to identify various ignition regimes. The strategy has mainly two components:

- **Number of exhausted modes** (M): Exhausted time-scales are identified based on the relative and absolute error thresholds. The number of exhausted modes, denoted by M, show distinct values in the active reaction zone, the downstream zone and the near-equilibrium product zone. For hydrogen/air mixtures under LTC conditions considered herein, the front structure was identified by the pattern of M = 2-3-2-1 (from upstream to downstream) near the propagating front. The presence of $M = 3$ layer was found to be a useful indicator to identify the direction of the front propagation.
- **Importance Index** (I^T): Using the M diagnostics, the relative dominance between transport and chemistry in the upstream zone is investigated by defining the importance index based on the slow dynamics of temperature. In the $M = 2$ region ahead of the active reaction zone, $I^T = 1$ implies pure deflagration, whereas $I^T = 0$ implies pure spontaneous ignition. The magnitude of I^T

thus determines the quantitative measure of the dominant characteristics of the ignition front.

The new criterion serves as a generalized diagnostic tool to characterize the ignition process under steady and unsteady conditions without relying on intuitive decision. This diagnostic tool, applied to 2-D constant volume turbulent ignition with temperature inhomogeneities, properly captured regions of interest and identified the ignition regimes under hostile condition of multi-dimensional, turbulent, multi-mode combustion events. In the next chapter, we will use this tool to study auto-ignition characteristics of multi-stage n-heptane/air chemistry.

CHAPTER IV

Analysis of n-Heptane Auto-Ignition Characteristics Using CSP

It is important to gain fundamental understanding of different auto-ignition characteristics of n-heptane/air mixtures as a result of various physical parameters in order to develop a predictive combustion model applicable to LTC engines for a wide range of operating conditions.

Following the pioneering work by Zeldovich [32], who established a theoretical framework to classify various ignition regimes depending on the level of temperature gradient, a number of studies have followed to develop a rational way to identify distinct ignition regimes. A large number of these studies considered a hydrogen-air mixture in favor of its simplicity in chemistry and temperature fluctuations only [33, 34, 52, 35], and various criteria for ignition regime identifications have been proposed. The study has been extended to consider both temperature and mixture stratifications [36] in which a more comprehensive criterion based on the radical Damkhler number was proposed. From a more practical standpoint towards reduced order full-cycle engine simulations, several studies considered a one-dimensional configuration with an iso-octane mixture, and provided simpler criteria for ignition regime identification based on global physical parameters [83, 37, 38].

The previous chapter demonstrated that the number of exhausted modes (M)

computed as a local variable serves as a convenient marker to detect the onset of ignition and, in multi-dimensional cases, the formation of ignition front and its direction of propagation. Moreover, given that the slow/fast importance index of the k^{th} process for the i^{th} species is the non-dimensional measure of its relative contribution to the slow/fast dynamics of that species, the quantity I^T was defined to measure the importance of the transport processes on the slow dynamics of temperature. It was found that I^T serves as a good metric to identify the ignition regime of various segments of the ignition fronts identified by the M profiles. Therefore, the CSP-based ignition diagnostics serves not only as a convenient automated tool, but also as a robust and generalized criterion applicable to highly transient conditions.

The present chapter extends the work of Chapter 3 by considering the detailed fuel chemistry of n-heptane, which at typical engine conditions exhibits the two-stage ignition behavior due to the negative temperature coefficient (NTC) chemistry. One of the key fundamental questions of the study is regarding how the NTC behavior affects the relative importance among different ignition regimes at given parametric conditions, such as temperature, pressure, and the level of temperature/composition fluctuations. Previous studies conducted in-depth analysis of auto-ignition of n-heptane mixture at engine conditions, but they considered temperature inhomogeneities only, and were rather case-specific [86] or focused on the changes in the ignition delay [74]. A CSP analysis of n-heptane ignition was also conducted [44], but with a limited scope of reaction pathway analysis.

Therefore, a further parametric study is needed in order to answer the questions raised herein. In the following, auto-ignition of n-heptane/air mixtures at various parametric conditions is simulated and the ignition regimes are investigated by the CSP analysis. In particular, two different temperature conditions are considered in order to represent NTC and non-NTC ignition behavior, and for each condition the effects of various parameters on the prominence of different ignition regimes are

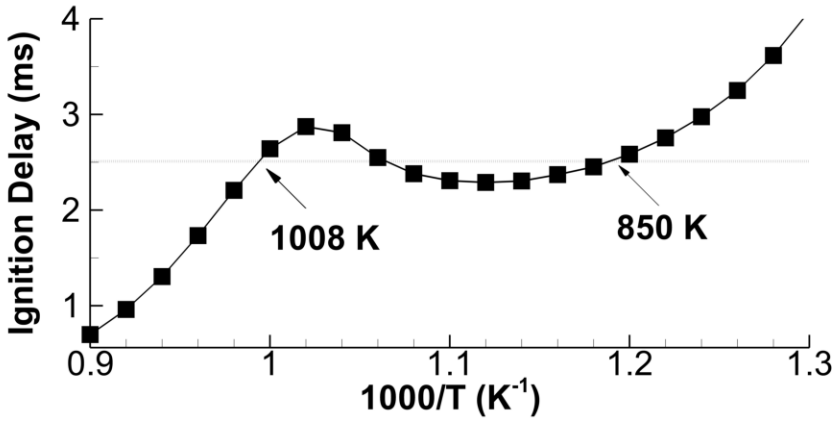

Figure 4.1: Homogeneous ignition delay as a function of temperature, at $P_{initial}$ = 40atm, $\phi_{initial} = 0.3$

studied.

4.1 Numerical Method and Initial Conditions

Test cases were simulated using S3D (Section 2.3). Periodic boundary conditions were employed at all the boundaries to simulate the constant volume ignition process. For the gas-phase chemistry, we adopted a 58 species, 387 step reduced n-heptane air reaction mechanism derived from the 88 species skeletal mechanism using directed relation graph, quasi-steady reduction, and isomer lumping [74]. The CSP analysis was carried out using a suite of tools developed by Valorani and coworkers [43, 64]. While the reduced mechanism was used in favor of its computational efficiency for extensive parametric studies, it contains 30 steady-state or lumped species variables that are not compatible with the CSP analysis. Therefore, as a pre-processing, the entire 88 species variables were retrieved from the solution data at a given time, based on which the chemical Jacobian was computed for the subsequent CSP analysis (so that, including temperature, a total of 89 modes exist). This approach inherently assumes that the steady-state approximation for the 30 species remains valid throughout the simulation. For a few representative cases, the results were validated against those

generated from the 88 species skeletal mechanism, and it was confirmed that all of the steady-state species remain exhausted and thus do not play a role as active modes in the CSP analysis.

The thermodynamic conditions for the initial field were close to those used in Yoo et al. [74]. The initial pressure at 40atm and the mean equivalence ratio (ϕ) at 0.3 were used, which correspond to the high load limit in LTC engines [21, 87]. Figure 4.1 shows the ignition delay versus temperature for the given pressure and equivalence ratio, from which two different initial temperatures, 1008 K and 850 K, were chosen in order to represent both NTC and non-NTC regimes, respectively. Note that the two temperature conditions yield comparable ignition delay of 2.5ms, which is relevant for the LTC engine operation. These conditions were used for the reference homogeneous ignition study.

4.1.1 Initial conditions for 1D ignition

Using the initial conditions in the homogeneous cases as the mean values, one-dimensional simulations were next conducted to investigate the effect of spatial temperature and composition inhomogeneities. For the initial conditions of $\phi = 0.3$ and p = 40 atm, a sinusoidal initial temperature profile with the maximum at the center of the domain was imposed with the RMS of the temperature fluctuations, $T_{rms} = 100$K, with respect to the mean initial temperature at 1008 K and 850 K. While typical LTC engines are likely to have T_{rms} of the order of 10-20K [88], it may reach up to 100 K under direct injection or delayed fuel injection conditions. The present study was intended to create a wider range of conditions to represent different ignition regimes, such that a large value of temperature fluctuation is considered. In the subsequent section, additional effects of composition stratification are investigated by imposing a sinusoidal equivalence ratio profile with respect to the mean value of $\phi = 0.3$, with its RMS fluctuations at $\phi_{rms} = 0.05$, either positively (in phase) or negatively (out of

phase) correlated with the temperature profile. The computational domain size was 1.24mm, for which 500 grid points was sufficient to resolve all physical scales.

4.1.2 Initial conditions for 2D turbulent ignition

Next, DNS studies of 2D turbulent auto-ignition were performed. The computational domain was 3.2mm x 3.2mm. A 640 x 640 grid was used, such that the spatial resolution was 5μm, which was enough to resolve the physical scales for the level of stratifications considered. Passot-Pouquet turbulence spectrum [89], wich has been used in a number of other DNS studies as well [34, 52, 36, 74] was used to initialize turbulence in the system.

Turbulence parameters were chosen such that the turbulence time scale (τ_t) was comparable to the homogeneous ignition delay (τ_0). Most energetic turbulent length scale, l_e was taken as 1.24mm, turbulence velocity fluctuation, u' was 0.5m/s. The most energetic length scale for temperature fluctuation was taken as 1.0mm. The initial temperature fluctuation T' was taken as 20K. As before, an equivalence ratio, ϕ of 0.3 was used.

To facilitate distinction of NTC and non-NTC ignition, two test cases based on different mean temperatures were considered. For case 1, T_{mean} = 1008K, such that it favors non-NTC ignition. For case 2, T_{mean} = 850K, such that it favors NTC ignition.

4.2 Homogeneous Ignition

As a baseline study, homogeneous ignition behavior is examined for both NTC and non-NTC conditions. A primary objective of this investigation is to understand key chemical processes at various stages during ignition. While the reaction pathways for n-heptane/air chemistry have been studied ([90, 91, 92, 93, 94, 95], in this study the CSP analysis is utilized as an automated diagnostics to identify the exhausted modes (M) and as an in-depth mode make-up analysis to understand the key reaction

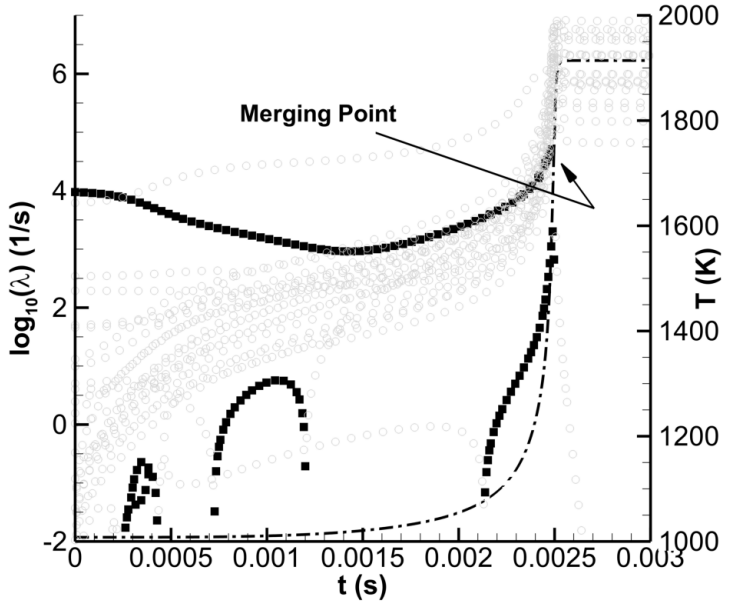

(a)

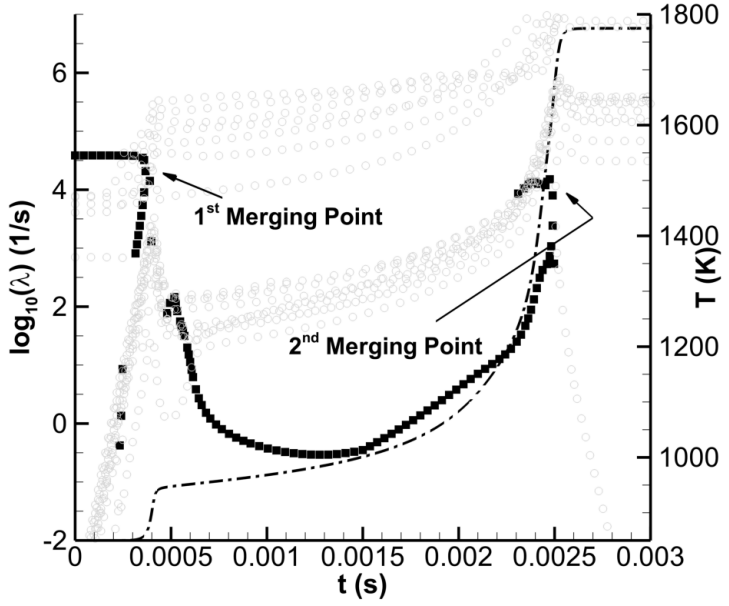

(b)

Figure 4.2: Temporal evolution of the real parts of the eigenvalues for homogeneous ignition, $P_{initial}$ = 40atm, $\phi_{initial}$ = 0.3: (a) non-NTC and (b) NTC conditions. Dark/grey symbols denote the positive/negative eigenvalues, respectively. The negative eigenvalues are plotted in magnitude in order to plot on the log scale.

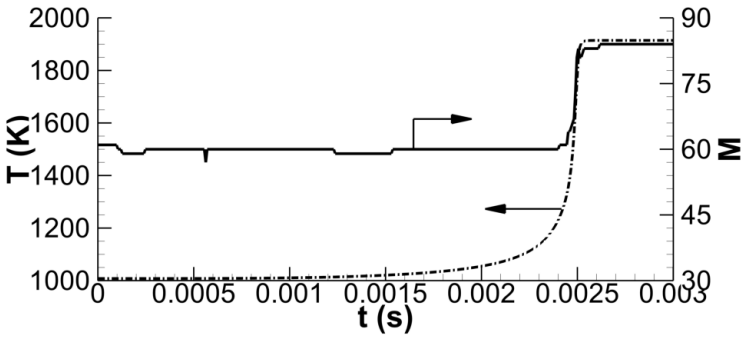

(a)

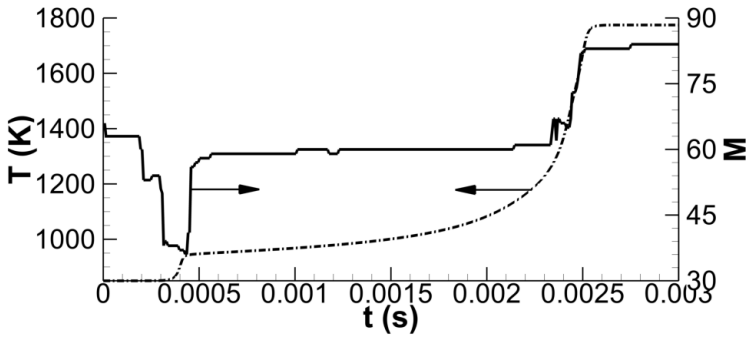

(b)

Figure 4.3: M (solid) and temperature (dash-dot) profiles for homogeneous ignition, $P_{initial} = 40$atm, $\phi_{initial} = 0.3$: (a) non-NTC and (b) NTC conditions.

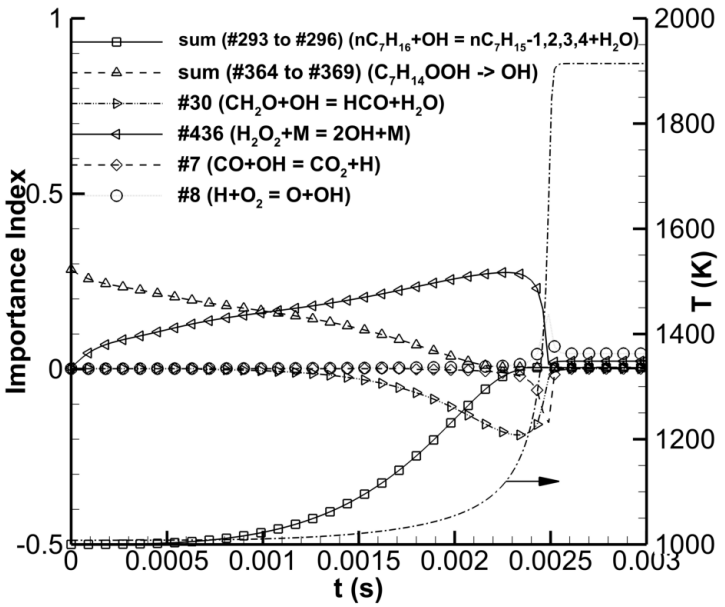

(a)

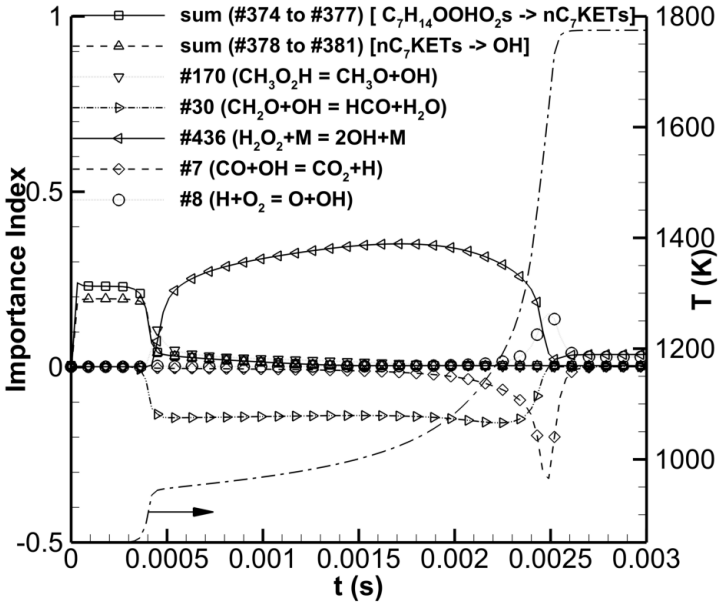

(b)

Figure 4.4: Temporal evolution of the importance index to the dynamics of *OH* for homogeneous ignition, $P_{initial} = 40$atm, $\phi_{initial} = 0.3$: (a) non-NTC and (b) NTC conditions.

steps responsible for important active modes. As discussed in Chapter 3, appropriate values of the error thresholds need to be determined so as to choose M such that the largest gap exists between modes M and $M+1$. After careful examination of all time scales at various conditions, the relative and absolute error thresholds of $\varepsilon_r = 10^{-3}$ and $\varepsilon_a = 10^{-6}$, respectively, were found to yield best results and have been used in this study.

We first examine the behavior of chemical modes near ignition. Previous studies [47, 85] found that explosive modes (positive eigenvalues) emerge during the ignition period, leading to an abrupt discontinuity [47] or merging of two branches [96, 85]. Figure 4.2 shows the evolution of explosive modes shown as dark symbols for both non-NTC and NTC cases. It is clearly seen that the merging point behavior is observed for all ignition conditions, including the 1^{st} and 2^{nd} stage ignitions for the NTC case, demonstrating that the merging of different explosive modes is a universal feature of ignition. Key reaction steps associated with various ignition stages will be discussed later.

Figure 4.3 shows the evolution of temperature and the corresponding number of exhausted modes (M) for (a) non-NTC (1008 K) and (b) NTC (850 K) conditions. For the non-NTC, single-stage ignition case (a), approximately 60 modes are exhausted throughout the induction period. As the ignition proceeds, the M profile shows an abrupt increase to reach the near-equilibrium condition with $M = 84$. For the NTC regime case, on the other hand, a slightly larger number of modes ($M = 65$) were exhausted at the beginning, but the M profile exhibits a sudden dip (down to $M = 37$) near the first stage ignition at 0.4 ms. After the completion of the first stage ignition, M increases up to 60 and retains a similar behavior as shown in the non-NTC case. Therefore, the M profile clearly indicates that there is a transition in the key chemical processes during the first stage ignition at intermediate temperatures. The CSP analysis provides a convenient tool to investigate this issue.

The slow importance index of the k$^{\text{th}}$ reaction step for the slow dynamics of the i$^{\text{th}}$ species is defined in equation 2.15 as:

$$(\mathbf{I}_k^i) = \frac{\sum_{s=M+1}^{N-N_c} a_s^i(\mathbf{b}^s.\mathbf{S}_k)R^k}{\sum_{j=1}^{N_p}\left|\sum_{s=M+1}^{N-N_c} a_s^i(\mathbf{b}^s.\mathbf{S}_j)R^j\right|} \tag{4.1}$$

The rate-controlling reaction processes at a given time of interest can be examined by their importance index for the slow dynamics of the CSP radical (species most parallel to the direction of a particular mode [43]) corresponding to the fastest active mode $(M+1)$. The importance index therefore delineates the primary reaction processes responsible for the key dynamics during ignition.

The analysis is conducted for the NTC case (850 K) near the first stage ignition (at 0.42ms), when M drops down to 37. At this time, the key radical that controls the 38$^{\text{th}}$ (fastest active) mode is nC_7KET42, and the associated reaction steps and the corresponding importance index values are:

$$C_7H_{14}OOH4 - 2O_2 \rightarrow nC_7KET42 + OH, \qquad I_k^i = 0.133 \quad (\#377)$$

$$nC_7KET42 \rightarrow CH_3CHO + nC_3H_7COCH_2 + OH, \qquad I_k^i = -0.158 \quad (\#381)$$

which implies that reaction #377 contributes to the production of nC_7KET42 by 13.3%, and #381 contributes to its consumption by 15.8%. Both reactions produce OH radicals, hence serve as the key chemical reactions leading to the first stage of ignition.

The same analysis is conducted for the same NTC case near the second stage ignition. At four different times during the 2$^{\text{nd}}$ stage ignition event, at 2.30, 2.34,

2.37, and 2.40 ms, respectively, the key reaction steps were found to be:

$$At\ 2.30ms : H_2O_2 + M \rightarrow 2OH + M, \qquad I_k^i = 0.144 \quad (\#436)$$

$$At\ 2.30ms : HO_2 + OH \rightarrow H_2O + O_2, \qquad I_k^i = 0.127 \quad (\#47)$$

$$At\ 2.34ms : C_5H_{10} - 1 + OH \rightarrow C_5H_9 + H_2O, \qquad I_k^i = 0.175 \quad (\#153)$$

$$At\ 2.37ms : nC_3H_7CHO + OH \rightarrow nC_3H_7CO + H_2O, \qquad I_k^I = 0.172 \quad (\#254)$$

$$At\ 2.40ms : C_2H_6 + OH \rightarrow C_2H_5 + H_2O, \qquad I_k^i = 0.126 \quad (\#18)$$

Therefore, the importance index and mode make-up analysis using CSP successfully identified the key chemical processes during the 2^{nd} stage ignition: the H_2O_2 dissociation branching followed by additional intermediate hydrocarbon decomposition by the OH radicals. These OH radicals then react first with HO_2, and then with higher hydrocarbons. The water formation reaction #47 is highly exothermic, providing the energy to sustain the reactions. Although not shown here, the same processes were identified during the ignition of the non-NTC test case (i.e. near 2.5ms in Figure 4.3(a)).

Considering that OH is an important active radical species, an alternative metric to identify key chemical processes is the importance index of various elementary reaction steps to the dynamics of OH, I_k^{OH}. Figure 4.4 shows the temporal evolution for the non-NTC and NTC cases. During the 1^{st} stage ignition for the NTC case, the prominence of reactions involving nC_7KET and isomers is evident. For the rest of the induction period (for both non-NTC and NTC cases), it is clearly seen that OH is primarily produced by the H_2O_2 branching reaction (#436), and is consumed to breakdown various hydrocarbon species. For the non-NTC case, the breakdown of n-heptane contributes to the consumption of OH (#293 through #296). For the NTC case, on the other hand, since n-heptane is mostly consumed during the 1st stage ignition, the main role of OH is found to be the oxidation of aldehyde (#30). As

the main ignition takes off for both non-NTC and NTC cases, the high temperature branching reaction (#8) takes over as the main producer of OH, and the oxidation of CO (#7) becomes larger as the final stage of oxidation.

The above analysis for homogeneous n-heptane systems demonstrated that the merging point of explosive modes serves as an accurate identification of the onset of ignition for both non-NTC and NTC regimes. Temporal evolution of the number of exhausted modes (M) was successfully used as an indicator to detect changes in the chemical dynamics of complex systems with a large number of time scales. Furthermore, the analysis of importance index revealed full details of key reaction processes during the entire period of ignition.

4.3 One-Dimensional Analysis: Ignition Regime Identification

In this section, various parametric cases of one-dimensional ignition simulations are analyzed in order to examine the ignition characteristics of non-NTC and NTC conditions. Following Chapter 3, the ignition front is located by monitoring the M profile, and identification of the ignition regime is determined by the importance index of transport to the slow dynamics of temperature, defined as in equation 3.1

By definition, I^T ranges between 0 and 1. If I^T value in the region upstream of the ignition front is close to one, then the front propagation is due to the transport-reaction balance and is identified as a deflagration wave. On the contrary, if I^T approaches zero, then the ignition front is a spontaneous ignition front dictated by chemical processes.

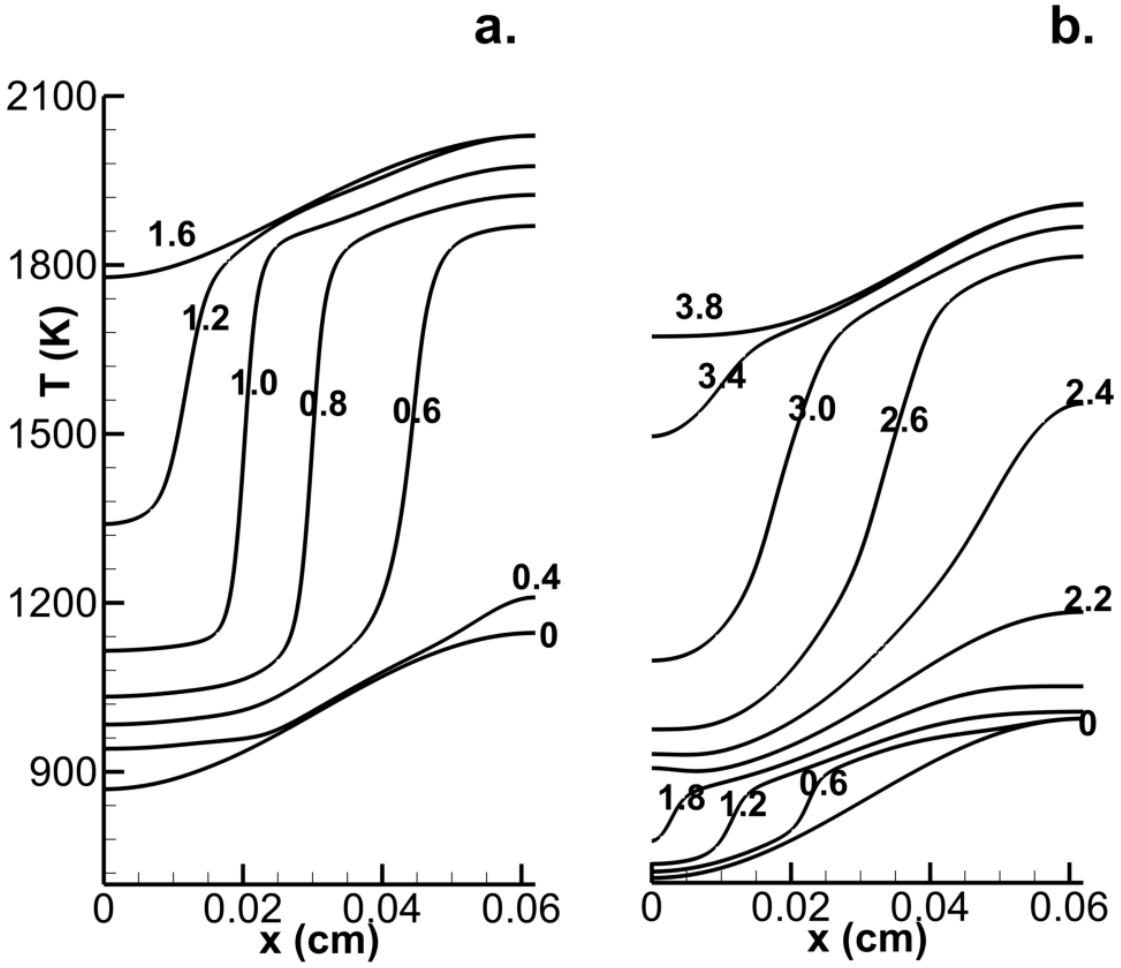

Figure 4.5: Temporal evolution of temperature profile for (a) non-NTC and (b) NTC conditions. Numbers indicate time in milliseconds. (a) non-NTC (b) NTC

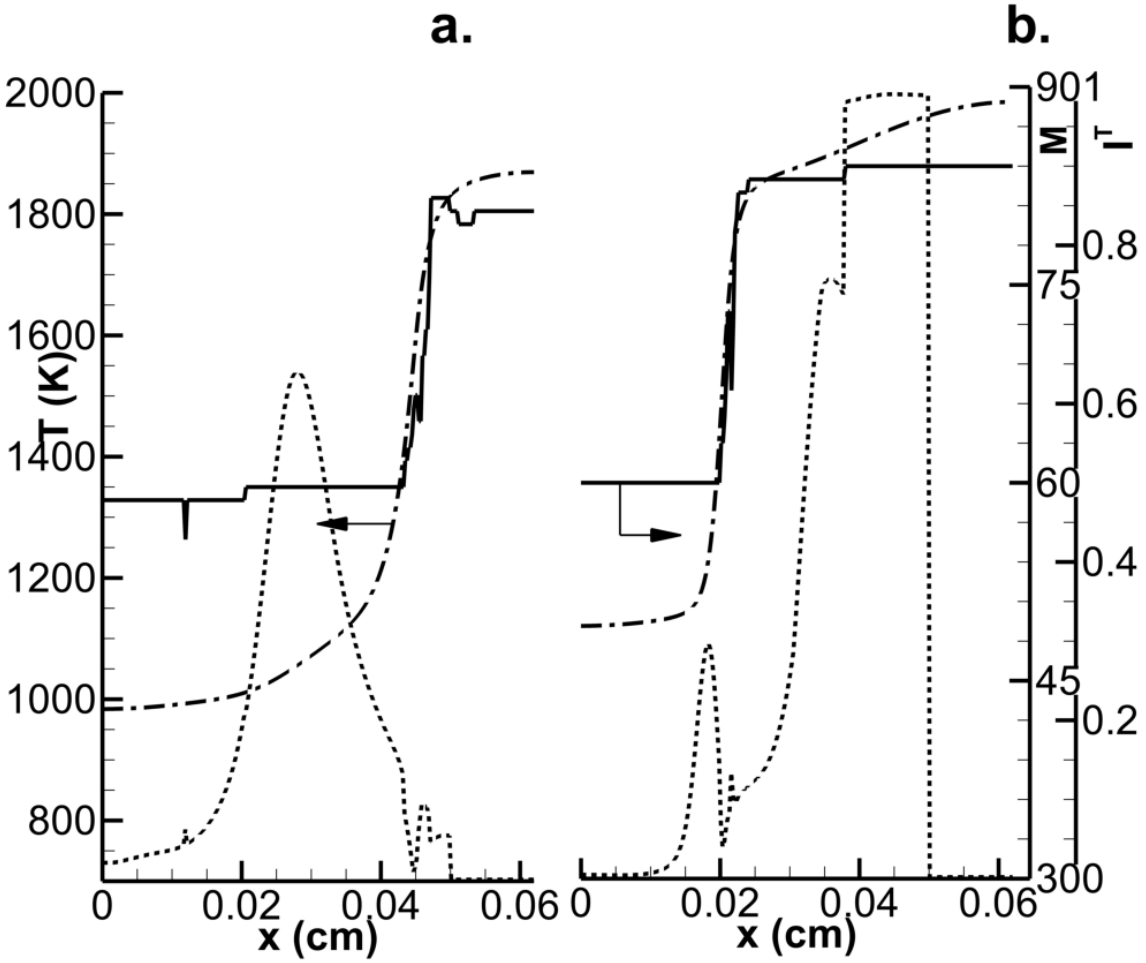

Figure 4.6: Instantaneous profiles of M (solid black), temperature (dash-dot) and I^T (dot) for the non-NTC case. (a) 0.6 ms (b) 1.0 ms

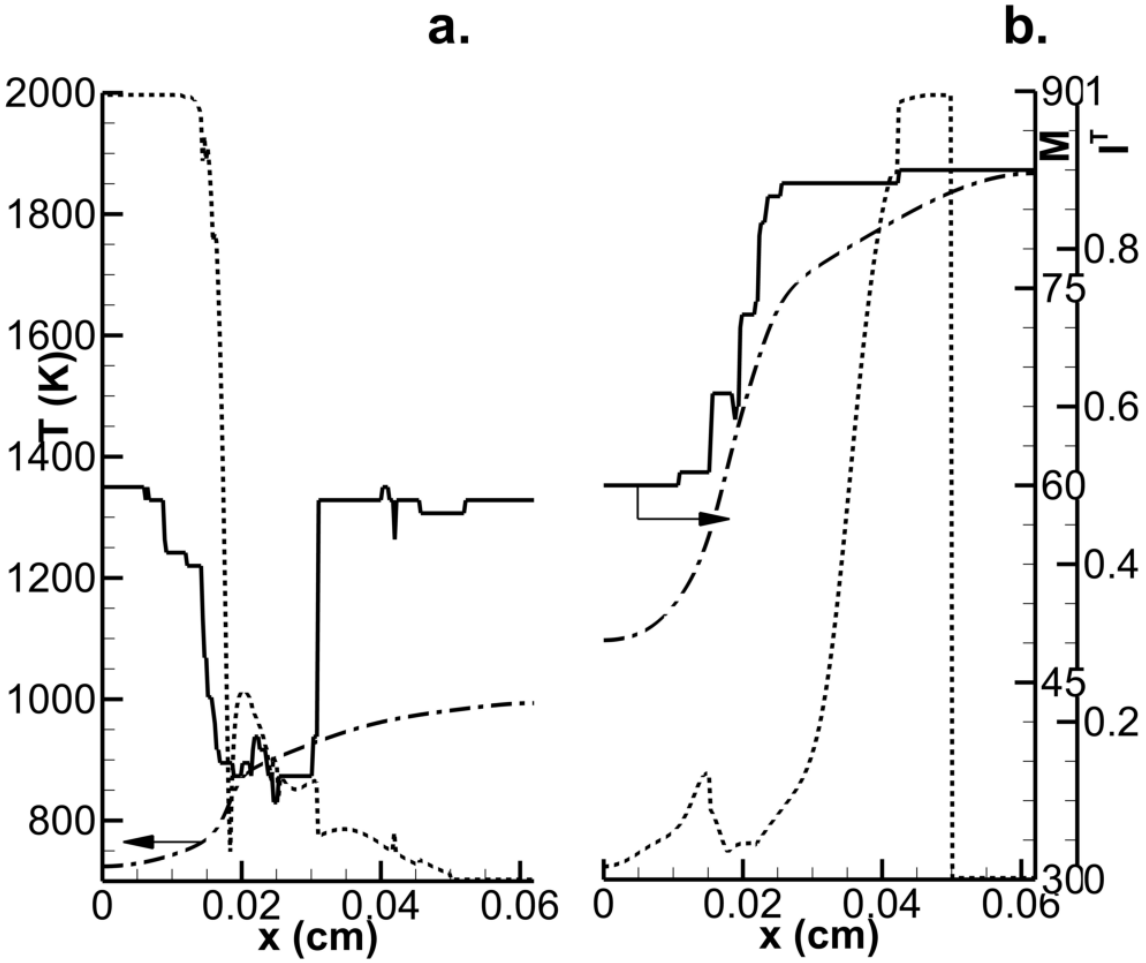

Figure 4.7: Instantaneous profiles of M (solid black), temperature (dash-dot) and I^T (dot) profiles for the NTC case. (a) 0.8 ms (b) 3.0 ms

4.3.1 Temperature Stratification Only

First, the effects of temperature stratifications are considered for a uniform mixture field at $\phi = 0.3$. Figure 4.5 shows the temporal evolution of the temperature profiles for (a) non-NTC and (b) NTC cases. Since the configuration is symmetric, only the left half of the domain is plotted in the results, such that the front is propagating to the left. While the conditions were chosen such that both cases ignite at approximately 2.5 ms at the corresponding mean temperature condition, in the presence of thermal stratification the ignition behavior changes significantly. The time to reach the near equilibrium condition is approximately 1.8 ms for non-NTC case and 3.8 ms for the NTC case. Furthermore, two distinct fronts are observed in the NTC case, one at 0-1.8ms and the other at 2.6-3.4ms, indicating the occurrence of the two-stage ignition process.

Figure 4.6 shows the spatial profiles of temperature, M, and I^T at two different times. As observed in the homogeneous case (Figure 4.3(a)), the M profile shows a transition from 60 to 84 across the front, thus serves as a good marker to locate the ignition front. While the front exhibits a steep temperature gradient (over 10,000 K/mm) and may appear as if it is a typical flame propagation, the importance index analysis shows that the I^T value in the upstream of the front changes from approximately 0.6 at 0.6ms to 0.2 at 1.0ms. Therefore, the ignition front observed during the non-NTC ignition is found to be in the deflagration initially, but it subsequently transforms to the spontaneous propagation regime as the mixture ahead of the front becomes hotter and more reactive.

The analysis is next conducted for the NTC ignition case. Figure 4.7 shows similar profiles at two different times for the NTC case. At 0.8 ms, only the ignition front associated with the 1st stage ignition is observed. Consistent with Figure 4.6, the M profile shows a dip from 60 to 40 across the front region. However, in contrast to the relatively smaller temperature gradient, the 1st stage ignition front is found to

be highly deflagrative, as indicated by the importance index value ahead of the front being close to unity. At a later time at 3.0 ms, the 2nd stage ignition front is established and the M and I^T profiles appear similar to those in figure 4.6; M undergoes a transition from 60 to 84, and the importance index diagnostics indicate that the front is again in the spontaneous propagation regime. Quantitatively, however, the magnitude of I^T is found to be significantly smaller than that observed in figure 4.6. Although the two fronts are both governed by the same 2^{nd} stage reaction processes, the 1^{st} stage ignition front occurring in the NTC case produces a high level of active radicals (mainly H_2O_2) which further promotes chemistry-driven auto-ignition of the mixture ahead of the ignition front.

4.3.2 Temperature and Composition Stratifications

Finally, the effects of spatial variations in the equivalence ratio are examined. In addition to the initial temperature profile, the same type of sinusoidal variations in the equivalence ratio with $\phi_{mean} = 0.3$ and $\phi_{rms} = 0.05$ were imposed, either positively (in phase) or negatively (out of phase) correlated with temperature. These cases will be referred to as T (temperature only), TFP (positively correlated), and TFN (negatively correlated). This is a practically relevant issue considering that in real engines temperature inhomogeneities are often associated with residual burned gases with lower fuel concentration.

Compared to the temperature-only cases shown above, it was in general found that the overall ignition delay becomes shorter for the positively correlated case, because the higher temperature region becomes more reactive due to the higher fuel concentration. By the same token, the negatively correlated case yields a longer ignition delay.

Figure 4.8 compare the temperature, M, and I^T profiles for the three (T/TFP/TFN) cases for the non-NTC condition. Figure 4.7 shows the same comparison for the NTC

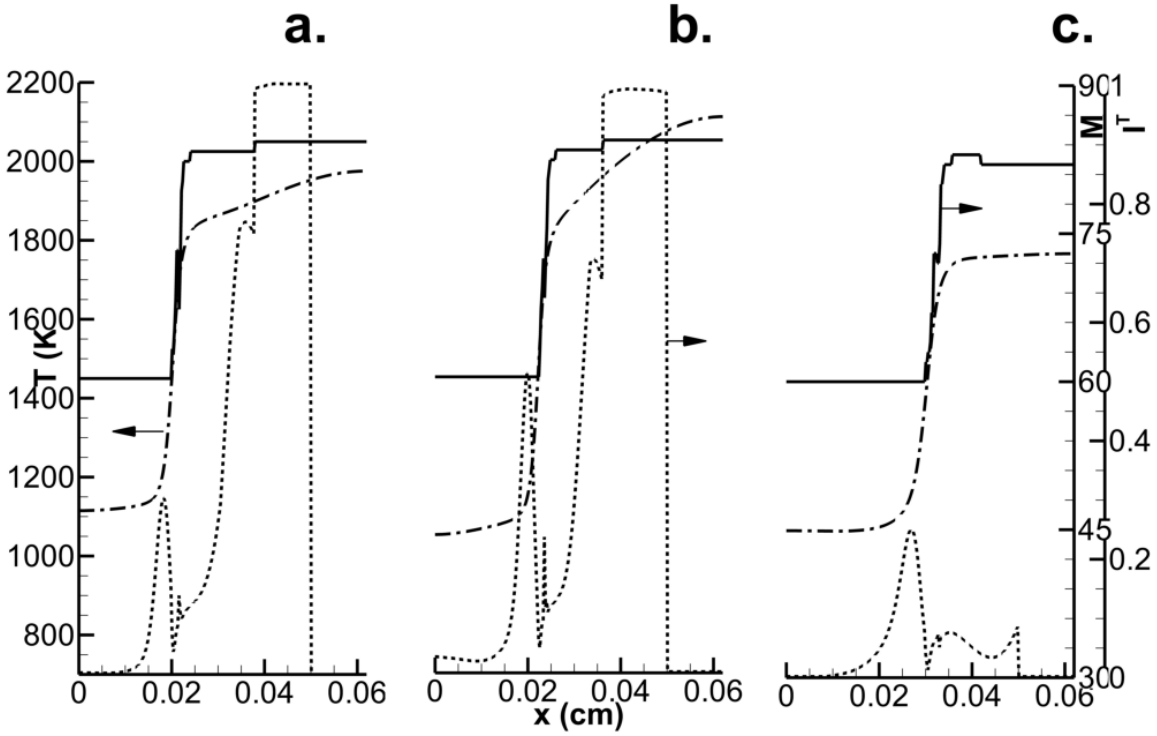

Figure 4.8: Comparison of instantaneous profiles of M (solid black), temperature (dash-dot) and I^T (dot) for the non-NTC case. (a) T (at 1 ms) (b) TFP (at 0.8 ms) (c) TFN (at 1 ms)

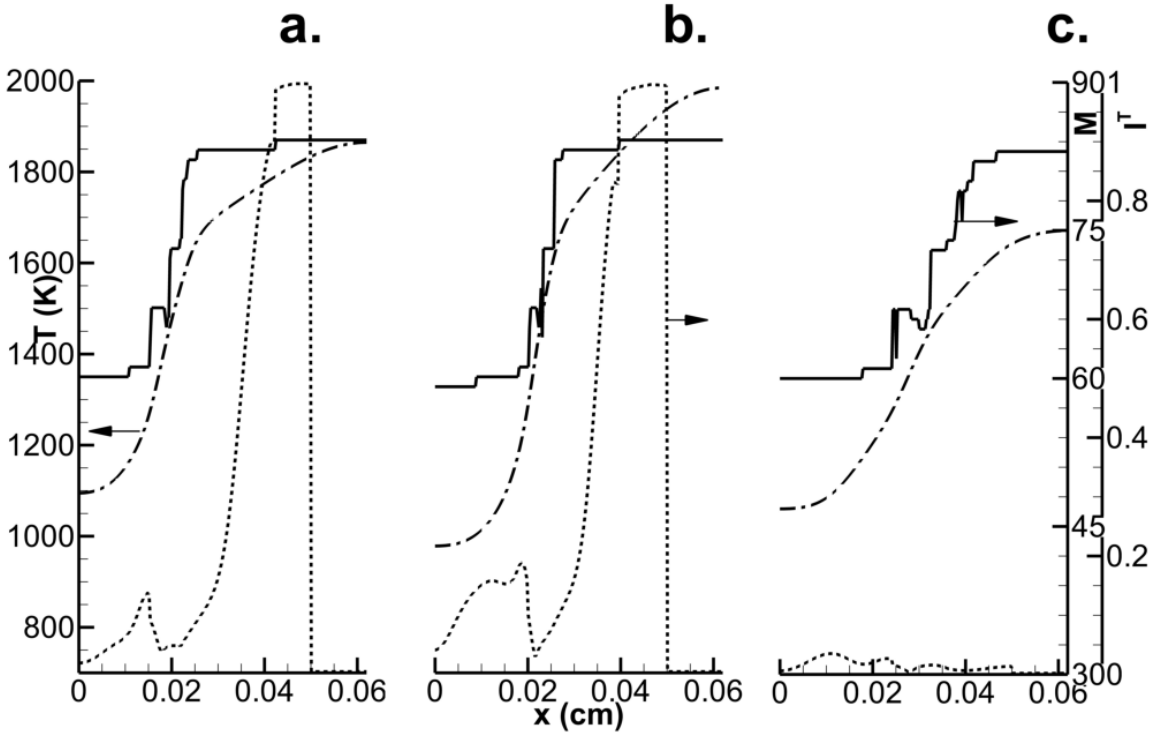

Figure 4.9: Comparison of instantaneous profiles of M (solid black), temperature (dash-dot) and I^T (dot) for the NTC case. (a) T (at 3 ms) (b) TFP (at 2.6 ms) (c) TFN (at 3 ms)

cases, after the 2nd stage ignition front appears. Although not shown here, the 1st stage ignition front for all three NTC cases was found to be in the deflagration regime. Time was arbitrarily chosen such that the 2nd stage ignition front appears at approximately the same location. For both non-NTC and NTC cases, the importance index profile ahead of the front clearly shows that the front becomes more deflagrative for the TFP case and less so for the TFN case. This is reasonable because the positively correlated case yields a less chemically reactive upstream mixture and more intense front. For the negatively correlated case, the effect of equivalence ratio variation offsets that of temperature, leading to a more uniform reactivity distribution and thus more homogeneous ignition characteristics. For all NTC cases considered, the M profiles are nearly the same in that it changes from 60 to 84 across the front, implying that the dominant chemical processes remain unchanged.

4.4 Two-Dimensional Analysis: Ignition Regimes in a Turbulent Mixture

In this section, results from the 2D DNS of turbulent ignition will be presented. The initial conditions were given in Section 4.1.2. Two test cases 1 and 2, with T_{mean} = 1008K and 850K respectively, have been considered.

In order to see distinct ignition behaviors, the integrated heat release rate for both the cases is shown in figure 4.10. Clearly, case 2 exhibits 2-stage ignition behavior with twin peaks, whereas case 1 pertains to 1-stage ignition. In order to analyze ignition regimes, we choose particular time instants representing points of maximum heat release rate. For case 1, it is 2.25ms; and for case2, it is 0.4ms (1st stage of ignition), and 2.45ms (2nd stage of ignition).

To gain insights into the dominant ignition regimes, we will look at the M and I^T contours for each case. M contours will help us identify various flow regions of

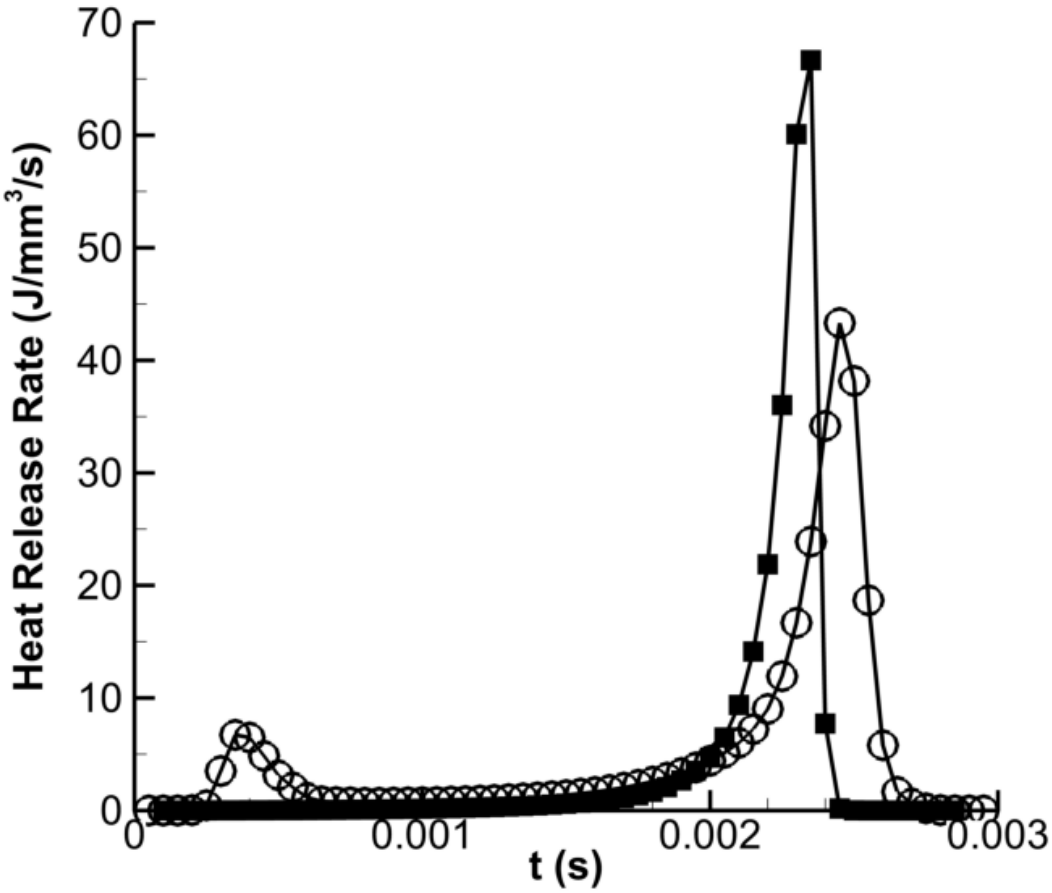

Figure 4.10: Comparison of integrated heat release rates. Squares denote case 1 (non-NTC) and circles represent case 2 (NTC)

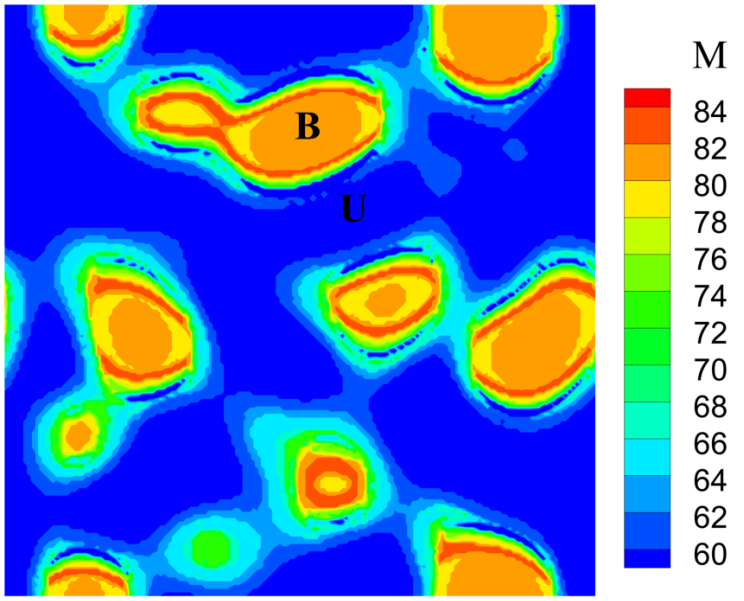

(a) M profile

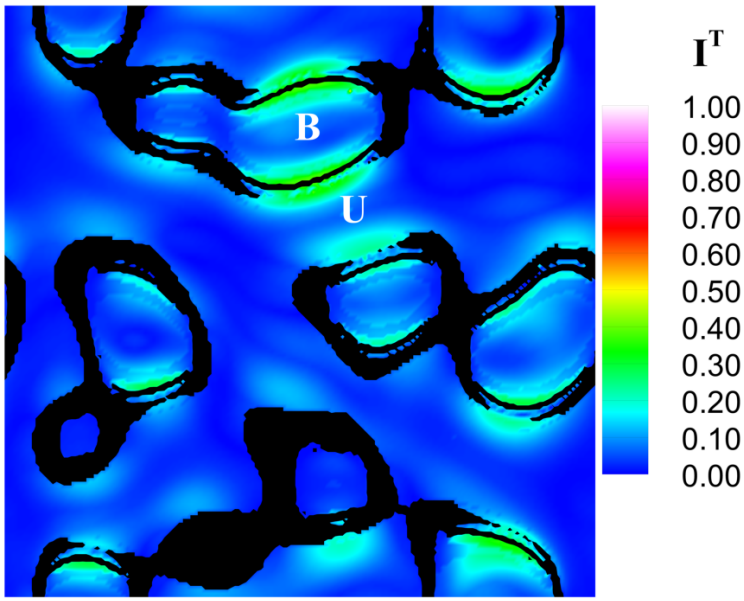

(b) Isocontours of I^T in color. $M = 64$ to 75 region is overlaid in black

Figure 4.11: Ignition regimes for case 1 (non-NTC) at 2.25ms

interest, and subsequent analysis of I^T will reveal the dominant ignition regime.

4.4.1 Non-NTC ignition

For case 1, contours of M are shown in figure 4.11. M profile for the corresponding 1D test case can be seen in figure 4.6. On comparison with the 1D profile, the M = 60 region in blue (figure 4.11(a)) is identified as the upstream unburned mixture, denoted by **U**. Similarly, M = 82 region in orange corresponds to the burned gas mixture (denoted by **B**). An interesting topological feature is the appearance of thin reddish-orange layers separating the yellowish-orange region on one side and greenish blue on the other side. These thin layers actually correspond to a little region of higher M just upstream of the burned gas mixture (at x $\sim$ 0.5mm) in figure 4.6(a). Thus, M profile gives detailed insights into various regions of the flow.

Next, we consider the I^T contours (figure 4.11(b)). From the corresponding 1D profile (figure 4.6), highly active regions representing ignition front location can be identified as the ones with M varying between 64 and 75. Therefore, to identify the same regions in 2D, contours corresponding to M = 64 to 75 are overlaid in black. The ignition front (in black) separating **B** and **U** regions has the magnitude of I^T close to 0.5, which means that it is halfway between a pure deflagration and a pure spontaneous ignition front. Most of the other regions have a very small value of I^T indicating that in general, spontaneous ignition regime is dominant.

Hence, the CSP analysis reveals that spontaneous ignition is the dominant ignition regime for non-NTC ignition, however, there are a few sites with local mixed-mode ignition.

4.4.2 NTC ignition

Next, we consider case 2 with 2-stage NTC behavior. The analysis will be done at two time instants: (i) at 0.4ms (corresponding to peak heat release rate for the 1st

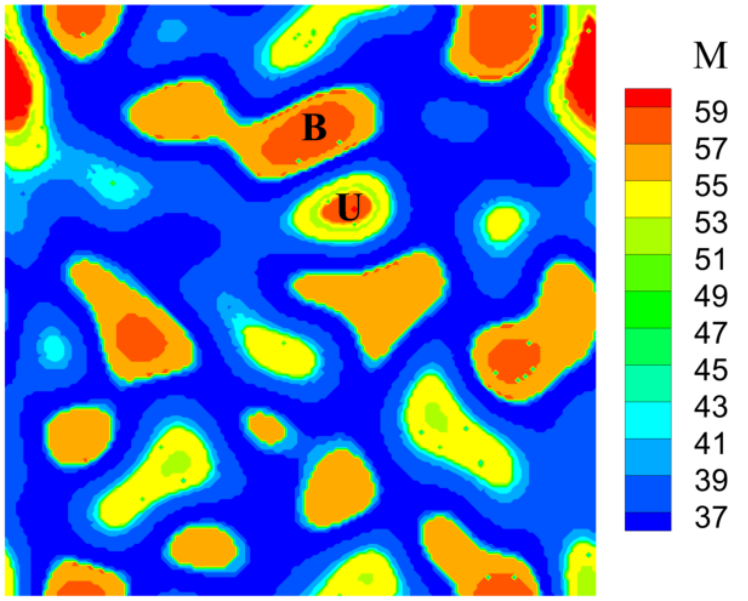

(a) M profile

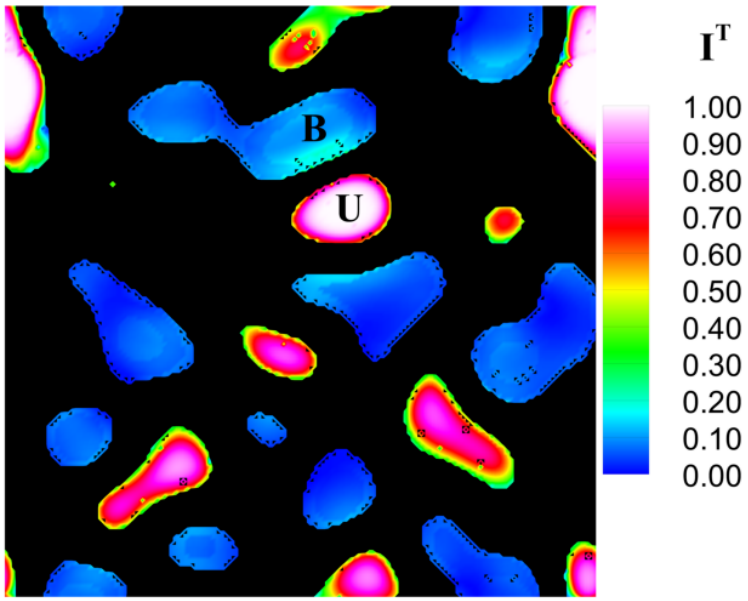

(b) Isocontours of I^T in color. $M = 37$ to 44 region is overlaid in black

Figure 4.12: Ignition regimes for case 2 (NTC) at 0.4ms

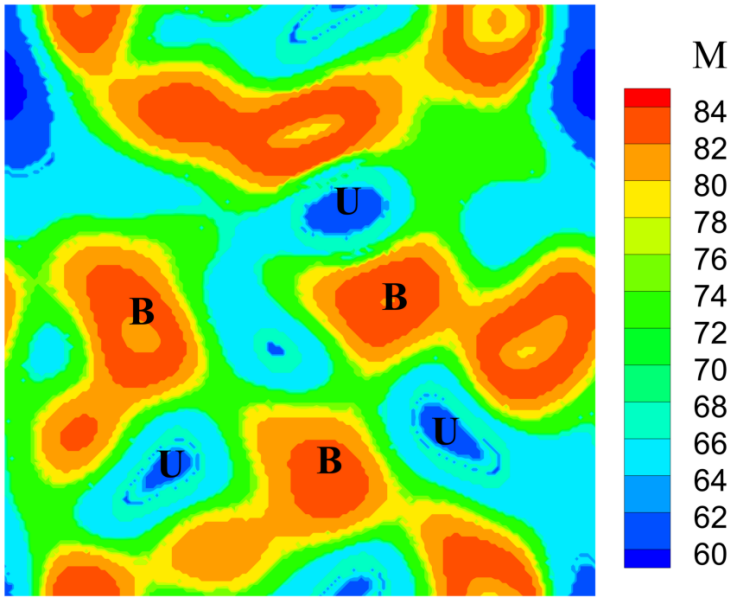

(a) M profile

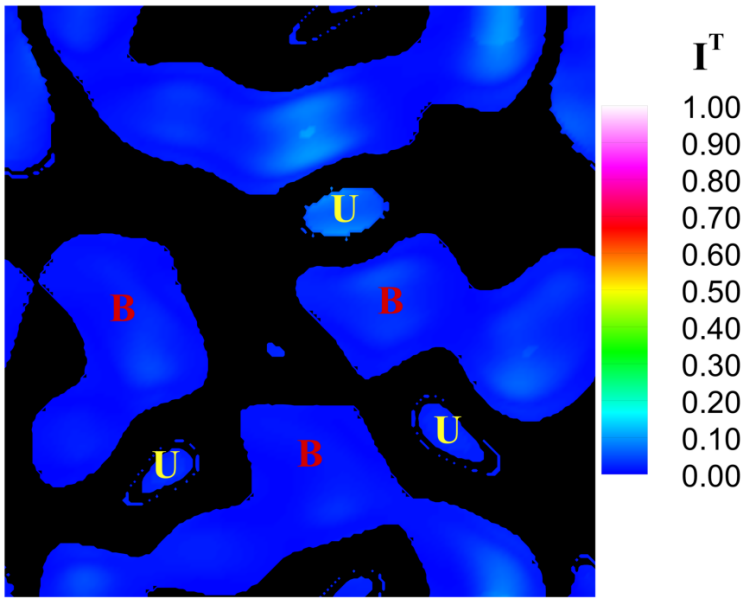

(b) Isocontours of I^T in color. $M = 64$ to 75 region is overlaid in black

Figure 4.13: Ignition regimes for case 2 (NTC) at 2.45ms

stage), and (ii) at 2.45ms (corresponding to peak heat release rate for the 2nd stage)

For 0.4ms (figure 4.12), the corresponding 1D test case is depicted in figure 4.7(a). From the 1D M-profile, it can be seen that both the upstream unburned mixture and the downstream burned mixture have $M = 60$. But, a small plateau of $M = 54$ exists close to the unburned mixture only. The same topology is reflected in the 2D contours (figure 4.12(a)). For the region labeled **U**, yellow $M = 54$ regions surround the red $M = 60$ zones. Therefore, they are identified as unburned mixtures. For the regions labeled **B**, no such yellow band appears and there is an abrupt transition from blue to orange-red. Figure 4.12(b) shows that almost all the unburned regions have a high value of I^T, indicating the dominance of deflagration regime.

The 2nd stage of ignition at 2.45ms (figure 4.13(a)) corresponds to the 1D test case in figure 4.7(b). The unburned M=60 regions in blue are depicted as **U**, whereas the burned $M = 84$ regions in red are depicted as **B**. The I^T contours (figure 4.13(b)) are all blue, suggesting that ignition is occurring in the spontaneous regime.

An interesting point to note here is that M profile can help distinguish even the 2nd stage of NTC ignition and the non-NTC ignition. For the former (figure 4.13(a)), the transition from unburned $M = 60$(blue) to burned $M = 84$(red) occurs smoothly through the green $M = 70$-74 band, whereas for the latter (figure 4.11(a)), the transition is relatively abrupt and the green layers are thinner.

4.5 Concluding Remarks

The main conclusions from this chapter are summarized below:

- **Homogeneous auto-ignition**: Homogeneous ignition at both non-NTC and NTC conditions were examined. It was found that the merging of two explosive modes appears to be a universal signature of onset of both 1st and 2nd stage auto-ignition. Monitoring M was found to be an effective way to detect

abrupt transient phenomena resulting from complex chemical systems with a large number of time scales. Detailed investigations into the reaction steps contributing to mode $M + 1$ clearly revealed the key chemical processes responsible for the ignition dynamics.

- **1D laminar ignition**: For the one-dimensional test cases considered, the non-NTC case exhibited ignition transition from the nearly deflagration to spontaneous ignition regimes during the evolution. For the NTC case, the 1st stage ignition front was found to be highly deflagrative, which was attributed to the reduced active chemical time scales combined with relatively low reactivity in the upstream mixture. On the other hand, the 2nd stage ignition front was found to be mostly in the spontaneous propagation regime, due to the larger production of active radicals left behind the 1st stage ignition front. When additional concentration stratification is added to the temperature field, the positively correlated cases yielded more deflagrative fronts, while the negatively correlated cases (which correspond to exhaust gas mixing in engines) showed more pronounced spontaneous propagation regime.

- **2D turbulent ignition**: In terms of the dominant ignition regimes, the discussion on 2D test cases reinforces the findings from the 1D study, i.e., for NTC ignition, 1^{st} stage deflagration is followed by 2^{nd} stage spontaneous ignition. For non-NTC ignition, the dominant ignition regime is spontaneous, together with mixed-mode ignition at some local sites. The 2D analysis also demonstrated the capability of CSP to differentiate between the 2^{nd} stage NTC and non-NTC ignition by the help of M profile.

CHAPTER V

Modeling of Scalar Dissipation Rates in Flamelet Models for LTC Engines

Turbulence plays a very important role under stratified LTC conditions, as described in Section 1.7. One of the most prominent modeling approaches which takes into account turbulence and mixture stratifications is flamelet modeling. The flamelet modeling approach and its inherent transport closure problem was introduced in Section 1.8, and its computational framework and the mathematical formulation of scalar dissipation rates was described in Section 2.4.

Scalar dissipation rates (mean and conditional) are of paramount importance in the context of flamelet modeling, as they are the only parameters which connect physical space to the flamelet space. Correct representation of scalar dissipation rates is therefore crucial to success of the flamelet modeling approach. In this DNS study, we look at the validation and development of models for scalar dissipation rates, based on a reference DNS data.

As an *a priori* test, two-dimensional DNS of auto-ignition of a turbulent H_2-air mixture with detailed chemistry has been used for validation [36]. The parametric studies differed in terms of the correlation of thermal and mixture inhomogeneities imposed as the initial condition. Three test cases were considered:

- Temperature inhomogeneities only (Case A)

- Uncorrelated temperature and compositional inhomogeneities (Case B)
- Negatively-correlated temperature and compositional inhomogeneities (Case C)

These cases represent vastly different combustion modes (homogeneous ignition, premixed flame propagation and sequential ignition). Therefore, the DNS data serve as a good reference to test the models on a multitude of different engine operation scenarios.

Although the fuel considered is hydrogen, practical relevance of this study lies in the fact that of late, hydrogen is being considered as an alternative automobile fuel for LTC engines [97, 98]. Moreover, hydrogen/air chemistry forms an integral part of the oxidation of almost all higher hydrocarbons. Gaining insights into mixing for hydrogen/air chemistry is hence the first step in understanding the complex mixing processes inside a real LTC engine.

In this study, Z is the Bilger's mixture fraction, calculated as in [99], and H is the total enthalpy, the sum of formation and sensible enthalpies. Both Z and H are normalized, based on their minimum and maximum magnitudes at each time step. Such a normalization is a common practice in the flamelet approach [58] because it considerably simplifies numerical computations in the flamelet space.

The main objectives of this chapter are to assess the performance of existing scalar dissipation rate models under LTC conditions, to understand the dynamics of turbulent mixing under such conditions, and finally to gain insights into the development of better modeling strategies. The results will be presented first in the context of RANS, and later in the context of LES.

5.1 Performance of existing RANS mixing models

We will assess the performance of existing RANS models for PDFs, conditional and mean scalar dissipation rates. Comparisons are made with the reference DNS data.

The mean values of various parameters are computed by taking a spatial average over the entire computational domain.

5.1.1 PDFs

PDF of a scalar gives its statistical distribution within the domain. Modeling PDF accurately is the first step for a good mixing model.

Figures 5.1(a) and 5.2(a) show the PDF of Z (calculated from DNS data) for cases B and C, respectively. PDF of H follows a similar trend, and so has not been shown here. Cases B and C have been chosen as they represent different combustion modes (Case B favors ignition front propagation, whereas case C favors homogeneous volumetric ignition [36]). For case B (Figure 5.1(a)), PDF starts off symmetrically (at t = 0ms) with its maximum value at Z = 0.5. At 1.5ms, the peak of PDF starts to shift left towards lower Z values, reaches a minimum Z location, and finally shifts right towards the fag end of ignition. However, for case C (Figure 5.2(a)), no such shift in the peak is observed. This difference in peak shift behavior between cases B and C suggests an underlying difference in their mixing processes. It will be explained in Section 5.4.1.

The most commonly used model for PDFs is the Beta PDF model, given by Equation 2.27. Figures 5.1(b) and 5.2(b) show Beta PDF for case B and case C, respectively. It can be seen that there is a decent agreement between the DNS and the Beta-PDF profiles for case C. For case B, however, the model under-predicts the DNS values at 2ms and 2.5ms.

5.1.2 Conditional scalar dissipation rates

Conditional scalar dissipation rates give the magnitude of scalar dissipation rate, conditioned on a particular scalar. They provide the functional dependence of scalar dissipation rate on the scalar under consideration. A brief discussion on the mathe-

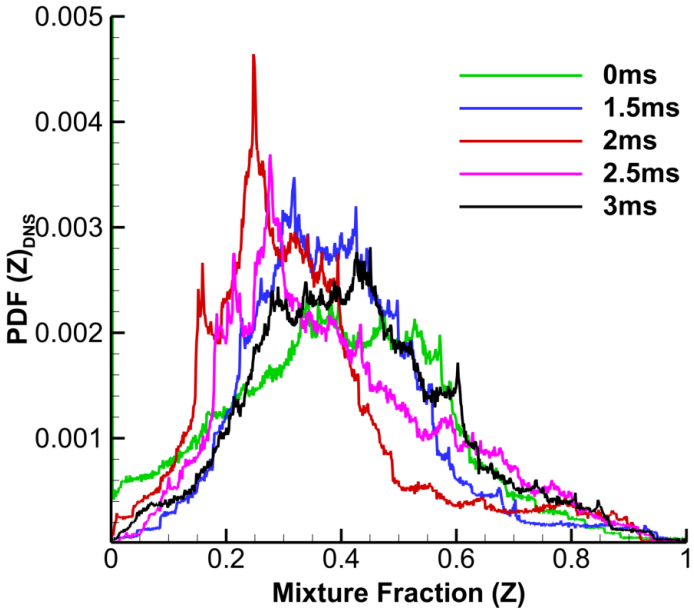

(a) PDF for Z calculated from DNS

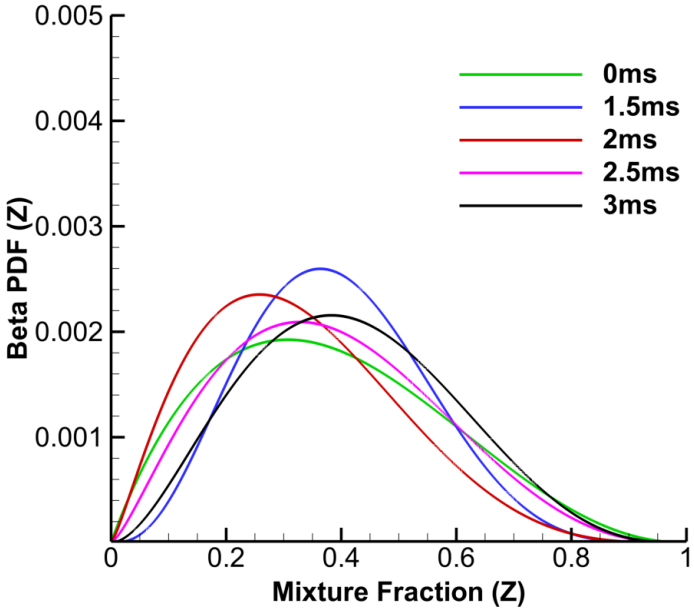

(b) Beta PDF for Z

Figure 5.1: DNS PDF vs. Beta PDF (Case B)

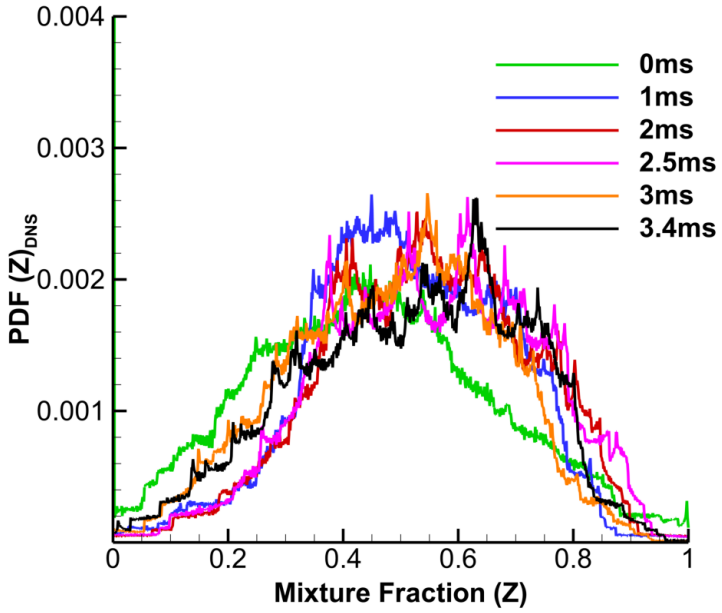

(a) PDF for Z calculated from DNS

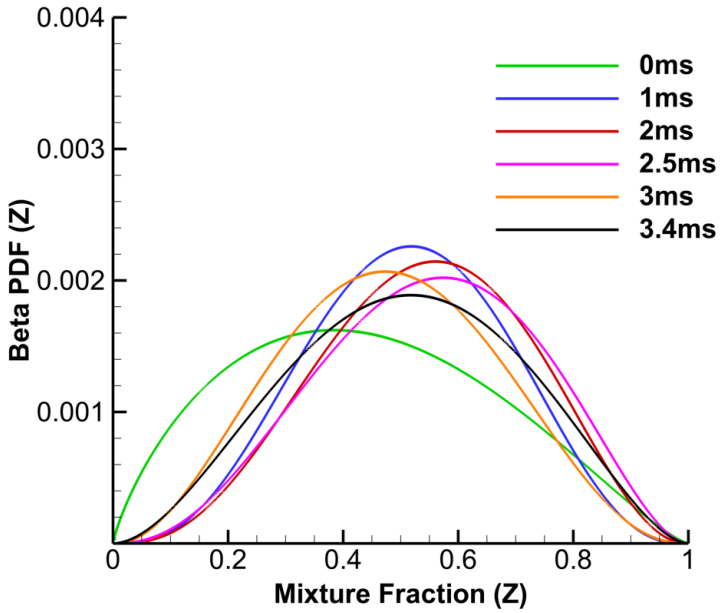

(b) Beta PDF for Z

Figure 5.2: DNS PDF vs. Beta PDF (Case C)

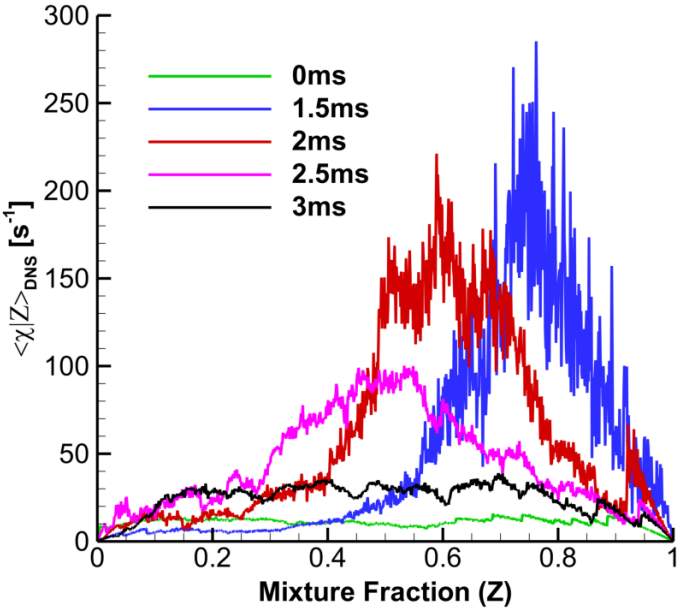

(a) $\langle \chi | Z \rangle_{DNS,mean}$)

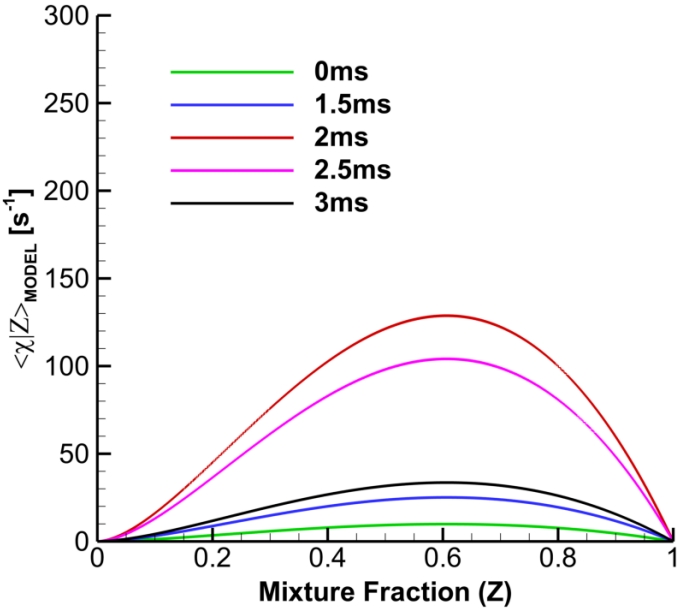

(b) $\langle \chi | Z \rangle_{MODEL}$

Figure 5.3: $\langle \chi | Z \rangle$: DNS vs. 1D infinite mixing layer model (Case B)

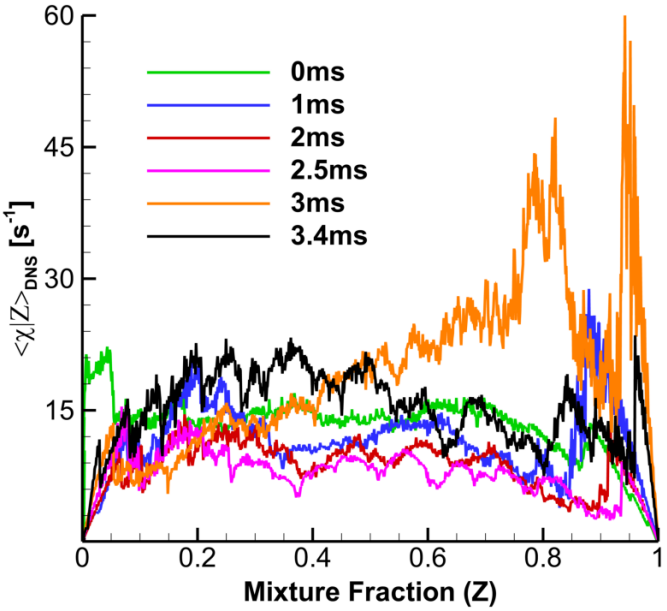

(a) $\langle \chi | Z \rangle_{DNS,mean}$

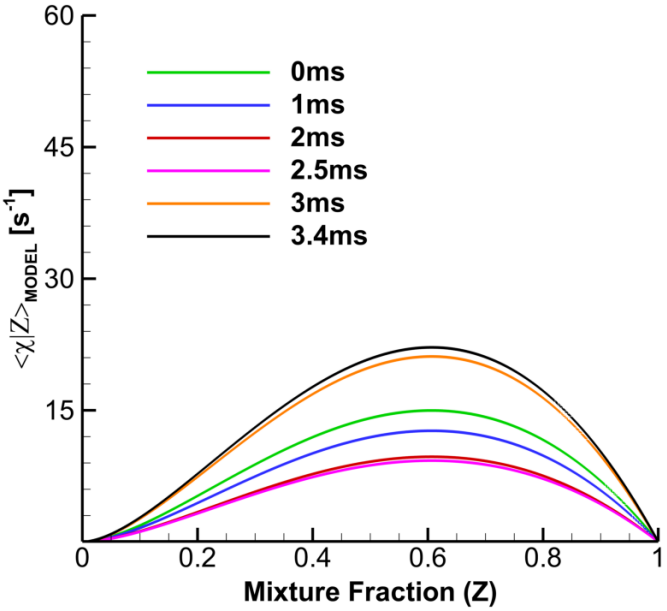

(b) $\langle \chi | Z \rangle_{MODEL}$

Figure 5.4: $\langle \chi | Z \rangle$: DNS vs. 1D infinite mixing layer model (Case C)

matical formulation and modeling approaches of conditional scalar dissipation rates was given in Section 2.4. There are two parts to the conditional scalar dissipation rate: the scaling factor, and the functional dependence on Z, i.e. $f(Z)$.

Here, we present results for the 1D infinite mixing layer model (Equation 2.26). Results for the counterflow profile [59] were found to be similar, and have not been presented. Figure 5.3 shows the conditional scalar dissipation rate profile at various time instants for case B, corresponding to DNS (Figure 5.3(a)) and model (Figure 5.3(b)). It can be seen that at 1.5ms and 2ms, DNS profiles have considerably higher peak values of scalar dissipation rate as compared to the model profiles, and are also skewed towards higher Z levels. For case C (Figure 5.4), however, there is no sudden rise in scalar dissipation rate, and the difference of the model and DNS values is relatively small. What causes this sudden increase and skewness in scalar dissipation rate profile for case B? Why do the model predictions not match with the DNS results? These questions will be answered in Section 5.4.2.

5.1.3 Mean scalar dissipation rates

Mean scalar dissipation rates serve as the only bridge between the flow field (CFD code) and combustion (Flamlet code), and appear as unclosed terms in the transport equations of variances of Z and H (Equation 2.21). Formulating accurate models for them is perhaps the most important aspect in the context of flamelet modeling.

As described in Section 2.4, we test the validity of the existing models for mean scalar dissipation rates (Equations 2.22 and 2.23) by looking at the magnitudes of the constants of proportionality (C_Z and C_H).

Figure 5.5 shows the value of the constant (open squares) for the three cases. It is observed that C_Z and C_H are almost constant in the non-reacting regime (before the onset of ignition) for all the cases, except for the initial rise (which is due to turbulent straining of the mixing field, as an artifact of the initial turbulence seed),

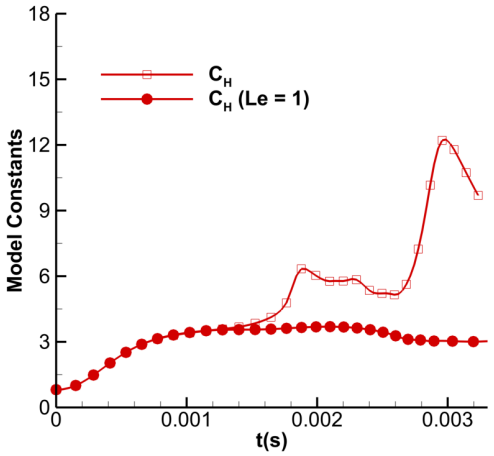

(a) Case A

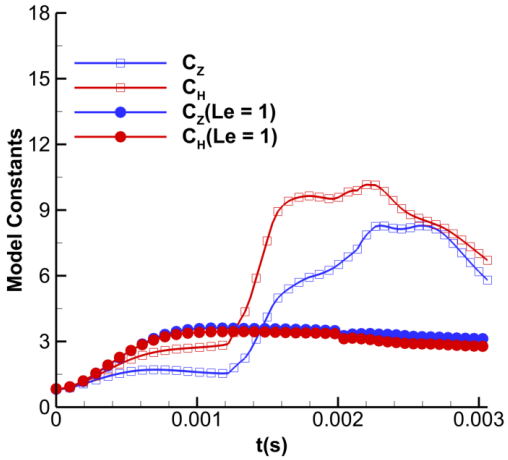

(b) Case B

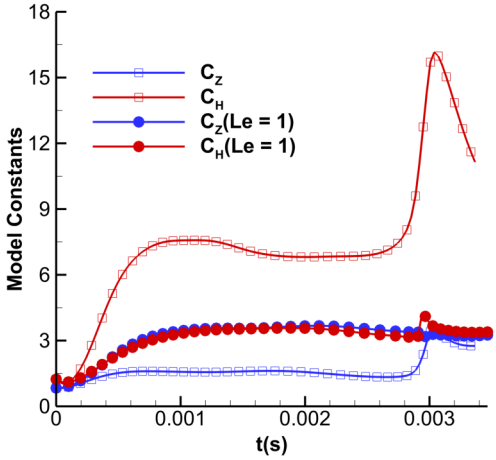

(c) Case C

Figure 5.5: Model constants for mean scalar dissipation rates

although the value of constant is different for each case, and also different for Z and H. We also see that C_H is always greater than C_Z by a factor of almost 2-3 (except for case A, which didn't have any initial Z fluctuations). In the reacting regime, C_Z and C_H are no longer a constant and have a non monotonic behavior for all the three cases, more so for cases A and B which favor ignition front formation. Such a huge deviation from the constant value may lead to an erroneous prediction of the mean scalar dissipation rate in the full cycle RANS simulations, leading to an inaccurate prediction of the ignition delay.

We have thus seen that the models for PDFs, conditional and mean scalar dissipation rates don't perform quite well, more so for case B, than for case C. In the next section, we will explore the dynamics of mixing and subsequently, find reasons for this poor performance.

5.2 Dynamics of mixing

In this section, we first look into the behavior of mixing (τ_Z, τ_H) and turbulent (τ_{turb}) timescales for all the three cases (Figure 5.6).

The mixing and turbulence timescales are defined as:

$$\tau_Z = \frac{\widetilde{Z''^2}}{\widetilde{\chi_Z}} \tag{5.1}$$

$$\tau_H = \frac{\widetilde{H''^2}}{\widetilde{\chi_H}} \tag{5.2}$$

$$\tau_{turb} = \frac{\widetilde{\varepsilon}}{\widetilde{\kappa}} \tag{5.3}$$

Also plotted is the logarithm of the inverse of Integrated Heat Release rate as a marker of the ignition event. The following trend is observed in all the cases. The initial turbulence seed causes turbulent straining of the mixing field, resulting in the decrease of mixing timescales. After sometime, when the effect of initial turbulence

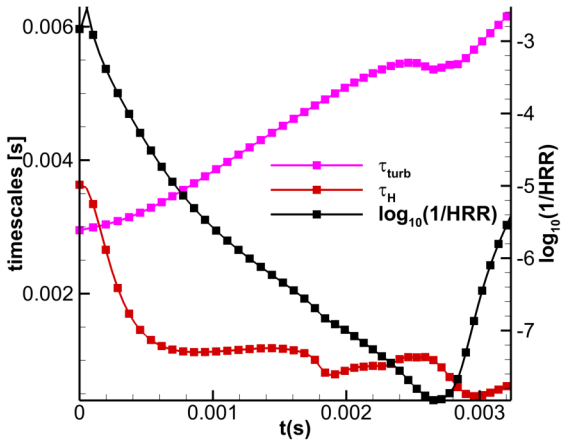

(a) Case A

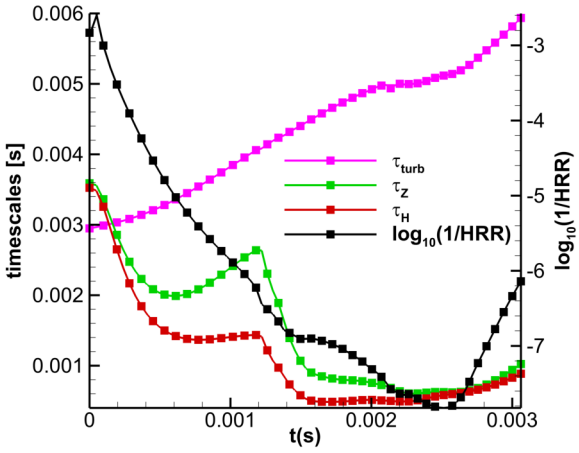

(b) Case B

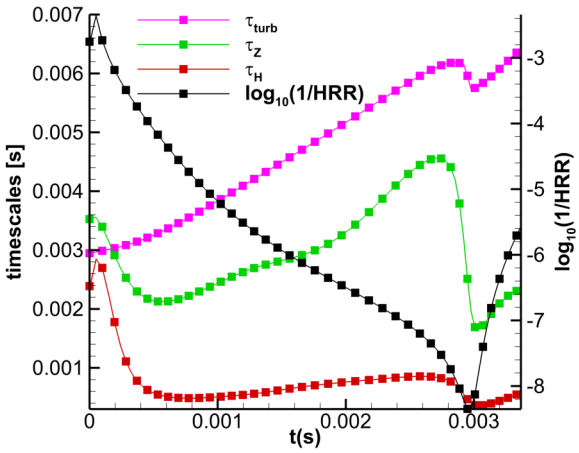

(c) Case C

Figure 5.6: Interaction of Mixing, Turbulent and Chemical Timescales

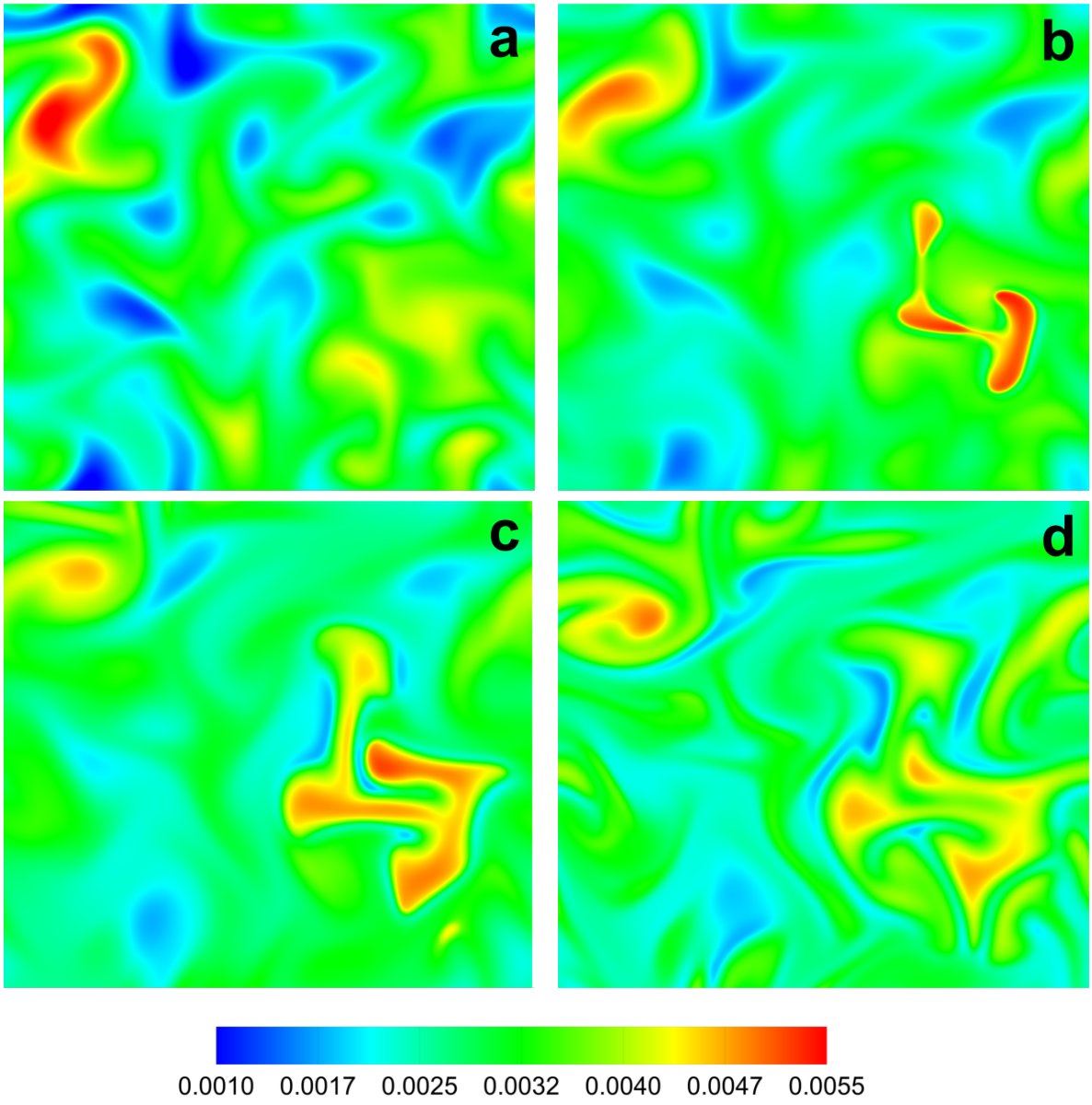

Figure 5.7: 2D Z field for Case B: a. 1ms, b. 1.5ms, c. 2ms, d. 2.5ms

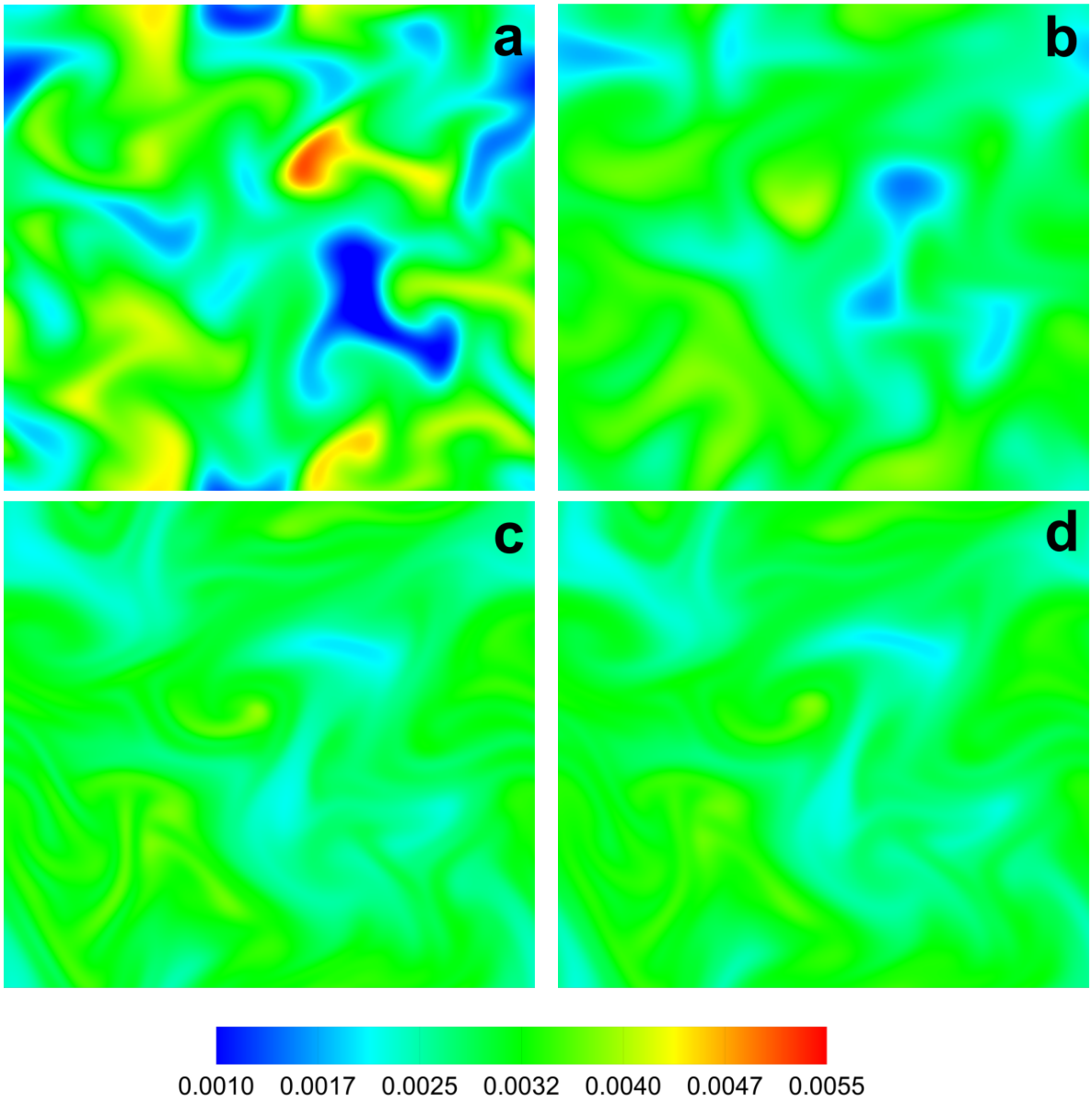

Figure 5.8: 2D Z field for Case C: a. 1ms, b. 2ms, c. 3ms, d. 3.2ms

straining has diminished, the mixture starts to become less inhomogeneous, thereby increasing the mixing timescales. The mixing timescales increase until a point when the ignition fronts start to form inside the domain (notable especially for case A (Figure 5.6(a)) and case B (Figure 5.6(b)) at 2ms and 1ms, respectively). From this point onwards until the volumetric ignition is reached, mixing timescales are small, and finally increase marginally when the spatial gradients within the domain decrease towards the end of combustion. However, for case C, which favors volumetric ignition, there is no sudden decrease of mixing timescales.

One important question to ask here is: Why do mixing timescales decrease at the onset of ignition front formation (2ms for case A and 1ms for case B)? To answer this question, we need to look into the local mixing dynamics.

Figures 5.7 and 5.8 show the evolution of mixture fraction field for cases B and C, respectively. For case B, ignition fronts form at around 1.5ms, which causes a sudden increase in gradient in mixture composition, with the ignition front separating the unburned and the burning region. As can be seen from Figure 5.7 at 1.5ms, there are sharp gradients in Z as well, and although not shown here, H also undergoes a similar type of behavior. For case C, Z field appears to decay smoothly, without any local creation of gradients.

The appearance of sharp gradients might at a first sight seem contradictory to the definition of a conserved scalar, as by definition, a conserved scalar cannot be generated by combustion. In fact, the volume averaged Z does not undergo any change at all during the course of combustion. Volume averaged H, however, does increase a little during heat release, because of the dp/dt term in its transport equation. As described next, the main reason has to do with the physical and chemical properties of hydrogen (H_2).

Hydrogen has a Lewis number much less than unity, and thus can diffuse much faster as compared to other species. So, as soon as the ignition fronts form, hydrogen

from the unburned mixture diffuses to the burned mixture, hence increasing the local Z value for the burning region, and decreasing it for the unburned region. Since hydrogen also has a high value of chemical enthalpy, the total enthalpy of burning region increases as soon as hydrogen diffuses there. On the same token, because of the loss of hydrogen, the total enthalpy of the unburned region reduces.

To further investigate how differential diffusion results in a sudden rise in scalar dissipation rate, we perform a theoretical analysis of the effects of differential diffusion on mixing.

5.3 Differential diffusion effects

It is commonly believed that in large Re flows, differential diffusion effects are negligible, because differential diffusion influences only the small length scales. But, in the presence of heat release, Re can reduce considerably, thereby making differential diffusion more important [100]. To quantify the effects of differential diffusion in this study, we first present the theoretical formulation, along the lines of Sutherland et al [101] for non-premixed combustion. This formulation is based only on Z. Similar expressions can be derived for H following the same approach.

5.3.1 Theoretical formulation of differential diffusion

Mass fraction of jth element is defined as:

$$Z_j = \sum_{i=1}^{n} \frac{a_{ij} W_j}{W_i} Y_i \tag{5.4}$$

Transport equations for species mass fractions are:

$$\rho \frac{\partial Y_i}{\partial t} + \rho \mathbf{v}.\nabla Y_i = -\nabla.j_i + \omega_i \tag{5.5}$$

where, $j_i = -\rho D_i \nabla Y_i$

Adding Equations 5.5 for all species, we get:

$$\rho\frac{\partial Z_j}{\partial t} + \rho\mathbf{v}.\nabla Z_j = -\nabla.(\sum_{i=1}^{n}\frac{a_{ij}W_j}{W_i}j_i) \tag{5.6}$$

If $D_i = D$, then

$$\rho\frac{\partial Z_j}{\partial t} + \rho\mathbf{v}.\nabla Z_j = \nabla.(\rho D\nabla Z_j) \tag{5.7}$$

Equation 5.7 is the original formulation of Z transport equation

However, if $D_i \neq D$, then

$$\rho\frac{\partial Z_j}{\partial t} + \rho\mathbf{v}.\nabla Z_j = \nabla.(\sum_{i=1}^{n}\frac{a_{ij}W_j}{W_i}\rho(D_i - D + D)\nabla Y_i) \tag{5.8}$$

$$\rho\frac{\partial Z_j}{\partial t} + \rho\mathbf{v}.\nabla Z_j = \nabla.(\rho D\nabla Z_j) + B_j \tag{5.9}$$

$$B_j = \nabla.(\sum_{i=1}^{n}\frac{a_{ij}W_j}{W_i}\rho(D_i - D)\nabla Y_i) \tag{5.10}$$

Bilger's mixture fraction can be represented as [99]:

$$Z = aZ_H + bZ_O + c \tag{5.11}$$

where a, b and c are constants dependent on the fuel and air composition.

$$\rho\frac{\partial Z_j}{\partial t} + \rho\mathbf{v}.\nabla Z_j = \nabla.(\rho D\nabla Z_j) + aB_H + bB_O \tag{5.12}$$

Let $B = B_H + B_O$, then we get:

$$\boxed{\rho\frac{\partial Z_j}{\partial t} + \rho\mathbf{v}.\nabla Z_j = \nabla.(\rho D\nabla Z_j) + B} \tag{5.13}$$

In Equation 5.13, B is the extra term due to differential diffusion, which is defined as:

$$\boxed{B = \sum_{i=1}^{n} \alpha(\frac{1}{Le_i} - 1)\nabla.(\rho\nabla Y_i)(\frac{aa_{iH}W_H + ba_{iO}W_O}{W_i})} \tag{5.14}$$

B acts as a source term in Equation 5.13, hence Z is no longer a conserved scalar. This in itself is a very important conclusion.

Starting from the modified Z transport Equation 5.13, the modified $\widetilde{Z''^2}$ equation is given as:

$$\boxed{\overline{\rho}\frac{\partial\widetilde{Z''^2}}{\partial t} + \overline{\rho}\widetilde{\mathbf{v}}.\nabla\widetilde{Z''^2} = \nabla.(\overline{\rho}\widetilde{\mathbf{v}''Z''^2}) + 2\overline{\rho}D_t(\nabla\widetilde{Z})^2 - \overline{\rho}\widetilde{\chi_Z} + 2\overline{\rho}[\widetilde{Z''(\frac{B}{\rho})''}]} \tag{5.15}$$

In Equation 5.15, the last term $DD(Z)_{term} = 2\overline{\rho}[\widetilde{Z''(\frac{B}{\rho})''}]$ is the source term which corresponds to the contribution of differential diffusion.

To compare the relative magnitude of various terms in Equation 5.15, we plot them for case B. Since our computational domain is fixed, the second term on LHS, and first and second terms on RHS will vanish. We are only left with three terms: the time rate of change of $\widetilde{Z''^2}$, the scalar dissipation rate term and the differential diffusion term.

Figure 5.9(a) shows the contribution of these three terms for case B as a function of time. Z_{var}(production term) is the difference of d(Z_{var})/dt and $\chi_{Z,mean}$. If the above theoretical formulation is correct, then Z_{var}(production term) should be equal to DD(Z)$_{term}$, which is indeed found to be true. Also, the magnitude of DD(Z)$_{term}$ is of the same order of magnitude as $\chi_{Z,mean}$, which implies that differential diffusion plays a very important role in mixing dynamics for this test case. It is interesting to note that DD(Z)$_{term}$ changes its sign as the combustion event takes place, which

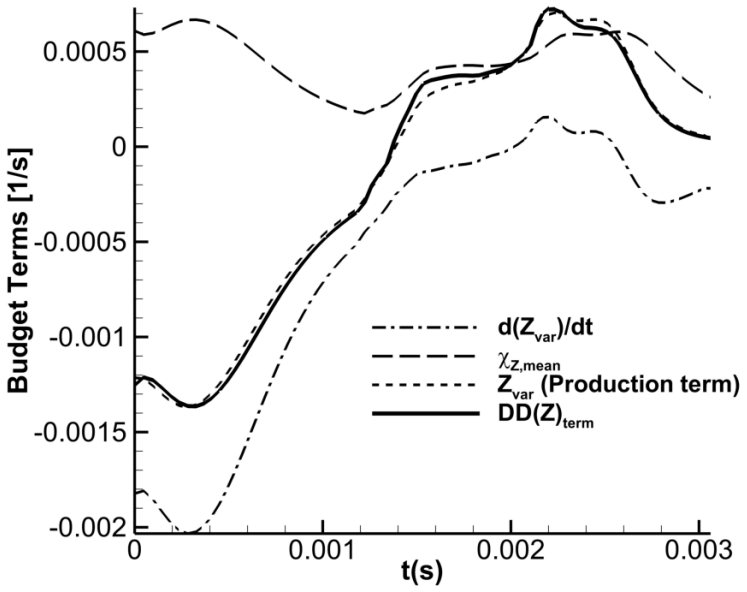

(a) Case B

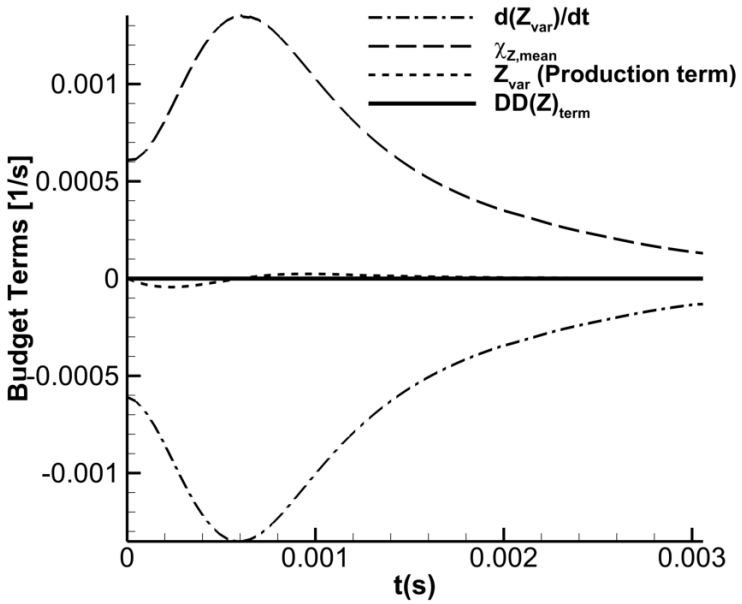

(b) Case B ($Le_i = 1$)

Figure 5.9: Budget term analysis of Equation 5.15

means that the fluctuations in B and those in Z change to positively correlated from being negatively correlated earlier. Further investigation into this subject can help us gain better insights into the local effects of ignition on mixing. This is a topic for future work.

In flamelet models, it is a common practice to assume unity Lewis number of all species, thereby making sure that mixture fraction is a conserved scalar. Even if the effects of non-unity Lewis numbers are considered [81], a separate transport equation without any source term is solved for the scalar, such that it remains conserved. Therefore, in order to gain insights into mixing models in the context of flamelet modeling, we need to work in the framework of a conserved scalar. To this end, we assume unity Lewis numbers of all species, and re-run all the three test cases. This will also give us an opportunity to study the effect of differential diffusion on global parameters, such as integrated heat release rate.

5.3.2 Effect of differential diffusion on ignition

Firstly, to confirm that differential diffusion is negligible for the unity Lewis number simulations, the budget terms of Equation 5.15 are plotted in Figure 5.9(b). We indeed find that the mean scalar dissipation rate balances the time rate of change of Z variance, such that there is no contribution of differential diffusion.

Next, let us see how differential diffusion impacts ignition. Figures 5.10 show the integrated heat release rate for all the three cases with and without unity Lewis number assumption. There has been a previous study [102] on the influence of differential diffusion on ignition of thermally stratified mixtures, and it was found that the effect becomes more prominent for larger stratification levels. The present study gives us a chance of extending the analysis to muxutres with both thermal and compositional stratifications.

From Figure 5.10(b), it can be seen that differential diffusion has the largest effect

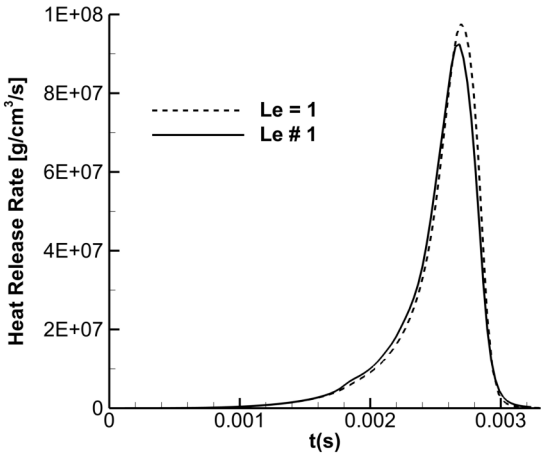

(a) Case A

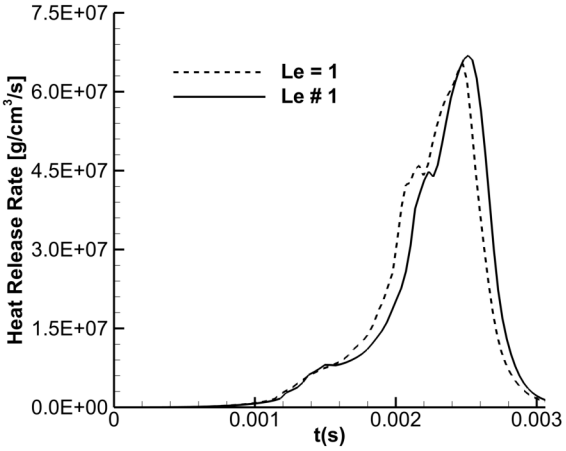

(b) Case B

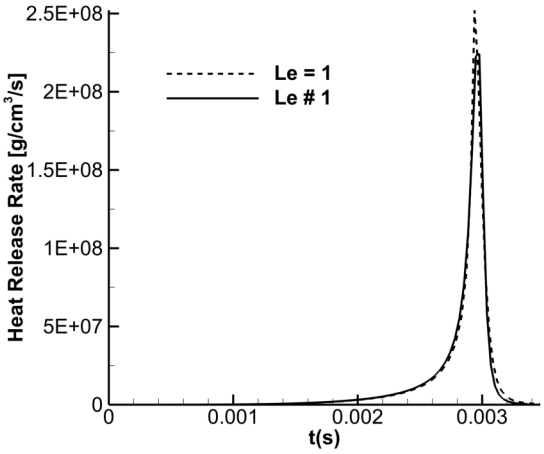

(c) Case C

Figure 5.10: Effect of differential diffusion on integrated heat release rate

on case B, where the ignition delay is reduced from its original value. There is a marginal effect on case C, where the magnitude of peak heat release rate increases a little bit. There is not much influence on case A. Hence, differential diffusion causes the ignition delay to reduce for positively correlated T-ϕ mixtures, and causes the peak heat release rate to increase for negatively correlated T-ϕ mixtures.

5.4 RANS modeling insights and strategies

After having identified differential diffusion as the reason for sudden rise in scalar dissipation rates during the formation and propagation of ignition fronts, let us try to find answers to the questions posed in Section 5.1.

5.4.1 PDFs

We can see from Figure 5.1(a) that the peaks shift leftwards up until 2ms. From t=1.5ms onwards, since the ignition front has formed, Z and H values within the unburned region decrease, because of differential diffusion, as explained before. Because most part of the mixture is still unburned, there is a high probability within the domain of finding low Z and low H values. Hence, the peak of the PDF shifts leftwards. But after 2ms, since the amount of unburned mixture is continuously decreasing, there is now a higher probability of finding moderately higher Z and H values. This is the reason why after 2ms, the peak shifts rightwards until it reaches the symmetry position towards the end of the combustion event. For case C (Figure 5.2(a)), which facilitates volumetric ignition, there are no sharp local gradients in Z (H has similar trends, hence not shown here), and hence no such shifts in PDF peak are observed.

Also, the magnitude of the modeled PDF is found to be smaller than the corresponding DNS profile. This is mainly because of the occurrence of small length scale ignition fronts, which create large local gradients in Z and H. Since beta PDF scales

as the volumetric mean and variance of Z (and H), it is difficult to get an accurate scaling to account for these local gradients.

Figure 5.11(a) shows that in the absence of differential diffusion there is no more leftwards shift of the peak. Also, Beta PDF 5.11(b) now matches well with DNS results. Hence, we can safely conclude that Beta PDF is a good modeling strategy for PDFs in the context of flamelet modeling.

5.4.2 Conditional scalar dissipation rates

The issues raised at the end of 5.1.2 will be discussed here. The increase in peak values of DNS profile 5.3(a) is due to the increase in gradients of Z and H during ignition front propagation because of differential diffusion. For the same test case with unity Lewis numbers 5.11, we see that the peak values don't increase as much.

Skewness towards larger Z values during ignition front propagation means that maximum scalar dissipation rates occur in fuel-rich regions. This is again attributed to differential diffusion of hydrogen from the unburned to burning mixture, thereby increasing Z gradients at higher hydrogen (thereby higher Z) locations. In the absence of differential diffusion (Figure 5.12(a)), the skewness disappears.

Also, there is a better agreement in Figure 5.13 between the DNS and model compared to Figure 5.3, as far as the magnitudes are concerned. However, there seems to be some difference in the shape of the profile. The DNS profile is twin-peaked at the lower and higher values of Z; whereas the model profile peaks at the center. This calls for further investigations into alternative ways of representing $f(Z)$, and is a subject of future study.

5.4.3 Mean scalar dissipation rates

We had seen earlier in Figure 5.5, that there is a large non-monotonic behavior of the model constants for all the three cases, more so for cases A and B. The same

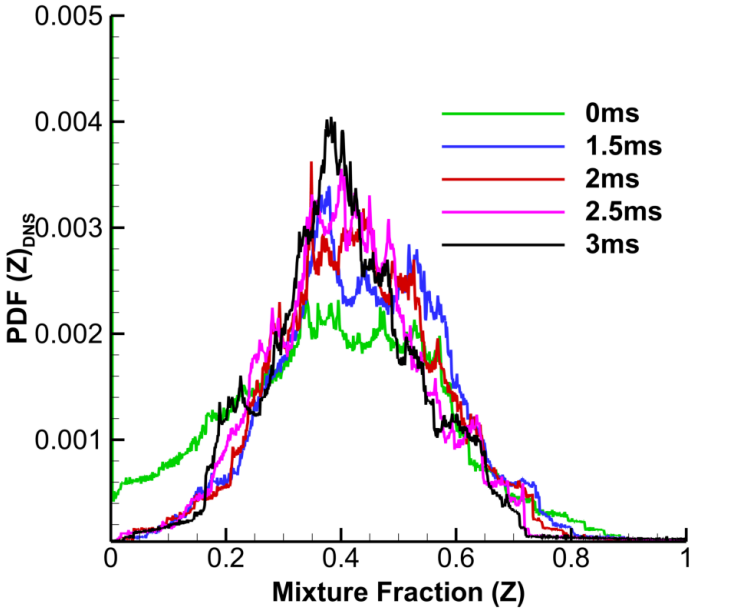

(a) PDF for Z calculated from DNS

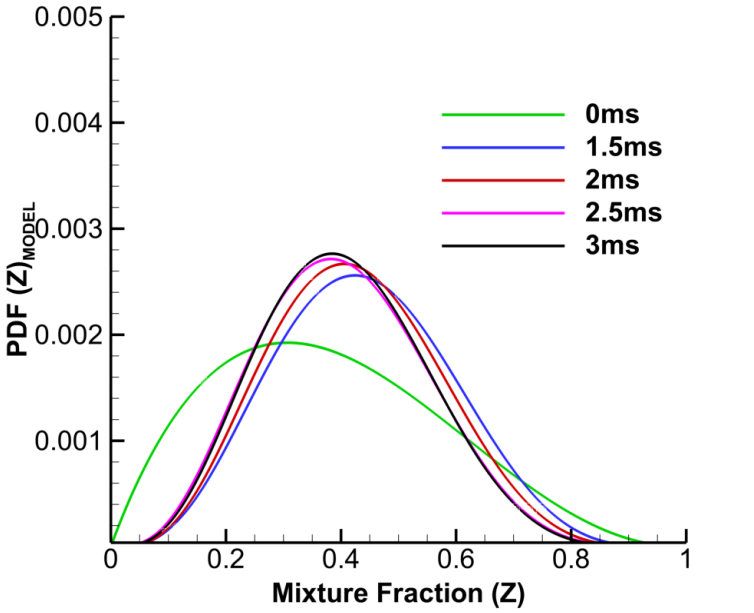

(b) Beta PDF for Z

Figure 5.11: DNS PDF vs. Beta PDF for case B, $Le_i = 1$

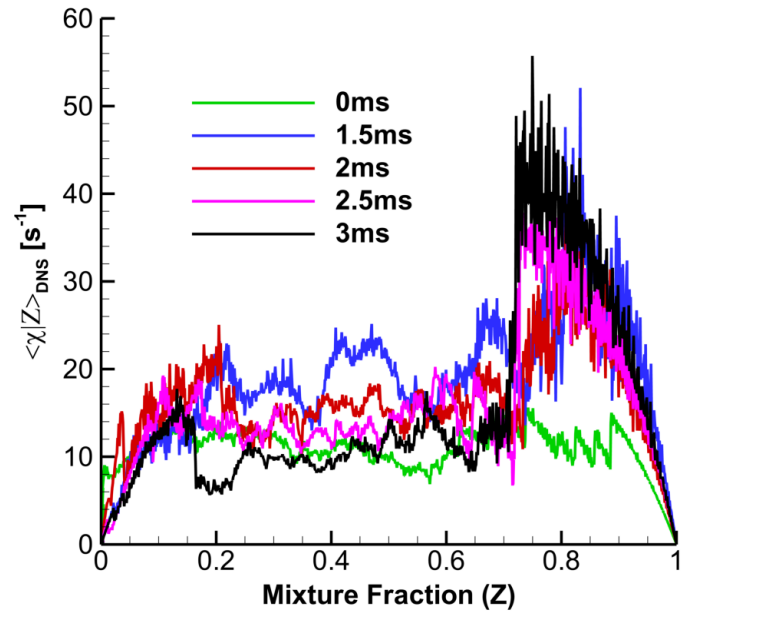

(a) $\langle \chi | Z \rangle_{DNS,mean}$

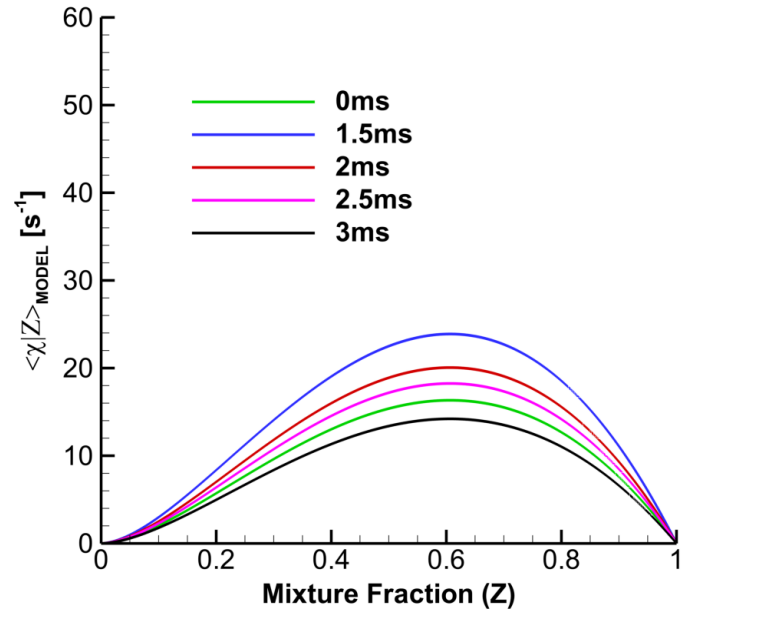

(b) $\langle \chi | Z \rangle_{MODEL}$

Figure 5.12: Comparison of $\langle \chi | Z \rangle$: DNS vs. 1D infinite mixing layer model (Case B, $Le_i = 1$)

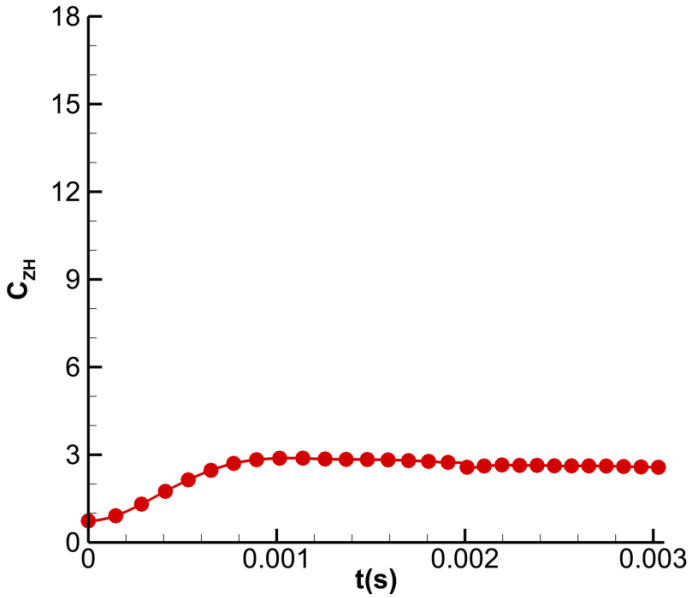

(a) Case B, ($Le_i = 1$)

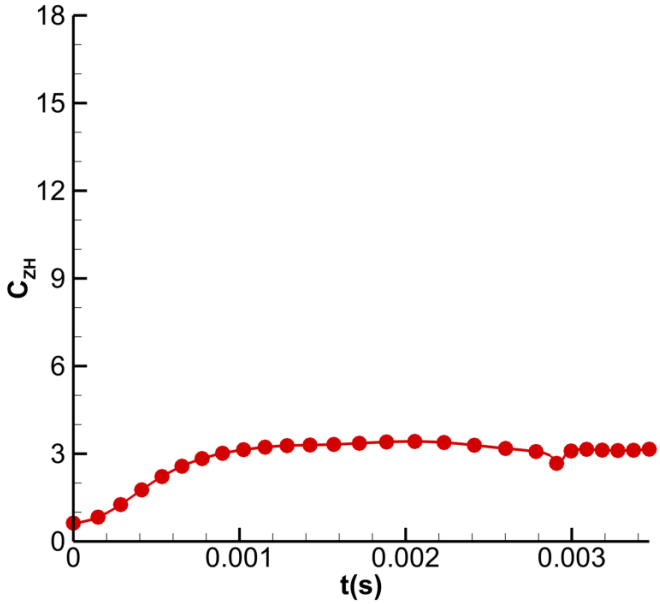

(b) Case C, ($Le_i = 1$)

Figure 5.13: Model constant for *Z-H* cross scalar dissipation rate

model constants for simulations with $Le_i = 1$ (Figure 5.5 with filled circles) give much better results, and the model constants attain a magnitude of 3.0 almost throughout the ignition event, except for the initial part which is an artifact of the initial turbulent seed. This is a very encouraging result, as it implies that the existing model for mean scalar dissipation rate works well by having a constant of proportionality of 3.0 instead of 2.0. It is of importance to note that the constant attains the same value for both Z and H, and for a multitude of different ignition regimes represented by the three test cases.

Based on the above findings, a very simplistic model for the mean cross Z-H scalar dissipation rate is proposed as:

$$\widetilde{\chi_{ZH}} = C_{ZH} \frac{\widetilde{\varepsilon}}{\widetilde{\kappa}} \sqrt{Z''^2 H''^2} \tag{5.16}$$

Figure 5.13 shows that C_{ZH} is indeed a constant with the same magnitude of 3.0

5.5 Mixing models for LES

For all the results discussed so far, the filter size (or averaging size) has been the entire volume. But, if we consider smaller filter sizes, the results could be relevant to LES. This is because the size of resolved eddies in LES is smaller than that in RANS. So, we next attempt to extend our study to LES by decreasing the filter size. Generally, the LES filter size is such that it is able to capture the large energy containing eddies, but it is not large enough to properly capture the scalar dissipation rate [103]. Figure 5.14 shows the typical profile of scalar dissipation rate relevant to our test cases, extracted from case B at 2ms. Its thickness is around 0.0058cm.

For LES applications, the filter size should lie between the Taylor microscale (λ) and the Integral length scale L [103]. These scales are related as [104]

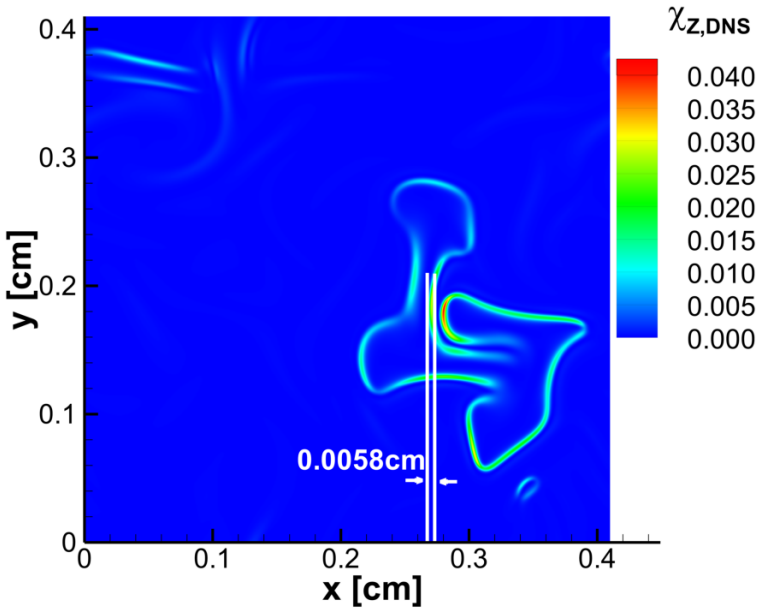

Figure 5.14: Characteristic thickness of H scalar dissipation rate (2ms, case B)

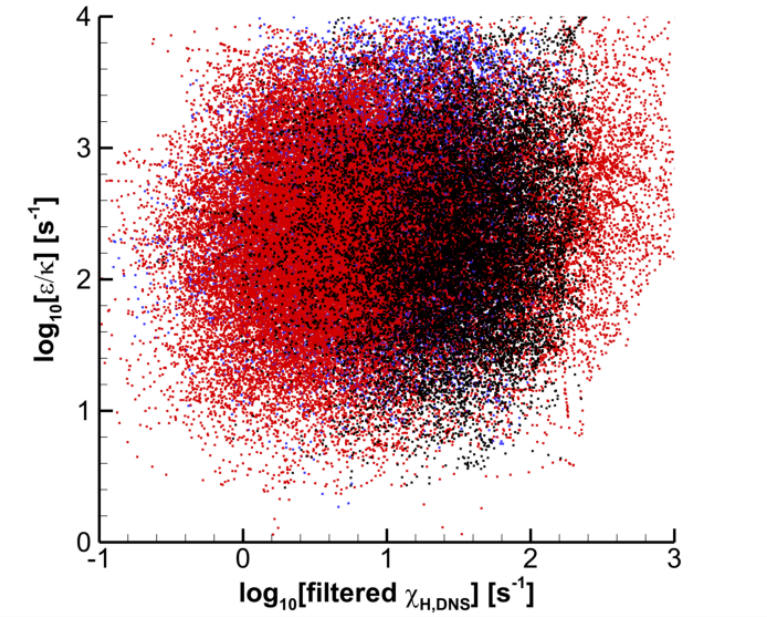

Figure 5.15: Correlation of inverse eddy turnover time with filtered $\chi_{Z,DNS}$ (filter size = $30\Delta_{DNS}$, case B)

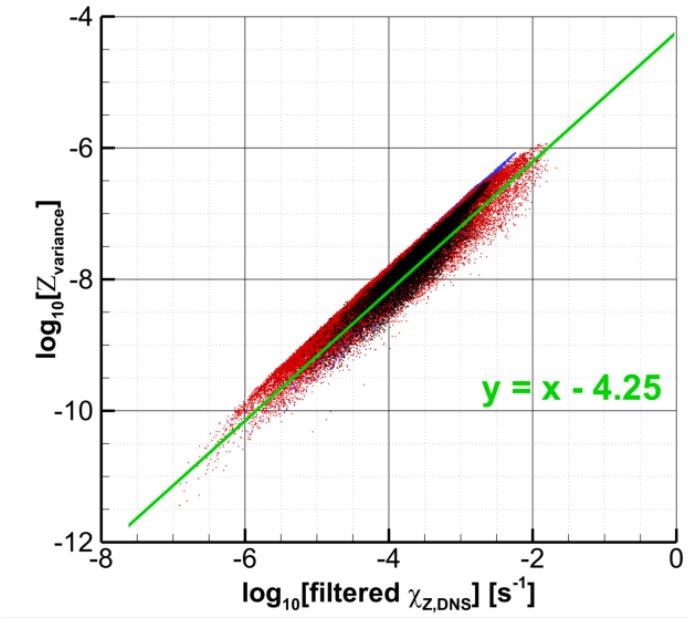

(a) for Z

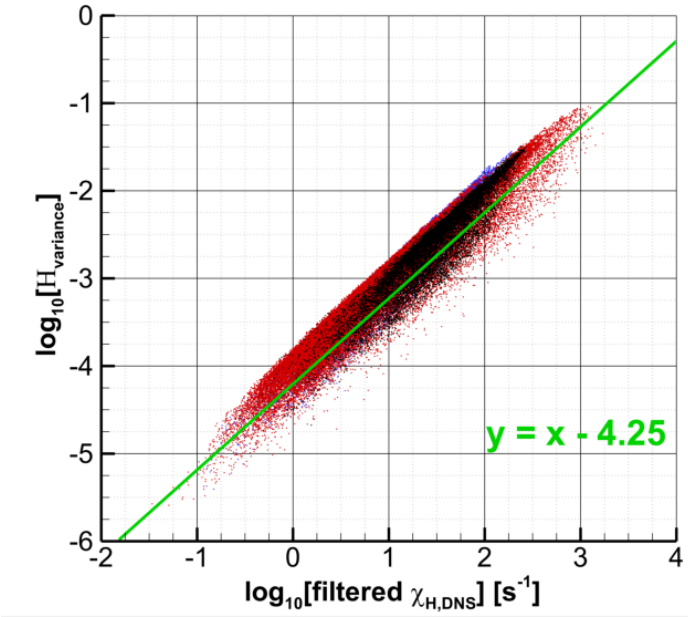

(b) for H

Figure 5.16: Mean scalar dissipation rates (filter size = $30\Delta_{DNS}$), case B

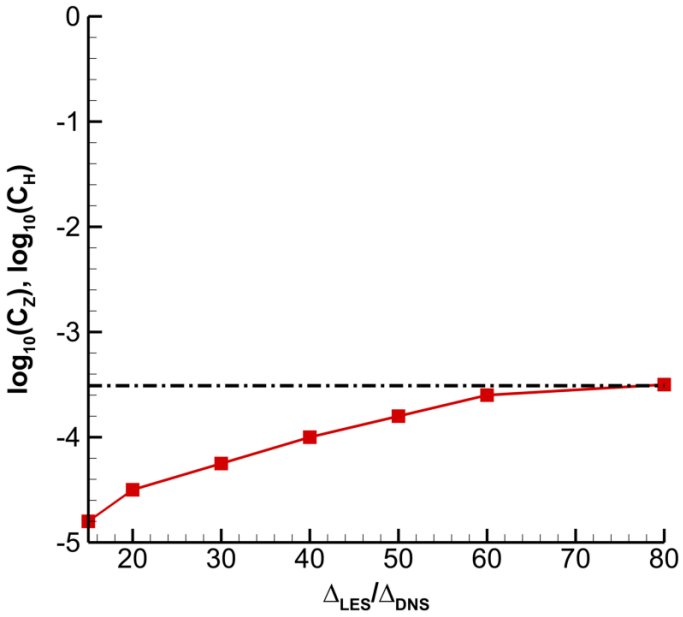

Figure 5.17: Variation of the model constants with filter size

$$\frac{\lambda}{L} \sim (Re_L)^{-1/2} \tag{5.17}$$

For our test cases, $L = 0.34mm$, and $Re_L = 50$. From Equation 5.17, $\lambda \sim 0.048mm$. Also, $\Delta_{DNS} = 0.00427mm$

Hence, the following are the upper and lower bounds for filter sizes applicable to LES studies:

$$\frac{\Delta_{filter,min}}{\Delta_{DNS}} \sim \frac{\lambda}{\Delta_{DNS}} \sim 12 \tag{5.18}$$

$$\frac{\Delta_{filter,max}}{\Delta_{DNS}} \sim \frac{L}{\Delta_{DNS}} \sim 80 \tag{5.19}$$

Based on the above discussions, we take the filter size as $30\Delta_{DNS}$, which is 0.0128cm (more than twice the size of the scalar dissipation rate thickness in Figure 5.14).

As a first step in model formulation, we compare the turbulence and mixing timescales. Here, we present results for case B only, since the RANS study showed

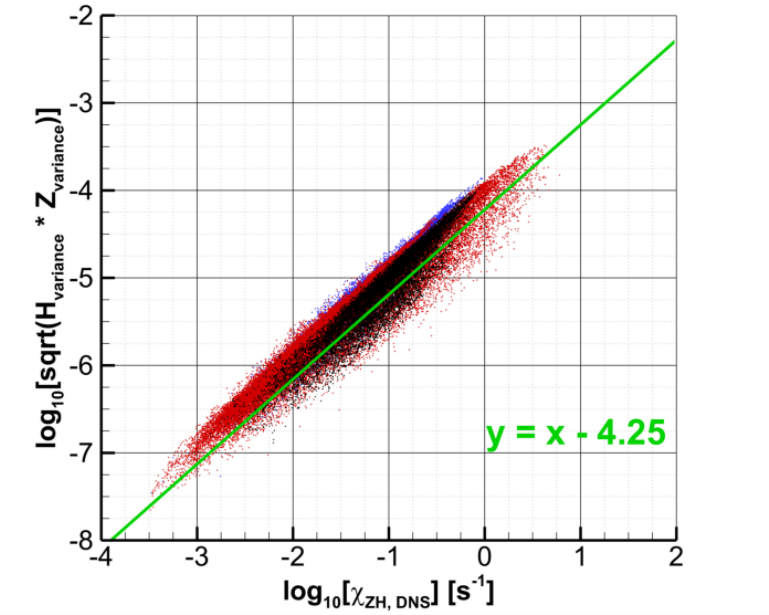

Figure 5.18: Model for mean cross scalar dissipation rate

maximum modeling challenges for this test case. Results for other cases were found to be similar. From figure 5.15, we see that turbulence is completely uncorrelated with the mean scalar dissipation rate. This suggests that the energy containing turbulence length scales are much larger than the filter size, and so are not able to affect mixing in any way.

The characteristic time scale model proposed by [105] contains only the variances and inverse eddy turnover time. Since we already found that turbulence is uncorrelated with mixing, we are inspired to next compare the correlation of the mean scalar dissipation rates with just the scalar variances. Figures 5.16(a) and 5.16(b) show the correlation of the variance of Z and H with the corresponding mean scalar dissipation rates. The results are excellent, which suggest the following modeling strategy:

$$\widetilde{\chi_Z} = C_Z \widetilde{Z''^2} \tag{5.20}$$

$$\widetilde{\chi_H} = C_H \widetilde{H''^2} \tag{5.21}$$

With C_Z and C_H having a constant value of $10^{-4.25}s^{-1}$ for the filter size considered herein. Figure 5.14 shows the variation of these constants with the filter size. Within LES bounds, C_Z and C_H asymptote to a value of $10^{-3.5}s^{-1}$.

This simple model implies that the mixing timescales for Z and H are constant and moreover have the same value. The same magnitude of the constants C_Z and C_H was observed for all the other test cases. This suggests that C_Z and C_H are independent of the type of correlation of compositional fluctuations with temperature fluctuations.

The results were also found to be the same for test cases with unity Lewis numbers, suggesting that differential diffusion is not important. Hence, it can be safely concluded that in the context of LES, mixing is not influenced by either turbulence or ignition.

Based on the above findings, a simplistic model for mean cross scalar dissipation rate is proposed:

$$\chi_{ZH} = C\sqrt{\widetilde{Z''^2}\widetilde{H''^2}} \tag{5.22}$$

Figure 5.18 shows that the model gives excellent results, with the same magnitude of the constant of proportionality as before.

5.6 Concluding Remarks

The main conclusions of this study are briefly summarized. In the context of RANS: The existing models of PDFs, and mean and conditional scalar dissipation rates don't perform well because they don't account for the local rise in scalar dissipation rate caused by differential diffusion of hydrogen from unburned region to burning region at the onset of ignition front formation. It was found that differential diffusion reduces the ignition delay more for mixtures with positive thermal and compositional stratifications. After discarding the differential diffusion effect by assuming unity Lewis numbers for all species, the following key conclusions can be drawn:

- The model constants for mean scalar dissipation rate, C_Z and C_H should be taken as 3.0 instead of 2.0.
- Conditional scalar dissipation rate profiles should incorporate the twin-peak behavior at low and high Z values.
- Beta-PDF gives sufficiently accurate results, and can be safely used in the model formulation.
- A simplistic model for mean cross scalar dissipation rate was proposed based on the square root of variances of Z and H, and gave good results.

In the context of LES, it was found that mixing is completely uncorrelated with turbulence. A simplistic model for mean scalar dissipation rates based on a constant mixing timescale was proposed. The mixing timescale was found to asymptote to a magnitude of $10^{-3.5}$s at the integral length scale filter for both Z and H and for all test cases. A simplistic model for mean cross scalar dissipation rate was also proposed based on the square root of variances of Z and H, and it gave good results.

CHAPTER VI

Conclusions and Future Work

This dissertation was aimed at gaining fundamental insights into ignition regime classification and turbulent mixing in LTC engines. Homogeneous, 1D laminar, and 2D turbulent model problems with hydrogen/air and n-heptane/air chemistry representing LTC conditions were simulated using direct numerical simulations (DNS).

The computational singular perturbation (CSP) analysis of hydrogen/air mixtures was used to develop a novel diagnostic strategy, based on the number of exhausted modes (M) and the slow importance index of transport of temperature (I^T), to identify various ignition regimes: homogeneous explosion, spontaneous propagation and deflagration. The new tool provided useful insights into the influence of n-heptane/air NTC chemistry on the prominence of ignition regimes. It was revealed that 1^{st} stage of ignition is either deflagration or spontaneous ignition depending on the level of stratifications, but the 2^{nd} stage is always spontaneous ignition, because of the presence of radical species left behind by the 1^{st} stage ignition front in the upstream mixture.

Many insights into the complex phenomenon of turbulent mixing were obtained from the 2D DNS of hydrogen/air. It was revealed that at the onset of ignition front formation, differential diffusion increased the gradients of mixture fraction and total enthalpy, thereby making them non-conserved scalars. This resulted in poor perfor-

mance of the existing RANS mixing models. By discarding the effect of differential diffusion in DNS, the existing models performed better, but with a different constant of proportionality. In the LES context, however, the differential diffusion effect was not found to be as critical in subgrid mixing models. One of the most important conclusions for LES applications was that turbulence and mixing were almost completely uncorrelated, suggesting a higher anticipation in developing improved models for scalar dissipation rates.

Key findings of the dissertation are summarized below.

6.1 Conclusions

6.1.1 Identification of ignition regimes in hydrogen/air mixtures using CSP analysis

CSP was utilized as a diagnostic tool to classify various ignition regimes in the auto-ignition of lean hydrogen-air mixture relevant to LTC conditions. Consistent with previous studies, an explosive eigenvalue analysis was carried out for the homogeneous problem, and it was found that two branches of explosive eigenvalues (corresponding to chain-branching and thermal ignition) exist in the high pressure environment. The merging point of these two branches was found to be a good indicator of the completion of the explosive phase of ignition. However, it was further found that the occurrence of the merging-point was not sufficient as a diagnostic indicator to distinguish between different ignition regimes. An alternative metric based on the exhausted mode analysis was proposed.

Exhausted time-scales were first identified based on the relative and absolute error thresholds. The number of exhausted modes, denoted by M, showed distinct values in the active reaction zone, the downstream zone and the near-equilibrium product zone. The front structure was identified by the pattern of M = 2-3-2-1 (from upstream to

downstream) near the propagating front. The presence of the $M = 3$ layer was found to be a useful indicator to identify the direction of the front propagation. Using the M diagnostics, the relative dominance between transport and chemistry in the upstream zone was investigated by defining the importance index based on the slow dynamics of temperature. In the $M = 2$ region ahead of the active reaction zone, $I^T = 1$ implies pure deflagration, whereas $I^T = 0$ implies pure spontaneous ignition. The magnitude of I^T thus determines the quantitative measure of the dominant characteristics of the ignition front. The new criterion serves as a generalized diagnostic tool to characterize the ignition process under steady and unsteady conditions without relying on intuitive decision.

The CSP-based diagnostics was subsequently applied to 2-D constant volume ignition with temperature inhomogeneities. The results showed that the new diagnostic tool properly captures regions of interest and identifies the ignition regimes under hostile condition of multi-dimensional, turbulent, mixed-mode combustion events.

6.1.2 Auto-ignition characteristics of n-heptane/air mixtures using CSP

This study demonstrated that CSP analysis serves as a powerful automated tool to distinguish explosive/dissipative and active/exhausted modes for highly complex chemically reacting systems such as the n-heptane/air auto-ignition. The CSP analysis also facilitates detailed investigation of dominant reaction processes at various stages of transient events by examining the importance index associated with the fastest active $(M + 1)$ mode. Furthermore, identification of auto-ignition regimes can be easily achieved by examining the importance index of transport processes to the slow dynamics of temperature.

Homogeneous ignition at both non-NTC and NTC conditions were examined in order to assess the validity of the CSP analysis in understanding chemical processes of n-heptane auto-ignition. It was found that the merging of two explosive modes

appears to be a universal signature of onset of both 1^{st} and 2^{nd} stage auto-ignition. Monitoring the number of explosive modes (M) was found to be an effective way to detect abrupt transient phenomena resulting from complex chemical systems with a large number of time scales. Detailed investigations into the reaction steps contributing to mode $M + 1$ clearly revealed the key chemical processes responsible for the ignition dynamics.

Ignition regime identification was subsequently studied by analyzing 1D simulations with temperature and concentration stratifications. A key fundamental issue was to understand the effects of the NTC chemistry on the relative importance between different ignition regimes. For the conditions considered, the non-NTC case exhibited ignition transition from the nearly deflagration to spontaneous ignition regimes during the evolution. For the NTC case, the 1^{st} stage ignition front was found to be highly deflagrative, which was attributed to the reduced active chemical time scales combined with relatively low reactivity in the upstream mixture. On the other hand, the 2^{nd} stage ignition front was found to be mostly in the spontaneous propagation regime, due to the larger production of active radicals left behind the 1^{st} stage ignition front. When additional concentration stratification is added to the temperature field, the positively-correlated cases yielded more deflagrative fronts, while the negatively-correlated cases (which correspond to exhaust gas mixing in engines) showed more pronounced spontaneous propagation regime.

Finally, to study the effect of turbulence on ignition regimes, two cases of 2D turbulent ignition with the same initial thermal fluctuation level, but with different initial mean temperatures (corresponding to NTC and non-NTC chemistry, respectively), were conducted. The dominant ignition regimes for both cases were found to be similar to those observed in 1D studies, suggesting that turbulence has little influence on ignition for the levels of thermal fluctuations considered.

6.1.3 Modeling of turbulent mixing in LTC conditions

This study provided fundamental insights into development of mixing models for RANS and LES modeling of stratified LTC using the flamelet approach. The reference DNS data pertained to three model problems of 2D turbulent ignition of hydrogen/air system with thermal and compositional inhomogeneities, corresponding to different ignition regimes.

In the RANS context, the existing models for PDFs of Z and H were considered. It was found that beta pdfs of Z and H yielded sufficiently accurate results, and thus can be safely used in the scalar dissipation rate modeling. Next, the existing model for the mean scalar dissipation rates, which is based on mixing timescale being proportional to the turbulent timescale, the constant of proportionality being $C = \tau_{turb}/\tau_{mix}$, was tested against DNS data. C was plotted for various test cases representing different ignition regimes, and it was observed that C attained a constant value prior to ignition, but as soon as the ignition fronts started to form, C became non-monotonic. The reason was identified as the increase in local scalar dissipation rate due to differential diffusion of hydrogen from the unburned to burning region. To verify that differential diffusion was indeed the cause, same test cases were repeated by artificially modifying transport properties such that the Lewis number for all species was assumed to be unity. The results confirmed that C remains constantat 3.0 for both Z and H throughout the entire ignition event. This demonstrated that differential diffusion plays a very crucial role in mixing, and it should be properly accounted for in the flamelet equations. The results also suggested that even with the unity Lewis number assumption for all species, the accurate value of C is close to 3.0 instead of 2.0 adopted in the existing models.

The conditional scalar dissipation rate model development had two-fold challenges: (i) to properly account for the scaling factor, and (ii) to account for the shape of the assumed function $f(Z)$. By discarding the differential diffusion, the scaling factor

was properly accounted for by the 1D doubly-infinite mixing layer model. Differential diffusion was also found to be responsible for the skewness of scalar dissipation rates towards higher Z values. The shape of DNS profile had two peaks, whereas the model profile exhibited a single peak. This inconsistency calls for further investigation into this subject.

For filter sizes corresponding to LES, it was revealed that turbulence is almost completely uncorrelated with mixing, and that the mean scalar dissipation rates can be simply modeled as being proportional to the corresponding scalar variances, the constant of proportionality turning out to be the same for Z and H. Based on this finding, a new model for cross scalar dissipation rate was proposed and it gave excellent correlations.

6.2 Directions for future work

In this dissertation, we have used high-fidelity DNS and various computational analysis tools to gain fundamental insights into ignition regimes and mixing in LTC engines. In order to better understand the underlying physics and for the subsequent implementation of LTC technology, there is a large scope for improvement in the areas of DNS, computational analysis strategies, and modeling of combustion and mixing.

Right now, we have conducted DNS studies with 2D turbulence, but turbulence is inherently a three-dimensional phenomenon. In 2D DNS, the three-dimensional vortex stretching term does not appear. Hence, it is a diminished representation of the realistic 3D picture. 3D DNS is difficult to perform because of the following challenges: (i) an exorbitant requirement of computing resources, (ii) difficulty in post-processing because of large data size, (iii) need for good feature-detection tools. Nevertheless, in recent years, there have been some efforts into performing 3D DNS studies [106]. Performing ignition regime identification and mixing studies for a realistic 3D turbulent ignition of large hydrocarbons will reveal better insights into LTC

behavior. The 2D DNS results presented in this dissertation will then provide as a basis for the analysis of 3D results.

Owing to environmental concerns, the use of bio-fuels is becoming more prominent. Performing DNS of such new fuels requires generation of efficient reduced chemical mechanisms, which can reduce the number of species and reactions, and at the same time not compromise on the solution accuracy. Development of such reduced mechanisms is another upcoming research direction. CSP has been used in the past for mechanism reduction as it can identify quasi steady state species and unimportant reactions through CSP radicals and importance indices. Moreover, even for solution of such highly stiff problems, CSP can be used on-the-fly to eliminate the fast exhausted timescales, thereby allowing the use of a much larger time step for DNS.

As 3D DNS becomes more common, the need for development of reliable data analysis or feature-detection tools will increase more than ever. In this dissertation, we have presented one such tool based on CSP, by combining M and I^T diagnostics. Many other criteria can be derived catering to different physical problems, based on the rich information produced by CSP analysis. The most significant contribution although, could be to develop a predictive tool instead, which could potentially give insights based on initial conditions. This is not a trivial task, as it would require a great depth of physical insights about a particular problem, and diagnostic studies such as the one presented here will serve as a first step in that direction. Another important area of research is to develop diagnostic tools to analyze the full cycle engine simulation data, which would be much more relevant to the experimentalists.

In terms of the full-cycle engine simulations, the use of LES is becoming more prominent, as it forms a bridge between industrial applications (RANS) and fundamental studies (DNS). One of the limitations of DNS is the possibility of very small domain sizes, because of which very low Reynolds numbers are attainable, and many

physical phenomenon involving the effects of turbulence on mixing and ignition are not properly accounted for. Moreover, as opposed to DNS, practical engine geometries can also be utilized in LES. Hence, the way to move forward is to use DNS to provide modeling insights for LES, and to use LES to study phenomena at engine length scales. Coupling LES with a good combustion model is another important area of research. Presently, there are research groups with either state of the art LES capabilities, or with advanced combustion modeling features, but only a combination of both will yield best results.

A key science question still remains as to how the inhomogeneities in temperature and mixture composition interact and correlate with one another. Insights into this issue will help in the development of better models for cross scalar dissipation rate and joint-PDFs of Z and H, which will help in the development of better mixing models. In the context of combustion modeling, over the past years, many parallel efforts have been made in the fields of flamelet modeling, multizone modeling, CMC etc. and all have given useful insights into problems of specific interest. Performing a comparative study of different combustion modeling approaches under a wide variety of operating conditions to determine the best modeling approach under LTC conditions merits further investigation.

BIBLIOGRAPHY

BIBLIOGRAPHY

[1] Gurpreet Singh. Overview of the DOE Advanced Combustion Engine Research and Development. *2011 Merit Review*. viii, 2

[2] D.J. Cook, H. Pitsch, and G. Nentwig. Numerical Investigation of Unburnt Hydrocarbon Emissions in a Homogeneous-Charge Late-Injection Diesel-Fueled Engine. *SAE Technical Paper, 2008-01-1666*, 2008. viii, 12, 13, 24

[3] U.S. Energy Information Administration (EIA). *http://eia.gov/*. 1

[4] U.S. Environmental Protection Agency (EPA). *http://epa.gov/*. 1

[5] F. Zhao, T. Asmus, D. Assanis, J. Dec, J. Eng, and P. Najt. *Homogeneous Charge Compression Ignition (HCCI) Engines, Key Research and Development Issues*. Society of Automotive Engineers, Inc., Warrendale, Pennsylvania, 2003. 2

[6] A University Consortium on Low Temperature Combustion for High-Efficiency Ultra-Low Emission Engines, directed by the University of Michigan, funded by Department of Energy under agreement DE-FC26-06NT42629. 2

[7] N. Milovanovic and R. Chen. A review of experimental and simulation studies on controlled auto-ignition combustion. *SAE Technical Report 2001-01-1890*, 2001. 2, 4

[8] D. Low and et al. 4-Stroke Active Combustion (Controlled Auto-Ignition) Investigations Using a Single Cylinder Engine with Lotus Active Valve Train (AVT). *Internal Report*, 2000. 3

[9] R.H. Thring. Homogenous Charge Compression Ignition (HCCI) Ehgines. *SAE Paper 892068*, 1989. 3

[10] P.M. Najt and D.E. Foster. Compression-Ignited Homogenous Charge Combustion. *SAE Paper 830264*, 1983. 3

[11] T. Aoyama, Y. Hattori, J. Mizuta, and Y. Sato. An Experimental Study on Premixed-Charge Compression Ignition Gasoline Engines. *SAE Paper 960081*, 1996. 3

[12] H. Yanagihara, Y. Sato, and M. Junichi. A Study of Diesel Combustion under Uniform Higher-Dispersed Mixture Formation. *JSAE 9733675*, 1997. 3

[13] J. Eng. Characterization of Pressure Waves in HCCI Combustion. *SAE Technical Paper, 2002-01-2859*, 2002. 3

[14] J. Dec. A Computational Study of the Effects of Low Fuel Loading and EGR on Heat Release Rates and Combustion Limits in HCCI Engines. *SAE Technical Paper, 2002-01-1309*, 2002. 3

[15] J. Yang, T. Culp, and T. Kenney. Development of a Gasoline Engine System Using HCCI Technology: The Concept and the Test Results. *SAE Technical Paper, 2002-01-2832*, 2002. 4

[16] J. Martinez-Frias, S.M. Aceves, D.L. Flowers, J.R. Smith, and R. Dibble. HCCI Engine Control by Thermal Management. *SAE Paper 2000-01-2869*, 2000. 4

[17] M. Christensen, A. Hultqvist, and B. Johansson. Demonstrating the Multi Fuel Capability of a Homogeneous Charge Compression Ignition Engine with Variable Compression Ratio. *SAE Paper 1999-01-3679*, 1999. 4

[18] N.B. Kaahaaina, A.J. Simon, P.A Caton, and C.F. Edwards. Use of Dynamic Valving to Achieve Residual-Affected Combustion. *SAE Paper 2001-01-0549*, 2001. 4

[19] T. Noda and D. Foster. A Numerical Study to Control Combustion Duration of Hydrogen-Fueled HCCI by Using Multi-Zone Chemical Kinetics Simulation. *SAE Technical Paper, 2001-01-0250*, 2001. 4

[20] M. Sjöberg, J. E. Dec, and N. P. Cernansky. Potential of Thermal Stratification and Combustion Retard for Reducing Pressure-Rise Rates in HCCI Engines, Based on Multi-Zone Modelling and Experiments. *SAE Technical Paper, 2005-01-0113*, 2005. 5

[21] John E. Dec, Hwang Wontae, and Magnus Sjberg. An Investigation of Thermal Stratification in HCCI Engines Using Chemiluminescence Imaging. *SAE Technical Paper, 2006-01-1518*, 2006. 5, 6, 50

[22] Satoshi S. Morimoto, Yasuharu Kawabata, Teruhiro Sakurai, and Toshiji Amano. Operating Characteristics of a Natural Gas-Fired Homogeneous Charge Compression Ignition Engine (Performance Improvement Using EGR). *SAE Technical Paper, 2001-01-1034*, 2001. 5

[23] M. Richter, J. Engstrom, A. Franke, M. Alden, A. Hultqvist, and B. Johansson. The Influence of Charge Inhomogeneity on the HCCI Combustion Process. *SAE Technical Paper, 2000-01-2868*, 2000. 5

[24] H. Zhao, Z. Peng, J. Williams, and N. Ladommatos. Understanding the Effects of Recycled Burnt Gases on the Controlled Autoignition (CAI) Combustion in Four-Stroke Gasoline Engines. *SAE Technical Paper, 2001-01-3607*, 2001. 5

[25] James W. Girard, Robert W. Dibble, Daniel L. Flowers, and Salvador M. Aceves. An Investigation of the Effect of Fuel-Air Mixedness on the Emissions from an HCCI Engine. *SAE Technical Paper, 2002-01-1758*, 2002. 5

[26] R. E. Herold, J. M. Krasselt, D. E. Foster, and J. B. Ghandhi. Investigations into the Effects of Thermal and Compositional Stratification on HCCI Combustion - Part II: Optical Engine Results. *SAE Technical Paper, 2009-01-1106*, 2009. 5

[27] S.M. Aceves, D.L. Flowers, C.K. Westbrook, J.R. Smith, W. Pitz, R. Dibble, M. Christensen, and B. Johansson. A Multi-Zone Model for Prediction of HCCI Combustion and Emissions. *SAE Technical Paper, 2000-01-0327*, 2000. 5, 12

[28] A. Hultqvist, M. Christensen, B. Johansson, M. Richter, J. Nygren, J. Hult, and M. AldJn. The HCCI Combustion Process in a Single Cycle Speed Fuel Tracer LIF and Chemiluminescence Imaging. *SAE Paper 2002-01-0424*, 2002. 6

[29] E.W. Kaiser, J. Yang, T. Culp, N. Xu, and M.M. Maricq. Homogeneous charge compression ignition engine-out emissions does flame propagation occur in homogeneous charge compression ignition? *International Journal of Engine Research*, 3, 2002. 6

[30] S.M. Walton, X. He, B.T. Zigler, M.S. Wooldridge, and A. Atreya. An experimental investigation of iso-octane ignition phenomena. *Combustion and Flame*, 150:246–262, 2007. 6

[31] B.T. Zigler, S.M. Walton, D. Assanis, E. Perez, M.S. Wooldridge, and S.T Wooldridge. An experimental investigation of iso-octane ignition phenomena. *Journal of Engineering for Gas Turbines and Power*, 130:052803–1, 2008. 6

[32] YA.B. Zeldovich. Regime Classification of an Exothermic Reaction with Nonuniform Initial Conditions. *Combustion and Flame*, 39:211–214, 1980. 6, 27, 47

[33] X.J. Gu, D.R. Emerson, and D.B. Bradley. Modes of reaction front propagation from hot spots. *Combustion and Flame*, 133:63–74, 2003. 7, 47

[34] R. Sankaran, H.G. Im, E.R. Hawkes, and J.H. Chen. The effects of non-uniform temperature distribution on the ignition of a lean homogeneous hydrogenair mixture. *Proceedings of the Combustion Institute*, 30:875–882, 2005. 7, 47, 51

[35] E.R. Hawkes, R. Sankaran, P. Pebay, and J.H. Chen. Direct numerical simulation of ignition front propagation in a constant volume with temperature inhomogeneities II. Parametric study. *Combustion and Flame*, 145:145–159, 2006. 7, 11, 47

[36] G. Bansal and H.G. Im. Autoignition and front propagation in low temperature combustion engine environments. *Combustion and Flame*, 158:2105–2112, 2011. 7, 11, 28, 47, 51, 74, 76

[37] J.B. Martz, H. Kwak, H.G. Im, G.A. Lavoie, and D.N. Assanis. Combustion regime of a reacting front propagating into an auto-igniting mixture. *Proceedings of the Combustion Institute*, 33:3001–3006, 2011. 7, 47

[38] J.B. Martz, G.A. Lavoie, H.G. Im, R.J. Middleton, A. Babajimopoulos, and D.N. Assanis. The propagation of a laminar reaction front during end-gas auto-ignition. *Combustion and Flame*, 159:2077–2086, 2012. 7, 47

[39] S.H. Lam and D.A. Goussis. Understanding Complex Chemical Kinetics with Computational Singular Perturbation. *Twenty-Second Symposium (International) on Combustion*, pages 931–941, 1988. 8, 28

[40] D. Goussis, S.H. Lam, and P. Gnoffo. Reduced and Simplified Chemical Kinetics for Air-Dissociation Using Computational Singular Perturbation. *28th Aerospace Sciences Meeting, AIAA-90-0644*. 8, 28

[41] S.H. Lam. Using CSP to Understand Complex Chemical Kinetics. *Combustion Science and Technology*, 89, 1993. 8, 17

[42] S.H. Lam and D.A. Goussis. The CSP Method for Simplifying Kinetics. *International Journal of Chemical Kinetics*, 26:461–486, 1994. 8, 21

[43] M. Valorani, H.N. Najm, and D.A. Goussis. CSP analysis of a transient flame-vortex interaction: time scales and manifolds. *Combustion and Flame*, 134:35–53, 2003. 9, 16, 28, 31, 34, 36, 38, 49, 56

[44] Andrei Kazakov, Marcos Chaos, Zhenwei Zhao, and Frederick L. Dryer. Computational Singular Perturbation Analysis of Two-Stage Ignition of Large Hydrocarbons. *The Journal of Physical Chemistry A*, 110, 2006. 9, 48

[45] D.A. Goussis and H.N. Najm. Model Reduction and Physical Understanding of Slowly Oscillating Process: The Circadian Cycle. *Multiscale Modeling and Simulation*, 5, 2006. 9

[46] T. Lu and C.K. Law. A criterion based on computational singular perturbation for the identification of quasi steady state species: A reduced mechanism for methane oxidation with NO chemistry. *Combustion and Flame*, 154:761–774, 2008. 9, 31, 34

[47] T.F. Lu, C.S. Yoo, J.H. Chen, and C.K. Law. Three-dimensional direct numerical simulation of a turbulent lifted hydrogen jet flame in heated coflow: a chemical explosive mode analysis. *Journal of Fluid Mechanics*, 652:45–64, 2010. 9, 55

[48] M. Christensen, B. Johansson, and A. Hultqvist. The Effect of Combustion Chamber Geometry on HCCI Operation. *SAE Technical Paper, 2002-01-0425*, 2002. 11

[49] M. Christensen and B. Johansson. The Effect of In-Cylinder Flow and Turbulence on HCCI Operation. *SAE Technical Paper, 2002-01-2864*, 2002. 11

[50] S.C. Kong, R.D. Reitz, M. Christensen, and B. Johansson. Modeling the Effects of Geometry Generated Turbulence on HCCI Engine Combustion. *SAE Technical Paper, 2003-01-1088*, 2003. 11, 12

[51] Y.Z. Zhang, E.H. Kung, and D.C. Haworth. A PDF method for multidimensional modeling of HCCI engine combustion: effects of turbulence/chemistry interactions on ignition timing and emissions. *Proceedings of the Combustion Institute*, 30:2763–2771, 2005. 11

[52] J.H. Chen, E.R. Hawkes, R. Sankaran, S.D. Mason, and H.G. Im. Direct numerical simulation of ignition front propagation in a constant volume with temperature inhomogeneities I. Fundamental analysis and diagnostics. *Combustion and Flame*, 145:128–144, 2006. 11, 28, 47, 51

[53] R.W. Bilger, S.B. Pope, K.N.C. Bray, and J.F. Driscoll. Paradigms in turbulent combustion research. *Proceedings of the Combustion Institute*, 30:21–42, 2005. 12

[54] S.B. Fiveland and D.N. Assanis. Development of a Two-Zone HCCI Combustion Model Accounting for Boundary Layer Effects. *SAE Technical Paper, 2001-01-1028*, 2001. 12

[55] M. Kraft, P. Maigaard, F. Mauss, M. Christensen, and B. Johansson. Investigation of Combustion Emissions in a Homogeneous Charge Compression Injection Engine: Measurements and a New Computatinal Model. *Proceedings of the Combustion Institute*, 28:1195–1201, 2000. 12

[56] M. Embouazza, D.C. Haworth, and N. Darabiha. Implementation of Detailed Chemical Mechanisms into Multidimensional CFD Using in situ Adaptive Tabulation: Application to HCCI Engines. *SAE Technical Paper, 2002-01-2773*, 2002. 12

[57] F. Bisetti, J.Y. Chen, E.R. Hawkes, and J.H. Chen. Probability density function treatment of turbulence/chemistry interactions during the ignition of a temperature-stratified mixture for application to HCCI engine modeling. *Combustion and Flame*, 155:571–584, 2008. 12

[58] D.J. Cook, H. Pitsch, J.H. Chen, and E.R. Hawkes. Flamelet-based modeling of auto-ignition with thermal inhomogeneities for application to HCCI engines. *Proceedings of the Combustion Institute*, 31:2903–2911, 2007. 12, 75

[59] N. Peters. Laminar Diffusion Flamelet Models in Non-Premixed Turbulent Combustion. *Progress in Energy and Combustion Science*, 10:319–339, 1984. 12, 25, 81

[60] H. Pitsch, Y.P. Wan, and N. Peters. Numerical Investigation of Soot Formation and Oxidation Under Diesel Engine Conditions. *SAE Technical Paper, 952357*, 1995. 12

[61] N. Peters. *Turbulent Combustion*. Cambridge University Press, 2002. 13, 24, 25

[62] H. Pitsch, H. Barths, and N. Peters. Three-Dimensional Modeling of NOx and Soot Formation in DI-Diesel Engines Using Detailed Chemistry Based on the Interactive Flamelet Approach. *SAE Technical Paper, 962057*, 1996. 13

[63] M. Valorani, D.A. Goussis, F. Creta, and H.N. Najm. Higher order corrections in the approximation of low-dimensional manifolds and the construction of simplified problems with the CSP method. *Journal of Computational Physics*, 209:754–786, 2005. 19

[64] M. Valorani, F. Creta, D.A. Goussis, J.C. Lee, and H.N. Najm. An Automatic Procedure for the Simplification of Chemical Kinetic Mechanisms Based on CSP. *Combustion and Flame*, 146, 2006. 20, 21, 49

[65] J.C. Lee, H.N. Najm, S. Lefantzi, J. Ray, M. Frenklach, M. Valorani, and D.A. Goussis. A CSP and Tabulation-based Adaptive Chemistry Model. *Combustion Theory and Modelling*, 11, 2007. 21

[66] A. Zagaris, H.G. Kaper, and T.J. Kaper. Analysis of the Computational Singular Perturbation Reduction Method for Chemical Kinetics. *Journal of Nonlinear Science*, 14, 2004. 21

[67] A. Zagaris, H.G. Kaper, and T.J. Kaper. Two Perspectives on Reduction of Ordinary Differential Equations. *Mathematische Nachrichten*, 278, 2005. 21

[68] H.G. Im, A. Trouvé, C.J. Rutland, and J.H. Chen. Terascale high-fidelity simulations of turbulent combustion with detailed chemistry. *Available from: http://purl.org/net/tstc*, 2005. 22

[69] C.S. Yoo. Direct Numerical Simulations of Strained Laminar and Turbulent Nonpremixed Flames: Computational and Physical Aspects. *Ph.D. Dissertation, University of Michigan, Ann Arbor*. 22

[70] H.G. Im, A. Trouvé, C.J. Rutland, and J.H. Chen. Terascale high-fidelity simulations of turbulent combustion with detailed chemistry. *SciDAC Program, U.S. Department of Energy, Office of Basic Energy Sciences*, 2001. 22

[71] C.A. Kennedy, M.H. Carpenter, and R.H. Lewis. Low-storage, explicit Runge-Kutta schemes for the compressible Navier-Stokes equations. *Applied Numerical Mathematics*, 35:177–219, 2000. 23

[72] R.J. Kee, J.F. Grcar, M.D. Smooke, and J.A. Miller. A Fortran Program for Modeling Steady Laminar One-Dimensional Premixed Flames. *Sandia National Laboratories Report SAND85-8240*, 1985. 23

[73] M. A. Mueller, T. Kim, R. Yetter, and F. Dryer. Flow Reactor Studies and Kinetic Modeling of the H//2/O//2 Reaction. *International Journal of Chemical Kinetics*, 31:113–125, 1999. 23

[74] C.S. Yoo, T. Lu, J.H. Chen, and C.K. Law. Direct numerical simulations of ignition of a lean n-heptane/air mixture with temperature inhomogeneities at constant volume: Parametric study. *Combustion and Flame*, 158:1727–1741, 2011. 23, 48, 49, 50, 51

[75] R.J. Kee, G. Dixon-Lewis, J. Warnatz, M.E. Coltrin, and J.A. Miller. A Fortran Computer Code Package for the Evaluation of Gas-phase Multicomponent Transport Properties. *Tech. Rep. SAND86-8246, Sandia National Laboratories*, 1986. 23

[76] R.J. Kee, F.M. Rupley, E. Meeks, and J.A. Miller. CHEMKIN-III: A Fortran Chemical Kinetic Package for the Anaylsis of Gas-phase Chemical and Plasma Knietics. *Tech. Rep. SAND96-8216, Sandia National Laboratories*, 1996. 23

[77] W.P. Jones and J.H. Whitelaw. Calculation Methods for Reacting Turbulent Flows: A Review. *Combustion and Flame*, 48:1–26, 1982. 24

[78] M.R. Overholt and S.B. Pope. Direct numerical simulation of a passive scalar with imposed mean gradient in isotropic turbulence. *Physics of Fluids*, 8:3128–3148, 1996. 24

[79] A. Juneja and S.B. Pope. A DNS study of turbulent mixing of two passive scalars. *Physics of Fluids*, 8:2177–2184, 1996. 24

[80] A.W. Cook, J.J. Riley, and G. Kosly. A Laminar Flamelet Approach to Subgrid-Scale Chemistry in Turbulent Flows. *Combustion and Flame*, 109:332–341, 1997. 25

[81] H. Pitsch and N. Peters. A Consistent Flamelet Formulation for Non-Premixed Combustion Considering Differential Diffusion Effects. *Combustion and Flame*, 114:26–40, 1998. 25, 92

[82] H. Pitsch, M. Chen, and N. Peters. Unsteady Flamelet Modeling of Turbulent Hydrogen-Air Diffusion Flames. *Twenty-Seventh Symposium (International) on Combustion*, page 10571064, 1993. 25

[83] R. Sankaran and H.G. Im. Characteristics of auto-ignition in a stratified iso-octane mixture with exhaust gases under homogeneous charge compression ignition conditions. *Combustion Theory and Modelling*, 9:417–432, 2005. 28, 47

[84] G. Bansal and H.G. Im. Autoignition of Hydrogen-Air Mixture with Temperature and Composition Inhomogeneities. *47th Aerospace Sciences Meeting and Exhibit, Orlando, FL, Paper AIAA 2009-1559*. 28, 32, 34, 41

[85] D. Diamantis, D. Kyritsis, and D.A. Goussis. Two Stage Ignition of n-heptane: Identifying the Chemistry Setting the Explosive Time Scales. *Second International Workshop on Model Reduction in Reacting Flows, Notre Dame, Indiana, USA,*, March 30-April 1, 2009. 31, 55

[86] Y. Ju, W. Sun, M.P. Burke, X. Gou, and Z. Chen. Multi-timescale modeling of ignition and flame regimes of n-heptane-air mixtures near spark assisted homogeneous charge compression ignition conditions. *Proceedings of the Combustion Institute*, 33:1245–1251, 2011. 48

[87] J.E. Dec. Advanced compression-ignition enginesunderstanding the in-cylinder processes. *Proceedings of the Combustion Institute*, 32:2727–2742, 2009. 50

[88] W. Hwang, J.E. Dec, and M. Sjberg. Fuel Stratification for Low-Load HCCI Combustion: Performance and Fuel-PLIF Measurements. *SAE Technical Paper, 2007-01-4130*, 2007. 50

[89] T. Passot and Pouquet. Numerical simulation of compressible homogeneous flows in the turbulent regime. *Journal of Fluid Mechanics*, 118:441–466, 1987. 51

[90] H. Curren, P. Gaffuri, W. Pitz, and C.K. Westbrook. *A Comprehensive Modeling Study of n-Heptane Oxidation*. Lawrence Livermore National Laboratory, Livermore, CA 94550, 2000. 51

[91] R. Ognik. Computer Modeling of HCCI Combustion. *PhD Thesis, Chalmers University*, 2004. 51

[92] S. Tanaka, F. Ayala, and J. Keck. A reduced chemical kinetic model for HCCI combustion of primary reference fuels in a rapid compression machine. *Combustion and Flame*, 133:467–481, 2003. 51

[93] J. Zheng, W. Yang, D.L. Miller, and N.P. Cernansky. A Skeletal Chemical Kinetic Model for the HCCI Combustion Process. *SAE Technical Paper, 2002-01-0423*, 2002. 51

[94] H. Li, D. Miller, and N. Cernansky. Development of a Reduced Chemical Kinetic Model for Prediction of Preignition Reactivity and Autoignition of Primary Reference Fuels. *SAE Paper, SAE960498*, 1996. 51

[95] H. Machrafi, K. Lombaert, S. Cavadias, and P. Guibert. Reduced Chemical Reaction Mechanisms: Experimental and HCCI Modelling Investigations of Autoignition Processes of n-Heptane in Internal Combustion Engines. *SAE Technical Paper, 2005-24-035*, 1996. 51

[96] S. Gupta, H.G. Im, and M. Valorani. Classification of Ignition Regimes in HCCI Combustion Using Computational Singular Perturbation. *Proceedings of the Combustion Institute*, 33:2991–2999, 2011. 55

[97] O. Stenls, M. Christensen, R. Egnell, and B. Johansson. Hydrogen as homogenous charge compression ignition engine fuel. *SAE Technical Paper 2004-01-1976*, 2004. 75

[98] M.L. Wyszynski, A. Megaritis, S.M. Peucheret, D. Yap, and H. Xu. Effect of hydrogen addition on natural gas HCCI combustion. *SAE Technical Paper 2004-01-1972*, 2004. 75

[99] R.W. Bilger, M. Chen, and H. Starner. On Reduced Mechanisms for Methane-Air Combustion in Nonpremixed Flames. *Combustion and Flame*, 80:135–149, 1990. 75, 89

[100] R.W. Bilger. Molecular Transport Effects in Turbulent Diffusion Flames at Moderate Reynolds Number. *AIAA 81-0104R*, 20, 1982. 88

[101] J.C. Sutherland, P.J. Smith, and J.H. Chen. Quantification of differential diffusion in nonpremixed systems. *Combustion Theory and Modelling*, 9:365–383, 2005. 88

[102] F. Bisetti, J.Y. Chen, J.H. Chen, and E.R. Hawkes. Differential diffusion effects during the ignition of a thermally stratified premixed hydrogenair mixture subject to turbulence. *Proceedings of the Combustion Institute*, 32:1465–1472, 2009. 92

[103] Y. Zhang, J. Gandhi, B. Peterson, and C.J. Rutland. Large Eddy Simulation of Scalar Dissipation Rate in an Internal Combustion Engine. *SAE Technical Paper 2010-01-0625*, 2010. 99

[104] S.B. Pope. *Turbulent Flow*. Cambridge Press, 2000. 99

[105] C.F. Jimnez, F. Ducros, B. Cuenot, and B. Bdat. Subgrid scale variance and dissipation of a scalar field in large eddy simulations. *Physics of Fluids*, 13:1748–1754, 2001. 103

[106] J. H. Chen, C.S. Yoo, G. Bansal, Hongfeng Yu, A. Mascarhenas, R. Grout, T. Lu, and R. Sankaran. High Fidelity Direct Numerical Simulations of Turbulent Combustion. *SC10, New Orleans*. 111